AD-A048 079 ADVISORY GROUP FOR AEROSPACE RESEARCH AND DEVELOPMENT--ETC F/G 11/6
USE OF GENERAL FATIGUE DATA IN THE INTERPRETATION OF FULL-SCALE--ETC(U)
OCT 77 W BARROIS

UNCLASSIFIED AGARD-AG-228 NL

OF
AD
A048079

END
DATE FILMED
1-78
DDC

AGARD-AG-228

AGARD

ADVISORY GROUP FOR AEROSPACE RESEARCH & DEVELOPMENT

7 RUE ANCELLE 92200 NEUILLY SUR SEINE FRANCE

AGARDograph No. 228

Use of General Fatigue Data in the Interpretation of Full-scale Fatigue Tests

by

W. Barrois

NORTH ATLANTIC TREATY ORGANIZATION

DISTRIBUTION AND AVAILABILITY
ON BACK COVER

AGARD-AG-228

NORTH ATLANTIC TREATY ORGANIZATION

ADVISORY GROUP FOR AEROSPACE RESEARCH AND DEVELOPMENT

(ORGANISATION DU TRAITE DE L'ATLANTIQUE NORD)

AGARDograph No.228

USE OF GENERAL FATIGUE DATA IN THE INTERPRETATION OF FULL-SCALE FATIGUE TESTS

by

W.Barrois

Retired Military Air Chief Engineer
42, rue Larmeroux
92170 Vanves, France

Oct 77

80p.

This AGARDograph was sponsored by the Structures and Materials Panel of AGARD.

THE MISSION OF AGARD

The mission of AGARD is to bring together the leading personalities of the NATO nations in the fields of science and technology relating to aerospace for the following purposes:

- Exchanging of scientific and technical information;
- Continuously stimulating advances in the aerospace sciences relevant to strengthening the common defence posture;
- Improving the co-operation among member nations in aerospace research and development;
- Providing scientific and technical advice and assistance to the North Atlantic Military Committee in the field of aerospace research and development;
- Rendering scientific and technical assistance, as requested, to other NATO bodies and to member nations in connection with research and development problems in the aerospace field;
- Providing assistance to member nations for the purpose of increasing their scientific and technical potential;
- Recommending effective ways for the member nations to use their research and development capabilities for the common benefit of the NATO community.

The highest authority within AGARD is the National Delegates Board consisting of officially appointed senior representatives from each member nation. The mission of AGARD is carried out through the Panels which are composed of experts appointed by the National Delegates, the Consultant and Exchange Program and the Aerospace Applications Studies Program. The results of AGARD work are reported to the member nations and the NATO Authorities through the AGARD series of publications of which this is one.

Participation in AGARD activities is by invitation only and is normally limited to citizens of the NATO nations.

Published October 1977

ISBN 92-835-1250-2

Set and printed by Technical Editing and Reproduction Ltd
Harford House, 7–9 Charlotte St, London, W1P 1HD

PREFACE

The provision of adequate fatigue strength is generally recognized today as a major design requirement for aircraft structures.

Usually, new aircraft designs are subjected to full-scale fatigue testing in order to substantiate a sufficient life under the spectrum of loads expected in service.

However, the loads experienced in actual service may deviate considerably from the original design assumptions. Moreover, modifications of the aircraft may lead to local structural changes. In order to allow an extrapolation of fatigue test results towards actual service conditions a careful interpretative analysis of damage observed in the test will be necessary.

In the present report, Mr. Barrois gives a comprehensive survey of means and methods that are available and factors that must be considered in the interpretation of full-scale fatigue test results.

Mr. Barrois is one of the gifted engineers who combine a scientific mind with a large practical design experience in the field of structural fatigue.

Sincere gratitude is expressed to him for preparing this work, which will be of great value to all those concerned with providing and maintaining structural integrity of aircraft.

J.B. DE JONGE
Chairman,
Working Group on Fatigue Life Prediction
of Tactical Aircraft

SUMMARY

The fatigue behaviour of notched specimens depends on two elasticity parameters, namely, the stress concentration factor, K_T, and the relative stress gradient or the radius of curvature at the notch root, r. Laboratory fatigue test results are not always representative of the environmental conditions within aircraft structural assemblies, particularly because of water vapour condensation in gaps and recesses resulting from temperature variations. The frequency effect is mainly ascribable to humidity, and therefore to corrosion, owing to hydrogen penetration.

In structural assemblies, stress concentrations due to load transfer through fasteners are investigated for the case of asymmetric single shear of the fasteners – a case often critical in fatigue.

The breakdown of the applied loadings must include the peak-to-peak, ground-air-ground variation. In load transfer by fastener bearing stresses, the low compressive loads may be neglected, the local highest stresses varying from zero to the maximum. Interpretation of full-scale fatigue results, either for a different loading or for a slightly modified local design of the structure, is essentially comparative. In order to locate the computation points within a suitable region of the $(K_T S_n - N) - K_T S_m - r$ curves, the stress concentration factor K_T is multiplied by a damage adjustment factor, k_{DA}, such that the Miner damage is 1 for the local failure of the structure considered. A structure may provide as many k_{DA}-values as the various damage failures observed during the full-scale fatigue test. A number of further investigations would enable the variation of k_{DA} with structural assembly parameters to be investigated.

CONTENTS

USE OF GENERAL FATIGUE DATA IN THE INTERPRETATION OF FULL-SCALE FATIGUE TESTS

W.Barrois

1. INTRODUCTION

Previously, in most cases, the interpretation of fatigue tests of full-scale structures, sub-structures or small assemblies, have been limited to initial test aims, such as the confirmation of a sufficient life under the spectrum of loads expected in service, or a comparative investigation of several detail designs in order to obtain the best solution.

A more advanced interpretation becomes necessary when complementary information modifies the assumed load spectrum, or if a development of the aircraft type implies a change in the expected loading and in the local dimensions of structural elements. Every instance of damage should be subjected to interpretative calculations, the results of which could be entered in a data bank. *Thus, one fatigue test could supply as many pieces of information on local fatigue behaviour as there are points where fatigue damage has been detected and possibly the propagation recorded.*

Although this type of interpretation may take place at any time after the fatigue test has ended, it would be useful to begin it as soon as the damage appears, so as to obtain easily complementary information which may be needed, such as stress measurements around the damage areas under fatigue loading.

In general, the forecasted, computed fatigue life of a structure under a given loading may be considered as being reliable only to the same extent as forecast weather conditions; although generally good, these can occasionally be wildly erratic. This state of affairs is considerably improved if one or several test results allow adjustment of the computation to take into account the actual properties of the structure in the area considered. Thus, computation will permit:

- evaluation of the life of the structure tested for a different fatigue loading;
- appraisal of the improvements afforded by local changes in shape or size;
- forecasting of the fatigue behaviour of other structures made from the same material by using similar technology.

The two components of calculation are:

(i) The set of $(S_a\text{–}N)\text{–}S_m$ curves characterizing the fatigue life, expressed as the number, N, of cycles, under constant amplitude stress, $S = S_m \pm S_a$, of notched specimens having a notch radius r, the fatigue behaviour of which is assumed similar to that of the area of structure considered.

(ii) The programme of variation of the stress S during test loading cycles and the expected stress development in service. Knowledge of these implies that the states of stresses are well defined for test and in-service loadings.

These two components are used in evaluating the theoretical Miner-Palmgren damage

$$d = \sum_i \frac{n_i(S_i)}{N_i(S_i)},$$

where n_i is the number of applications of the stress S_i during the loading cycle representing, for example, one average flight, while N_i is the number of applications of this stress level which, applied alone, would cause fatigue failure.

The stress development during the fatigue test is defined by the load development from the knowledge of local stresses that correspond to unit loads. Local stresses may be deduced from a combination of calculation and strain measurements carried out on the particular structure during fatigue tests or static tests. From the local geometry it is possible to compute the state of stress in small areas where measurement is not possible, such as in notch roots, which are defined by a stress concentration factor and a notch radius.

2. REPRESENTATION OF S–N CURVES FOR THE INTERPRETATION OF STRUCTURAL FATIGUE TESTS

The large number of material conditions, such as sheet, plate, extrusions and forging, of specimen shapes, as well as of surface conditions resulting from machining or from corrosion-protective coatings, gives rise to wide variation in the $(S_a - N) - S_m$ curves that represent fatigue test results.

In specimens and structural elements, stress concentrations are often defined with poor accuracy by the stress concentration factor, the reference stress of which is not always known. Moreover, this factor does not define the extent of the material subjected to high stresses and therefore gives no information on the plastic accommodation that modifies the stress distribution during successive fatigue cycles and which is the main cause of the scale effect.

The scatter of fatigue test results includes an intrinsic scatter, resulting from the variation of fatigue properties for neighbouring points of the material in the damaged area, and another kind of scatter related to the average tensile properties. As shown by Gassmann[1], the cause of this latter lies in the variation of the strength properties from one end of a bar to the other, or among the various areas of a forging, and additionally in the variation from one batch of the material to another.

As illustrated in Figure 1 for a steel alloy, when the tensile strength of each fatigue specimen is measured by testing small tensile specimens machined from every fatigue-failed large specimen, a stress correction

$$S_N^* = S_N \frac{(S_{ult})_{average}}{(S_{ult})_{specimen}},$$

based on the assumption that the fatigue strength is proportional to the ultimate tensile strength, S_{ult}, gives a greatly reduced scatter.

When fatigue test specimens, taken from one element of material, and in close proximity to one another, are subjected to one load level, the average fatigue life will be well defined for the area of the element considered and for the particular load level. Nevertheless, with several load levels, as are needed in the determination of a S–N curve, the curve variations may well be due to the variation of strength properties among the various areas of one element or among several elements of the material batch. On the contrary, a random selection of specimens assigned to each load level may increase the scatter, thus necessitating a larger number of specimens for each load level.

The curves plotted in Figure 2 represent fatigue test results published by Crichlow et al.[2]. The plane specimens, containing a central, quasi-elliptical notch obtained by the intersection of circular holes, were taken from bare 7075-T6, thin aluminium alloy sheets. Each point corresponds to the median life of five specimens subjected to the same fatigue load level. Considering the four parameters: alternating stress S_a, mean stress S_m, the life N expressed in number of cycles, and the stress concentration factor K_T, the lack of uniformity in the S–N curves may possibly be attributed to the scatter of the strength properties of the material from one point of the surface of one sheet to another, and to scatter among the various sheets. In order to regularize the results, Crichlow et al. first plotted S–N curves of regular curvatures that passed, sometimes, outside the experimental median points. Then, remarking that, even for the 7075-T6 aluminium alloy sheets, results published by other authors showed variations of the same order of magnitude as those related to various aluminium alloys, Crichlow et al. used a standard set of S–N curves for several K_T values, assumed to be valid for any aluminium material, in the determination of the so-called "Fatigue Quality Index K", i.e., the "equivalent" stress concentration factor K_T interpolated from the standard S–N data and corresponding, for each region of a structure or an assembly damaged in fatigue, to the same fatigue life under the same fatigue stress. However, fatigue tests of notched specimens subjected to fatigue load spectra show that the fatigue quality index K depends on the shape of the fatigue load spectrum (rare or numerous higher loads). We think that this is due to the stress gradient effect and to residual stresses created by high loads and causing a change in the mean stress of the cycles and a decrease of alternating stress amplitudes.

Our opinion is that a better representation of the state of stresses at a notch root may be obtained from a knowledge of the surface stress $S_s = K_T S$ at the point of maximum stress and of the relative stress gradient along the direction perpendicular to the surface, $(1/S_s)(\partial S/\partial n)_s$. These two quantities govern the elastic behaviour when the fatigue test begins and, furthermore, the plastic accommodation of successive fatigue cycles.

As the relative stress gradient g is related to the notch radius r and, in the bending case, to the specimen thickness h by the relation

$$g = (1/S_s)(\partial S/\partial n)_s = -2\left(\frac{1}{r} + \frac{1}{h}\right),$$

the relative stress gradient may be replaced by the quantity $1/r$ in the tensile case.

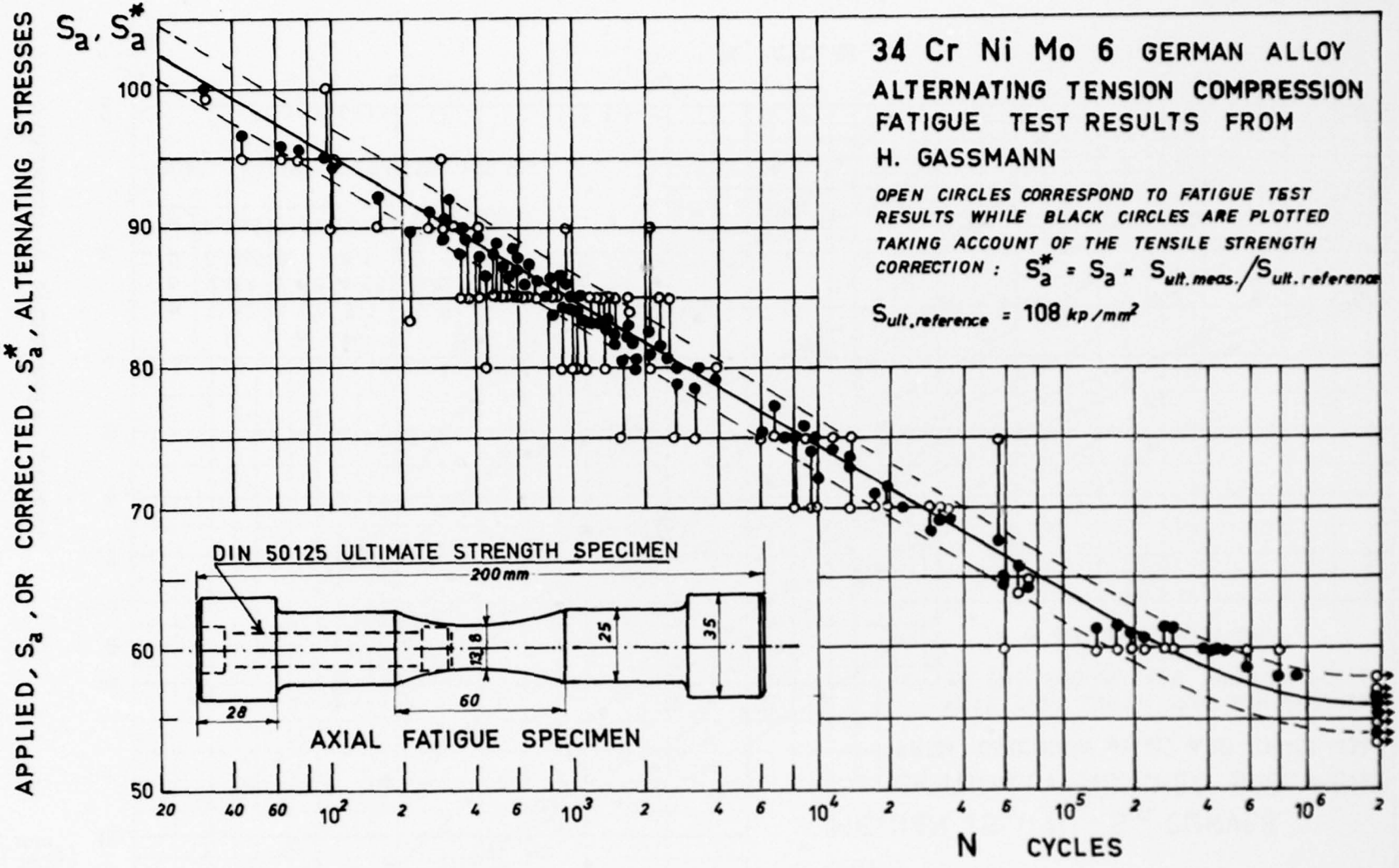

Fig.1 Reduction of the fatigue scatter using test results with a correction assuming fatigue strengths to be proportional to ultimate tensile strengths

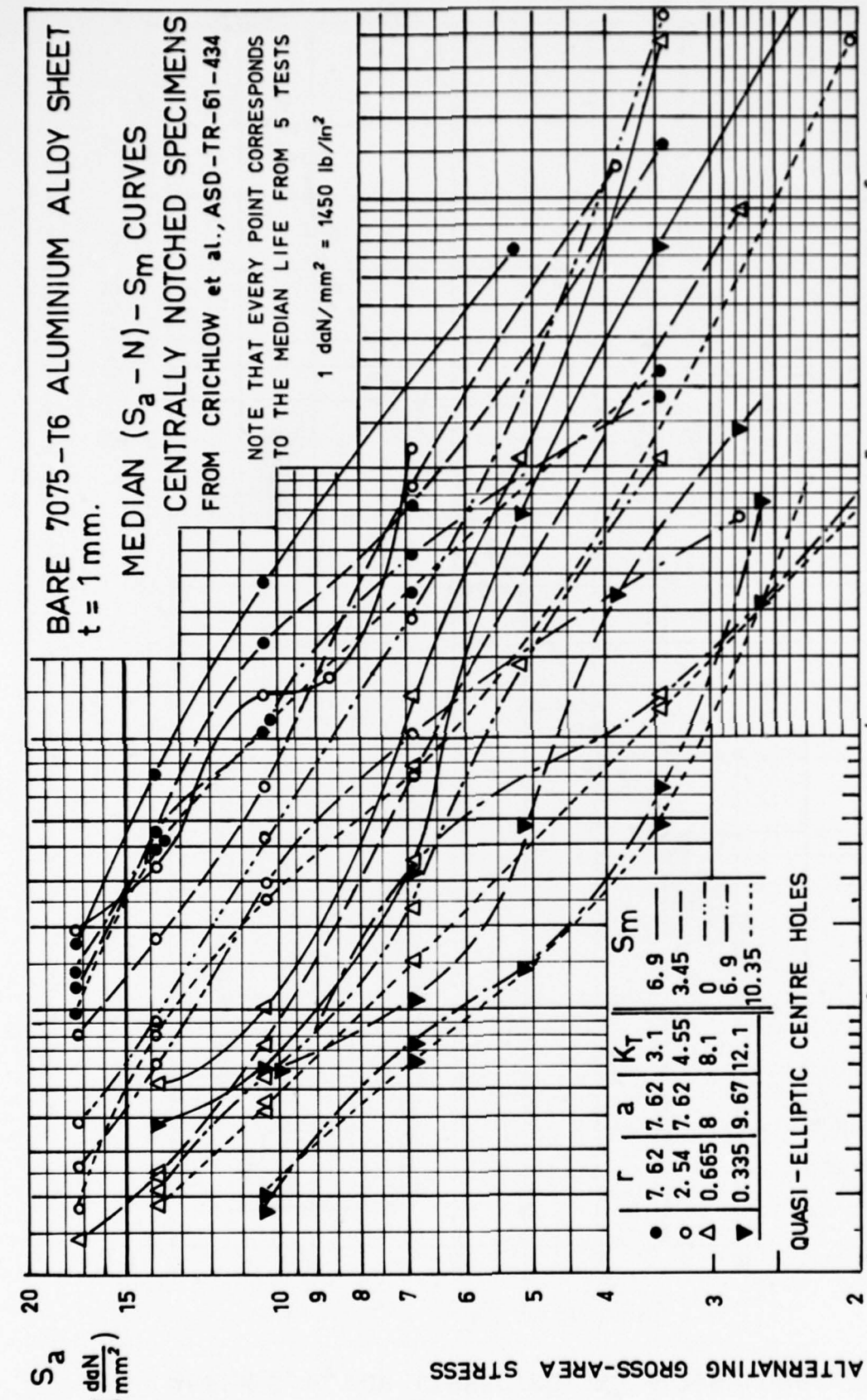
BARE 7075-T6 ALUMINIUM ALLOY SHEET
t = 1 mm.
MEDIAN (Sa - N) - Sm CURVES
CENTRALLY NOTCHED SPECIMENS
FROM CRICHLOW et al., ASD-TR-61-434
NOTE THAT EVERY POINT CORRESPONDS TO THE MEDIAN LIFE FROM 5 TESTS
1 daN/mm² = 1450 lb/in²
r | a | Kt | Sm
● 7.62 | 7.62 | 3.1 | 6.9
o 2.54 | 7.62 | 4.55 | 3.45
Δ 0.665 | 8 | 8.1 | 0
▼ 0.335 | 9.67 | 12.1 | 6.9
10.35
QUASI-ELLIPTIC CENTRE HOLES
Sa (daN/mm²)
ALTERNATING GROSS-AREA STRESS
N CYCLES

Figure 2

3. S–N CURVES FOR PLAIN OR NOTCHED SPECIMENS OF ALUMINIUM ALLOY

3.1 Thin Sheets of 7075-T6 Aluminium Alloy

Considering again the fatigue results of Crichlow et al.[2] from the regularized S–N curves, presented as $\log(K_T S_a)$ versus $\log N$, the reference curves plotted in Figure 3 are obtained. The K_T-values given by Crichlow are related to the nominal stress in the absence of the notch, but their method of evaluation was not reported. Here, the notch root surface stresses, S_s, are evaluated by using the expression

$$S_s = K_T S_{nom} = S_{nom}(1 + 2/(a/r))\sqrt{(1 - (2a/w)^2)},$$

where S_{nom} is the stress far away from the notch,

2a the width of the centre notch,

r the notch end radius and

w the specimen width.

$(1 + 2\sqrt{(a/r)})$ is the stress concentration factor for an elliptical hole at the centre of an infinite sheet, and $\sqrt{(1 - (2a/w)^2)}$ is the finite-width correction of Dixon[3]. For the various specimens used, w = 76.2 mm and:

r =	7.62	2.54	0.665	0.335 mm
a =	7.62	7.62	8	9.67 mm
$K_{T\,nominal}$, ESDU Data Sheets 69020	3.15			
$K_{T\,net}$, ESDU Data Sheets 69020		3.8	6.6	9.2
$K_{T\,nominal}$, expression (2)	3.1	4.55	8.1	12.1
$K_{T\,net}$, expression (2)	2.48	3.64	6.4	9.02
$K_{T\,nominal}$, Crichlow et al.	3	4	7	10

The K_T-values of the expression have been used to compute values of $K_T S_a = S_{sa}$ in Figure 3.

The perspective diagram in Figure 4 shows well the lack of regularity in the S–N curves plotted for various mean stress levels, S_m, and relative stress gradients, g. The more regular lines of Figure 5 may be obtained by altering the initial data. The reference set thus obtained for the $(S_{sa}–N)–S_m–r$ curves is peculiar to bare 7075-T6 aluminium alloy sheets and differs from the standard $(S_a–N)–S_m–K_T$ curves proposed by Crichlow et al.[2] for all aluminium alloys.

Peculiarities of certain fatigue test results have not been emphasised or explained. For example, Figure 6, S_a versus S_m, represents NACA fatigue test results, with constant values of $R = S_{min}/S_{max}$, of plain specimens taken from bare, 2.3 mm-thick, 7075-T6 aluminium alloy sheets[4]. Within the S_m-range from 20 to 30 ksi, the curves show abrupt changes corresponding to the test at R = 0.02, which are not attributable to an R-effect. It may be assumed that the anti-buckling guides used in compression-tension tests are related to this phenomenon. In this case, plain curves could be replaced by the dotted ones, which restores the regularity.

Using the same batch of bare 7075-T6 sheets, NACA[5,6,7] has carried out fatigue tests of notched specimens, the notch surface being finished by electrolytic polishing. Values of S_{max} have been taken from published curves and values of $K_T S_a$ have been computed with K_T-values corresponding to notch sizes and to data from the ESDU Data Sheets 69020. Figure 7 shows these results graphically, with logarithmic scales of surface alternating stresses at the notch root, $K_T S_a$, and of relative stress gradients, $(1/S)(\partial S/\partial n) = -2/r$, perpendicular to the notch root surface. Probably owing to differences in hole machining for the 38 mm-diameter hole, and differences in stress distributions for the shoulder specimens, the corresponding points are not likely to belong to the same family as the results of edge-notched specimens.

With r = 2.54 mm, corresponding to $g = -0.79\ mm^{-1}$, Figure 8 shows $(K_T S_a–N)–S_m$ curves interpolated from the curves in Figure 7. With the same scales, Figure 9 shows the $(K_T S_a–N)–S_m$ curves drawn from Crichlow's results modified in order to transfer from the curves of Figure 2 to those of Figure 5. Comparison for $S_m = 0$ and $S_m = 10\ daN/mm^2$ is legitimate owing to this small smoothing modification to the experimental results. It is:

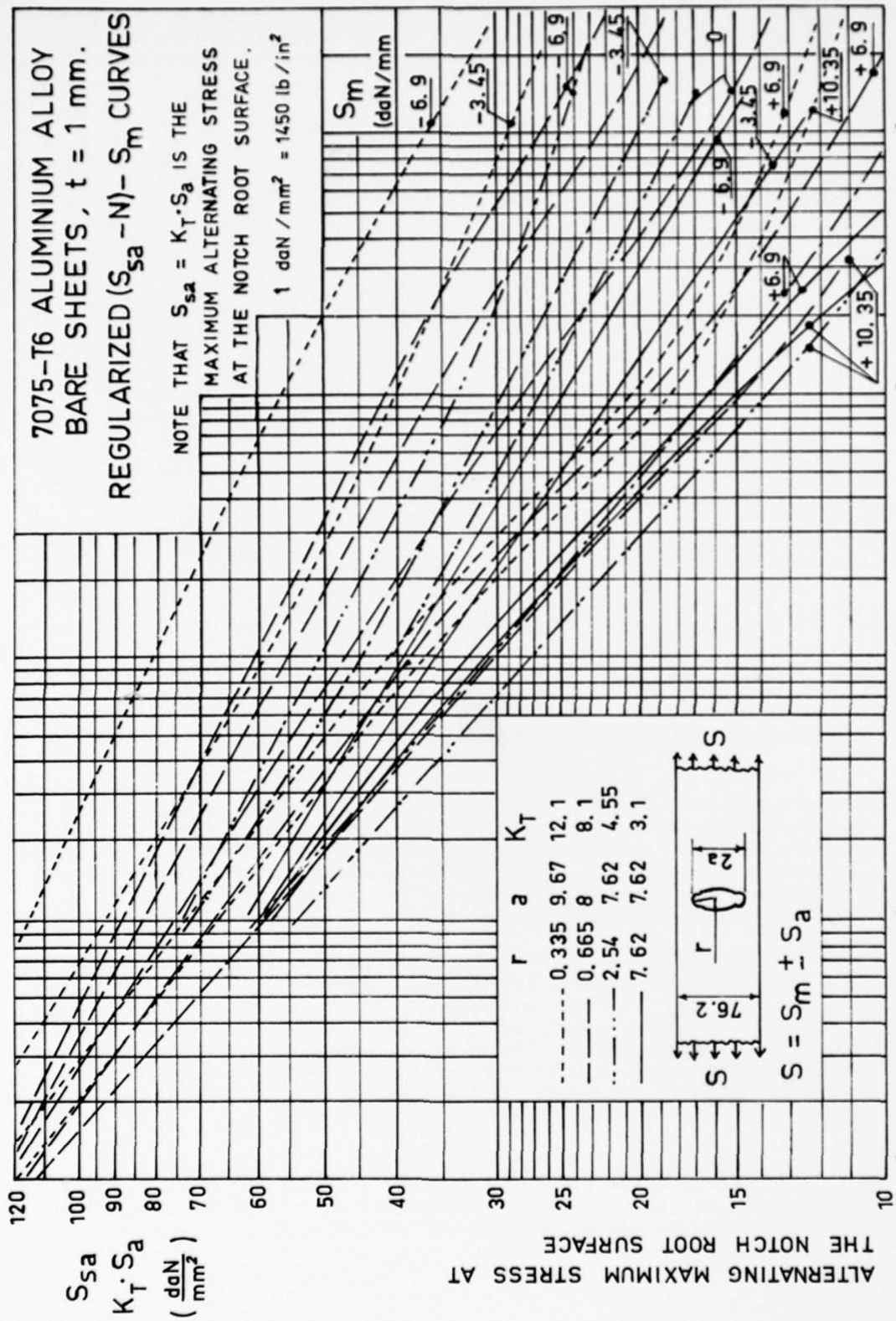
7075-T6 ALUMINIUM ALLOY
BARE SHEETS, t = 1 mm.
REGULARIZED (S_{sa}-N)- S_m CURVES
NOTE THAT $S_{sa} = K_T \cdot S_a$ IS THE MAXIMUM ALTERNATING STRESS AT THE NOTCH ROOT SURFACE.
1 daN / mm² = 1450 lb / in²
S_m (daN/mm)
-6.9
-3.45
0
+6.9
+10.35
$S_{sa} = K_T \cdot S_a$ (daN/mm²)
ALTERNATING MAXIMUM STRESS AT THE NOTCH ROOT SURFACE
N CYCLES
r a K_T
0.335 9.67 12.1
0.665 8 8.1
2.54 7.62 4.55
7.62 7.62 3.1
76.2
S = $S_m \pm S_a$

Figure 3

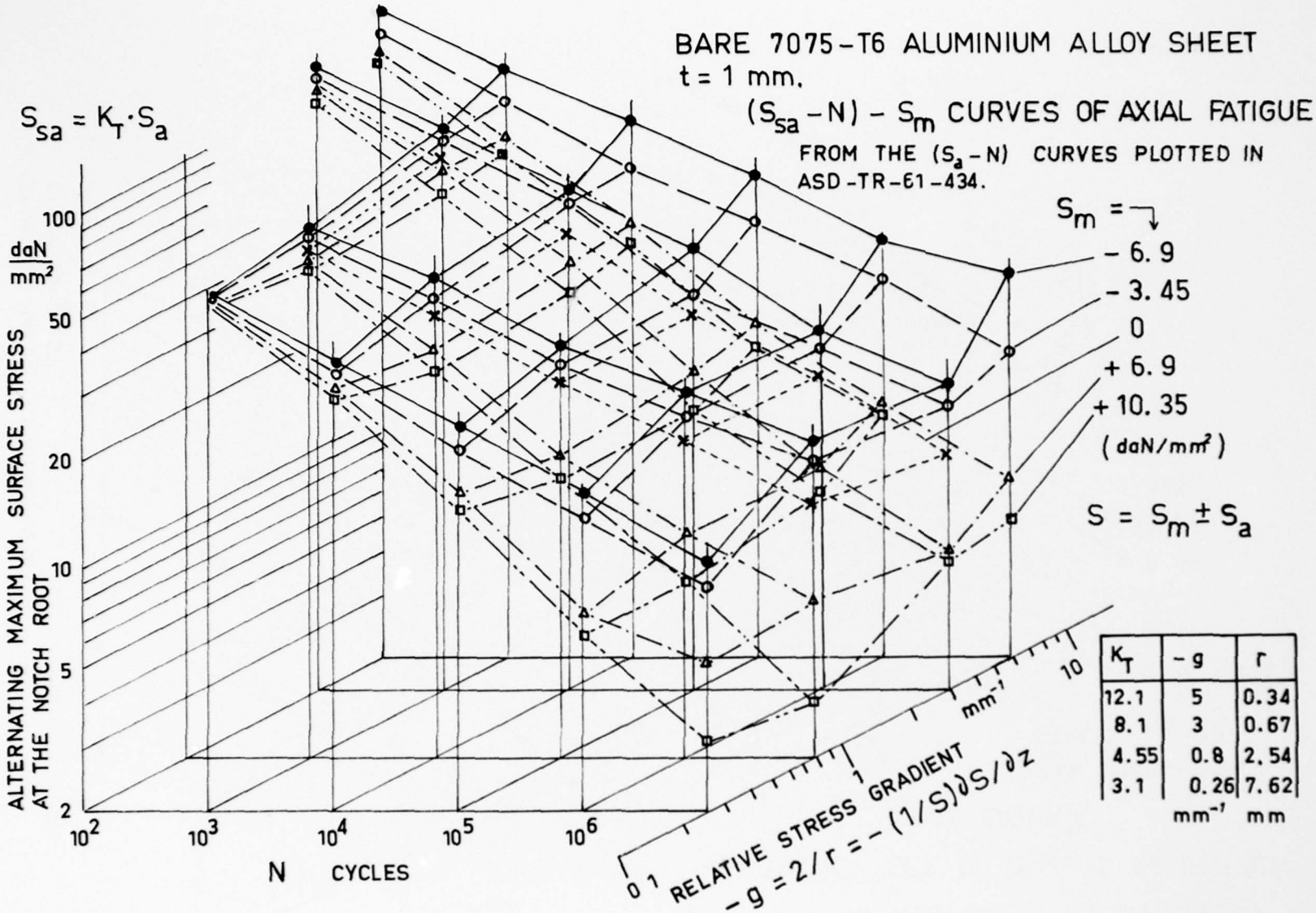
BARE 7075-T6 ALUMINIUM ALLOY SHEET
t = 1 mm.
(Ssa - N) - Sm CURVES OF AXIAL FATIGUE
FROM THE (Sa - N) CURVES PLOTTED IN ASD-TR-61-434.
Ssa = KT · Sa
Sm =
- 6.9
- 3.45
0
+ 6.9
+ 10.35
(daN/mm²)
S = Sm ± Sa
ALTERNATING MAXIMUM SURFACE STRESS AT THE NOTCH ROOT
daN/mm²
100
50
20
10
5
2
10²
10³
10⁴
10⁵
10⁶
N CYCLES
0 1
1
10
mm⁻¹
RELATIVE STRESS GRADIENT
- g = 2/r = - (1/S) ∂S/∂z
KT | - g | r
12.1 | 5 | 0.34
8.1 | 3 | 0.67
4.55 | 0.8 | 2.54
3.1 | 0.26 | 7.62
mm⁻¹ mm

Figure 4

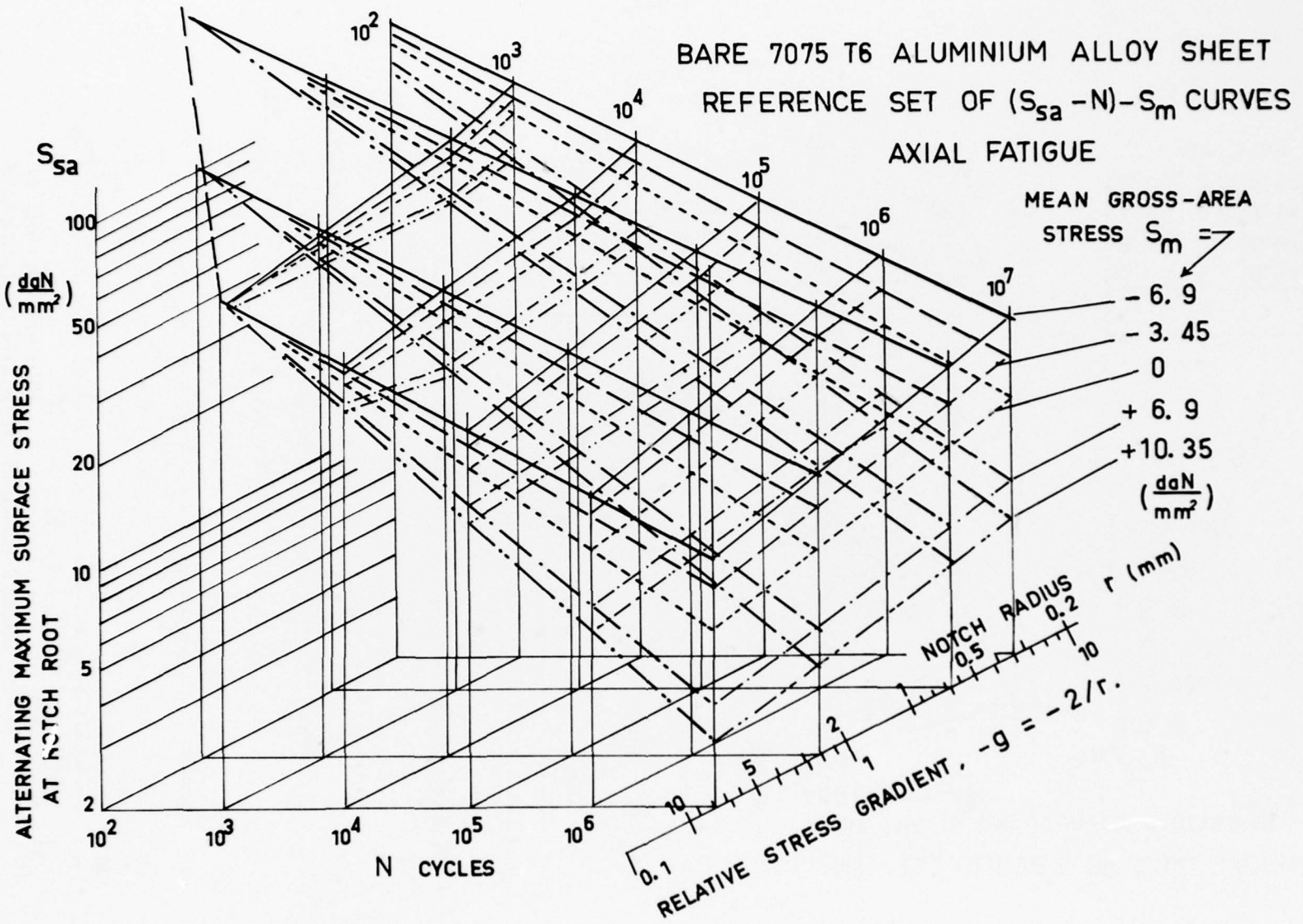
BARE 7075 T6 ALUMINIUM ALLOY SHEET
REFERENCE SET OF (S_{sa} – N) – S_m CURVES
AXIAL FATIGUE
S_{sa}
$(\frac{daN}{mm^2})$
ALTERNATING MAXIMUM SURFACE STRESS AT NOTCH ROOT
100
50
20
10
5
2
10^2
10^3
10^4
10^5
10^6
10^7
N CYCLES
MEAN GROSS-AREA STRESS S_m =
– 6. 9
– 3. 45
0
+ 6. 9
+10. 35
$(\frac{daN}{mm^2})$
NOTCH RADIUS r (mm)
0.1
0.2
0.5
1
2
5
10
RELATIVE STRESS GRADIENT, $-g = -2/r$.

Figure 5

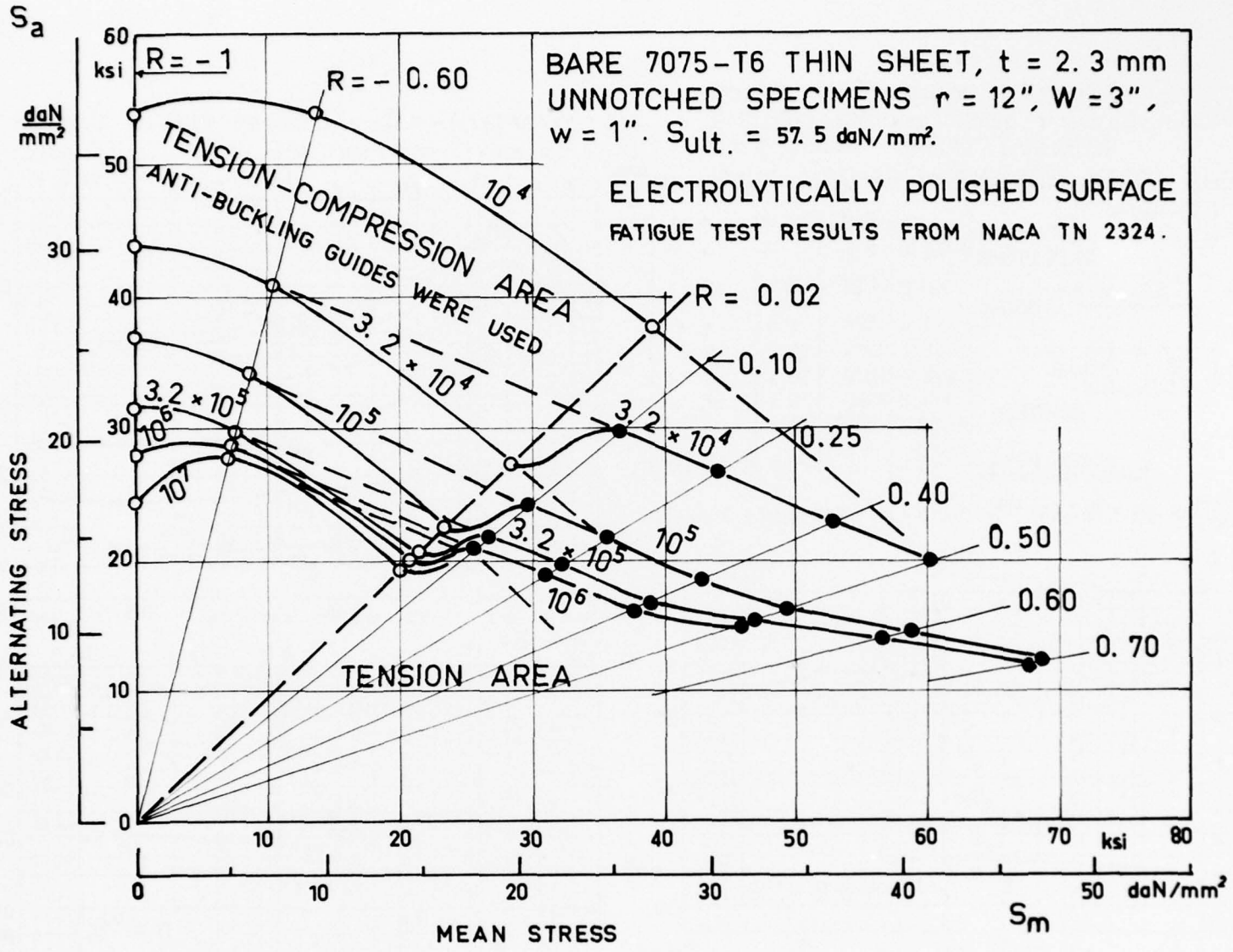
S_a
60
ksi
R = - 1
daN/mm²
50
30
40
30
20
20
10
10
0
R = - 0.60
TENSION-COMPRESSION AREA
ANTI-BUCKLING GUIDES WERE USED
10^4
3.2×10^4
3.2×10^5
10^5
10^6
10^7
BARE 7075-T6 THIN SHEET, t = 2.3 mm
UNNOTCHED SPECIMENS r = 12", W = 3",
w = 1". $S_{ult.}$ = 57.5 daN/mm².
ELECTROLYTICALLY POLISHED SURFACE
FATIGUE TEST RESULTS FROM NACA TN 2324.
R = 0.02
0.10
0.25
0.40
0.50
0.60
0.70
3.2×10^4
3.2×10^5
10^5
10^6
TENSION AREA
ALTERNATING STRESS
10
20
30
40
50
60
70
ksi
80
0
10
20
30
40
50
daN/mm²
MEAN STRESS
S_m

Figure 6

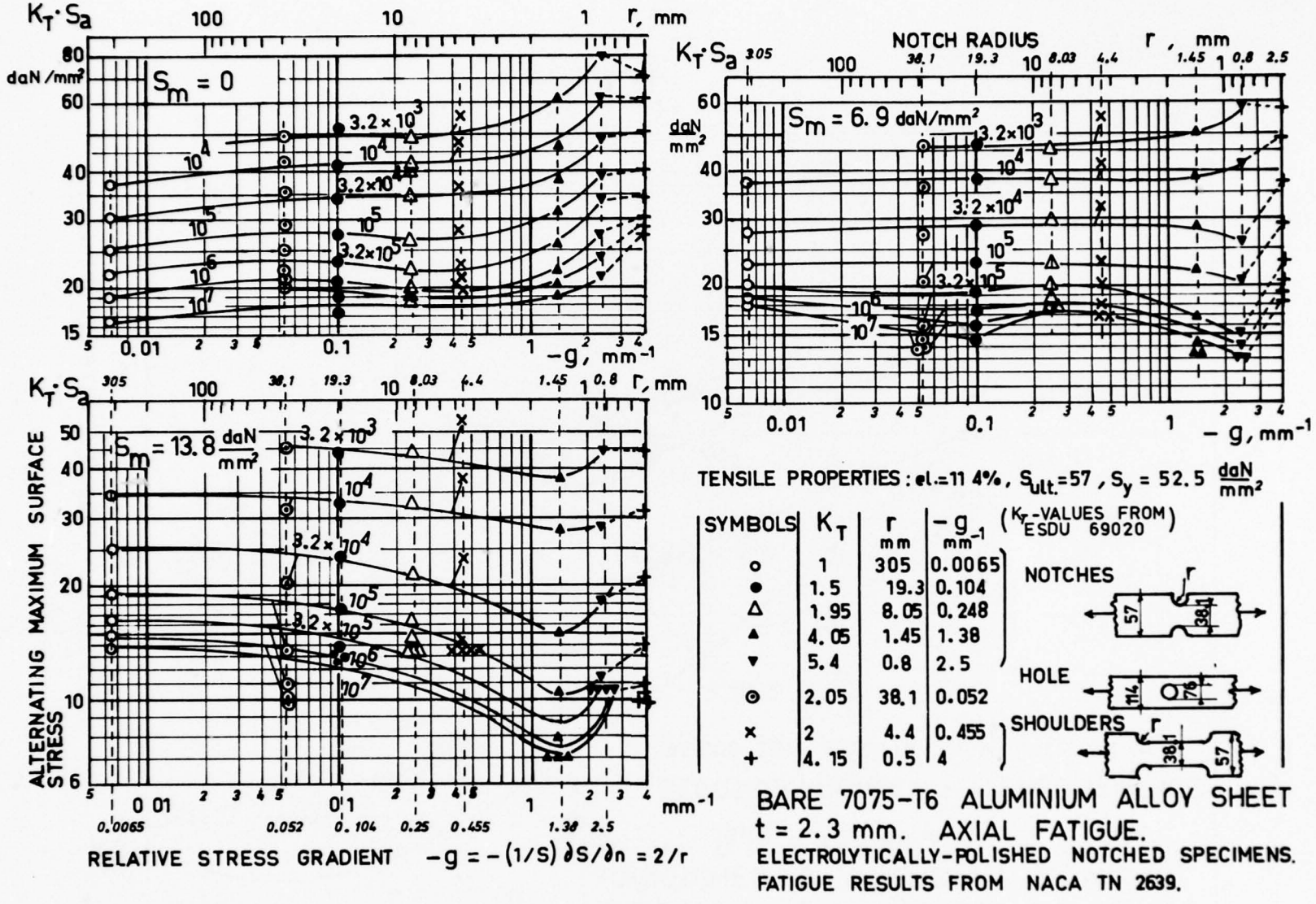
$K_T \cdot S_a$
daN/mm²
$S_m = 0$
$S_m = 13.8$ daN/mm²
$S_m = 6.9$ daN/mm²
NOTCH RADIUS r, mm
ALTERNATING MAXIMUM SURFACE STRESS
RELATIVE STRESS GRADIENT $-g = -(1/S)\,\partial S/\partial n = 2/r$
$-g$, mm⁻¹
TENSILE PROPERTIES : el.=11 4%, $S_{ult.}$=57, S_y = 52.5 daN/mm²
SYMBOLS | K_T | r mm | $-g$ mm⁻¹ (K_T-VALUES FROM ESDU 69020)
○ 1 | 305 | 0.0065
● 1.5 | 19.3 | 0.104
△ 1.95 | 8.05 | 0.248
▲ 4.05 | 1.45 | 1.38
▼ 5.4 | 0.8 | 2.5
⊙ 2.05 | 38.1 | 0.052
× 2 | 4.4 | 0.455
+ 4.15 | 0.5 | 4
NOTCHES
HOLE
SHOULDERS
BARE 7075-T6 ALUMINIUM ALLOY SHEET
t = 2.3 mm. AXIAL FATIGUE.
ELECTROLYTICALLY-POLISHED NOTCHED SPECIMENS.
FATIGUE RESULTS FROM NACA TN 2639.

Figure 7

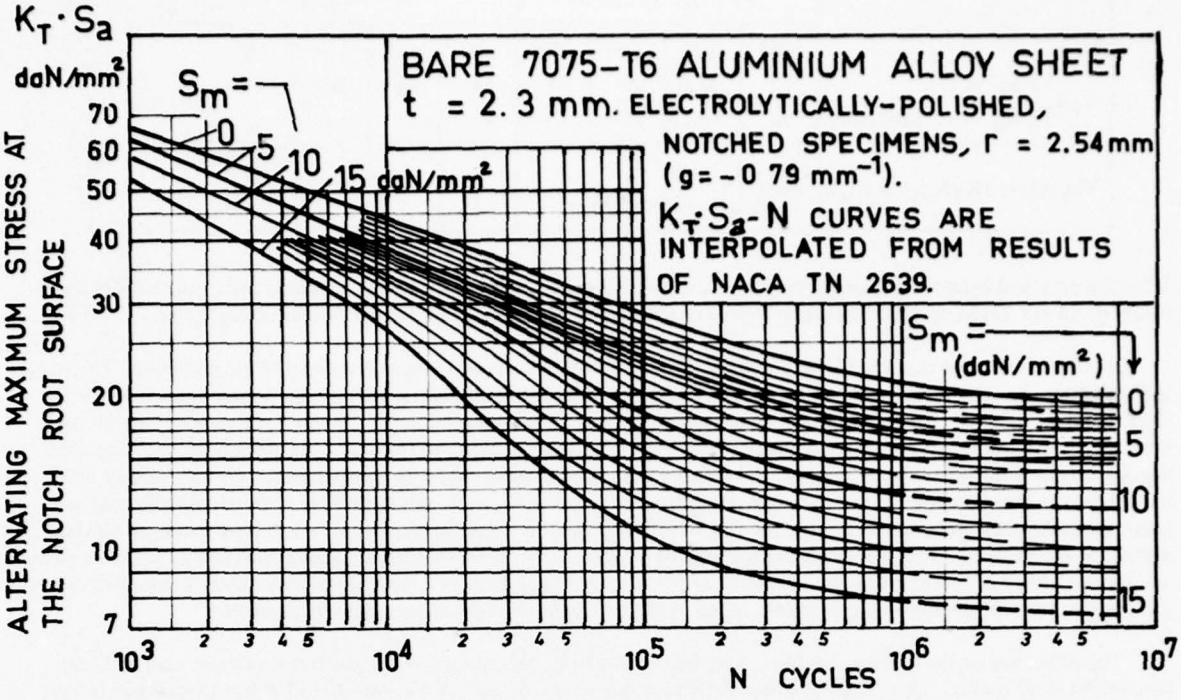

Figure 8

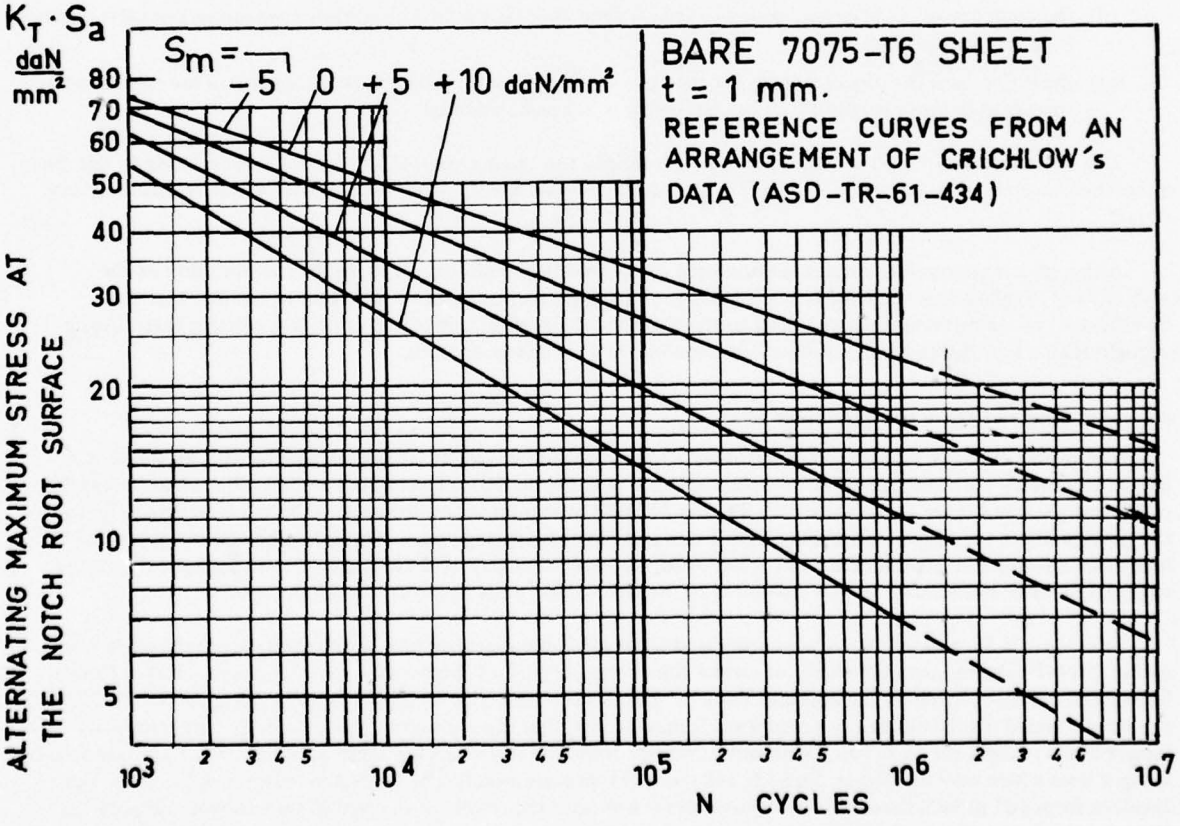

Figure 9

	I – NACA's results				*II – Crichlow's results*			
N =	10^3	10^4	10^5	10^6	10^3	10^4	10^5	10^6
$K_T S_a$ { $S_m = 0$	66	43.5	29	21	68	43	26.5	17 } daN/mm²
$K_T S_a$ { $S_m = 10$ daN/mm²	58	34.5	19	13	59	27	14.6	7 } daN/mm²
The ratios $(K_T S_a)_I/(K_T S_a)_{II}$ are { $S_m = 0$					1	1	1.1	1.2
The ratios $(K_T S_a)_I/(K_T S_a)_{II}$ are { $S_m = 10$ daN/mm²					1	1.3	1.3	1.9

Since for practical cases in evaluating the life of aircraft wings, S_m ranges from 0 to 10 daN/mm², and the life ranges from 10^4 to 10^5 flight cycles, the average values of the fatigue ratio would be 1.2 for fatigue strength and 2.5 for life.

It may be assumed that the higher fatigue strength of NACA tests was due to the electrolytic polishing. The longer the corrosion time the more important this effect may be. This would explain a shift of the fatigue limit towards the small numbers of cycles for the polished sheets and, from a practical point of view, the disappearance of the fatigue limit for service use in a humid environment. With high values of the mean stress, S_m, the absence of any corrosion damage on the polished surfaces permits the accommodation of fatigue cycles to be realized before any fatigue crack initiation; the mean stresses of accommodated cycles tend toward $S_m = 0$ and the effect of the nominally applied mean stress remains moderate as long as the test duration is small enough for corrosion not to have damaged the bare surface of the material. It is worth noting the benefit of preventing the corrosion of internal surfaces of fastener holes, and the difficulty of representing the corrosion effect during fatigue tests in a laboratory environment, which does not include the periodic condensation of water vapour onto the masked cold surfaces, gaps or recesses.

The influence of the surface condition may be better shown by comparing fatigue test results on clad and bare aluminium alloy sheets. The "Etablissement Aéronautique de Toulouse" (EAT, now CEAT)[8] has carried out fatigue tests on notched and unnotched specimens taken from clad or bare, 4 mm-thick, A-Z5GU-T6 (similar to 7075-T6) or A-U4G1-T3 (similar to 2024-T3) aluminium alloy sheets. For each alloy, bare or clad sheets came from the same casting, and they had undergone the same processing, rolling and treatment processes. Figures 10 and 11 show that:

(i) conventional fatigue limits at 10^7 cycles of bare sheets are 1.5 to 3 times higher than those of clad sheets;

(ii) the tendency of S–N curves to show a true fatigue limit (stress level asymptote) appears at a smaller number of cycles for clad sheets;

(iii) the differences in fatigue strength for the various materials with similar surface conditions are considerably smaller than those between bare or clad sheets of the same material.

This last conclusion is still supported by CEAT's fatigue test results, plotted in Figure 12 and relating to flat, plain or notched specimens made from AZ1 (1% Zn, remainder Al) clad A-Z5GU-T6 (7075-T6) or A-U2GN-T6 aluminium alloys[9].

Although a more rigorous service environment could modify the results, owing to the susceptibility of the A-Z5GU (7075) alloy to intergranular corrosion, the foregoing conclusions draw attention to the fact that the classification of materials by their chemical content and tensile properties is of less value in predicting their fatigue strength than a knowledge of their production processes and surface conditions.

3.2 Thin Sheets of 2024-T3 Aluminium Alloy

The master $K_T S$–N curves plotted in Figure 13 represent the results of fatigue tests performed by the NACA fatigue laboratory with the same set of notched specimens as for the 7075-T6 aluminium alloy, the fatigue strength of which was given in Figure 7. As with 7075-T6, the 2024-T3 aluminium alloy shows a significant beneficial effect of the stress gradient for notch radii smaller than 2 mm and pure alternating stress. This effect becomes detrimental for high mean stresses and large numbers of cycles. Also, the early tendency of S–N curves toward asymptotes for the larger numbers of cycles may well be attributed to the electrolytic polishing of the notch surfaces.

For $K_T = 2.55$ and $r = 1.6$ mm, corresponding to a 3.2 mm-diameter hole in flat strip specimens made from Alclad 2024-T3 aluminium alloy sheets of several thicknesses, Figure 14 shows $(K_T$–N)–S_m curves plotted from fatigue test results collated by Beckett and Vann[10]. These test results may be considered as typical for Alclad 2024-T3 thin sheets tested in a laboratory environment. It may be seen that the asymptotic trend of S–N curves towards fatigue limits is slight for $N < 10^7$. Within the N-range from 10^4 to 10^6 cycles, these curves are well approximated by straight lines which may be used as $K_T S$–N reference curves corresponding to the notch radius $r = 1.6$ mm. For N-values from 10^4 to 10^6, these reference curves agree well with the results of the NACA tests shown in Figure 13. However, for larger N-values, tendencies toward fatigue limits do not exist in aircraft service, owing to environmental conditions. Therefore straight reference lines are quite suitable for representing fatigue in service.

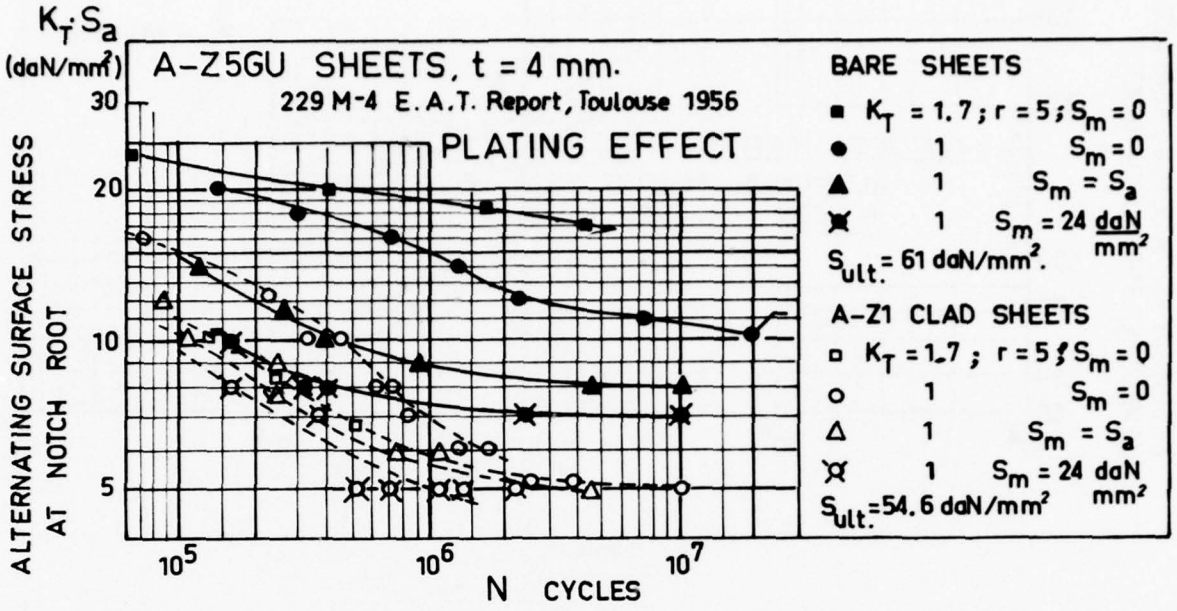

Figure 10

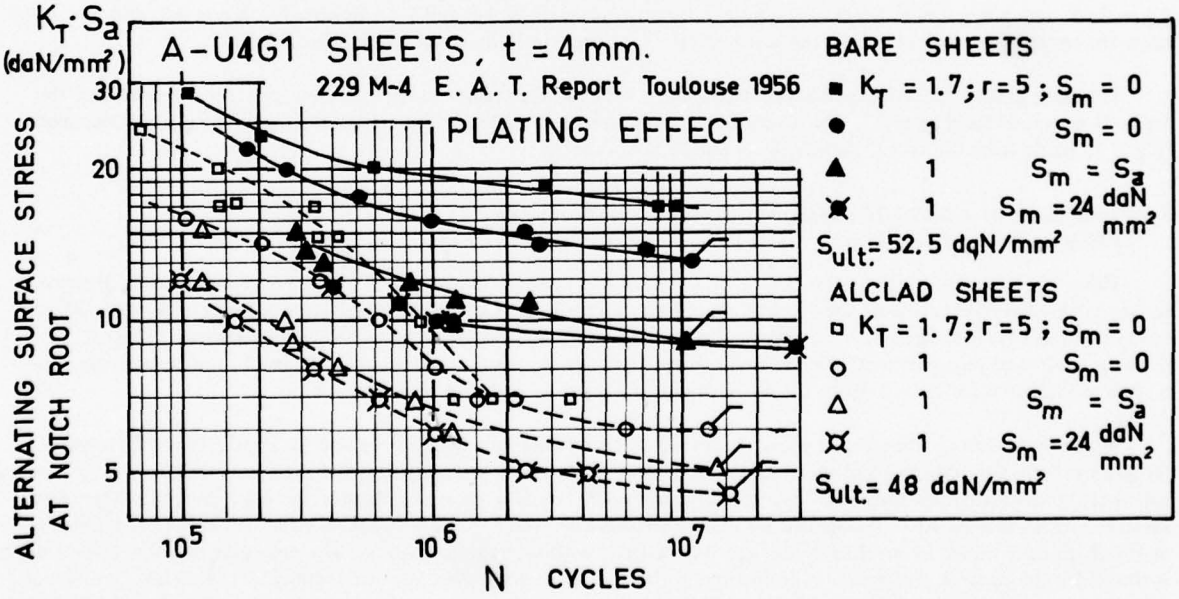

Figure 11

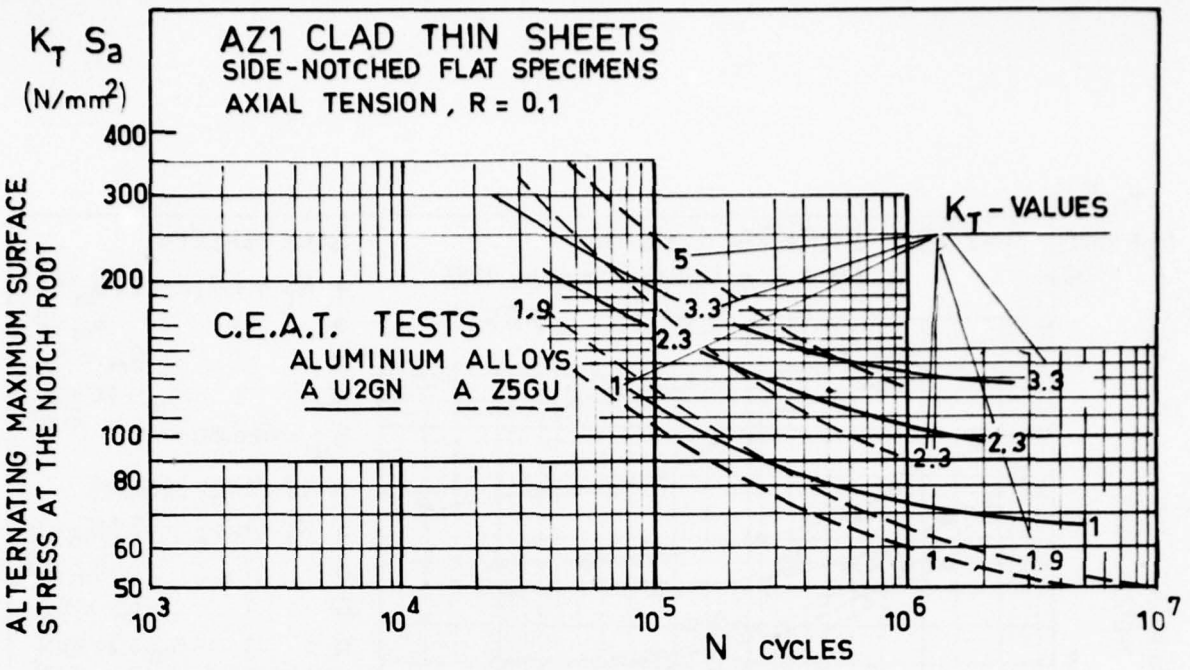

Figure 12

Figure 15 shows German fatigue test results from the Laboratorium für Bedienstfestigkeit (LBF)[11]. The centre notched (K_T = 3.1, r = 2 mm) specimens were made from bare, 5 mm-thick German 3.1354.5 (similar to 2024-T3) aluminium alloy sheet. The straight reference lines $K_T S$–N from Figure 14 are shown in Figure 15. The comparison shows discrepancies which are at most −20% in stress for S_m = 15 daN/mm², and −10% in stress for S_m = 0. Other results from the same source are reported in Figure 16. Again, reference straight lines that corresponded to K_T = 2.55 and r = 1.6 mm agree well with results for K_T-values of 1.5 and 2.1. Results for K_T = 4.5 and r = 1 mm show the usual improvement due to the gradient effect, as previously illustrated in Figures 7 and 13.

The same gradient effect explains the discrepancy between the reference lines (K_T = 2.55, r = 1.6 mm) and the $K_T S$–N curves of the Figure 17, which represent fatigue test data collated by Beckett and Vann[10] for plain specimens (K_T = 1) made from 0.8 to 1.2 mm-thick Alclad 2024-T3 sheet.

3.3 Thin Sheets of A-U4SG-T6 (similar to 2014-T6) Aluminium Alloy. Effect of Surface Conditions

There is a scarcity of fatigue test results on notched specimens made from 2014 aluminium alloy sheet. However, because A-U4SG-T6 sheets were used in French military aircraft, the CEAT fatigue laboratory undertook some fatigue tests intended to clarify the effect of surface conditions on fatigue strength. For unnotched specimens[12], Figure 18 shows a significant improvement when initially sharp-edged specimens have been vapour-blasted. For comparison, the S–N line evaluated for R = 0 from the S–N curves of Figure 17 is shown on Figure 18.

With respect to the strengths of plane specimens of rectangular cross section (curve 1), Figure 19 shows lower fatigue strengths for edge-grooved specimens[13]. The reason for this is probably that the specimen ends are not grooved and that the stress distributions at groove ends correspond to actual stress concentration factors higher than the value assumed, which is close to 1. No significant difference was observed in fatigue strength, either for different suppliers or for chemically milled or machined edge grooves, with or without vapour-blasting. The only case of poor, low strength is shown by the curve 4, which relates to loading in the transverse grain direction for chemically milled edge grooves and material from supplier A, which has a higher ultimate tensile strength. This particular behaviour was not explained. By comparison with curves 6 and 7 it can only be ascribed to the combination of chemical milling of edge grooves, transverse direction of loading and ageing treatment giving a higher ultimate strength. Each S–N curve being plotted from about 20 test results, it is impossible for scatter to explain this behaviour, particularly in the region of 10^7 cycles.

An investigation of other surface conditions[14] has been carried out by the CEAT fatigue laboratory using the same batch of bare 1.8 mm-thick A-U4SG-T6 aluminium alloy sheets. Figures 20(a) and 20(b) show S–N curves for materials from two different suppliers, A and B. Comparison of curves 1, 2 and 3 shows that chemical milling is detrimental in fatigue, even when a new solution- and ageing-treatment is carried out. Vapour-blast surface treatment on both sides of the sheet produces some fatigue improvement in the A-material, which has the highest ultimate tensile strength, but

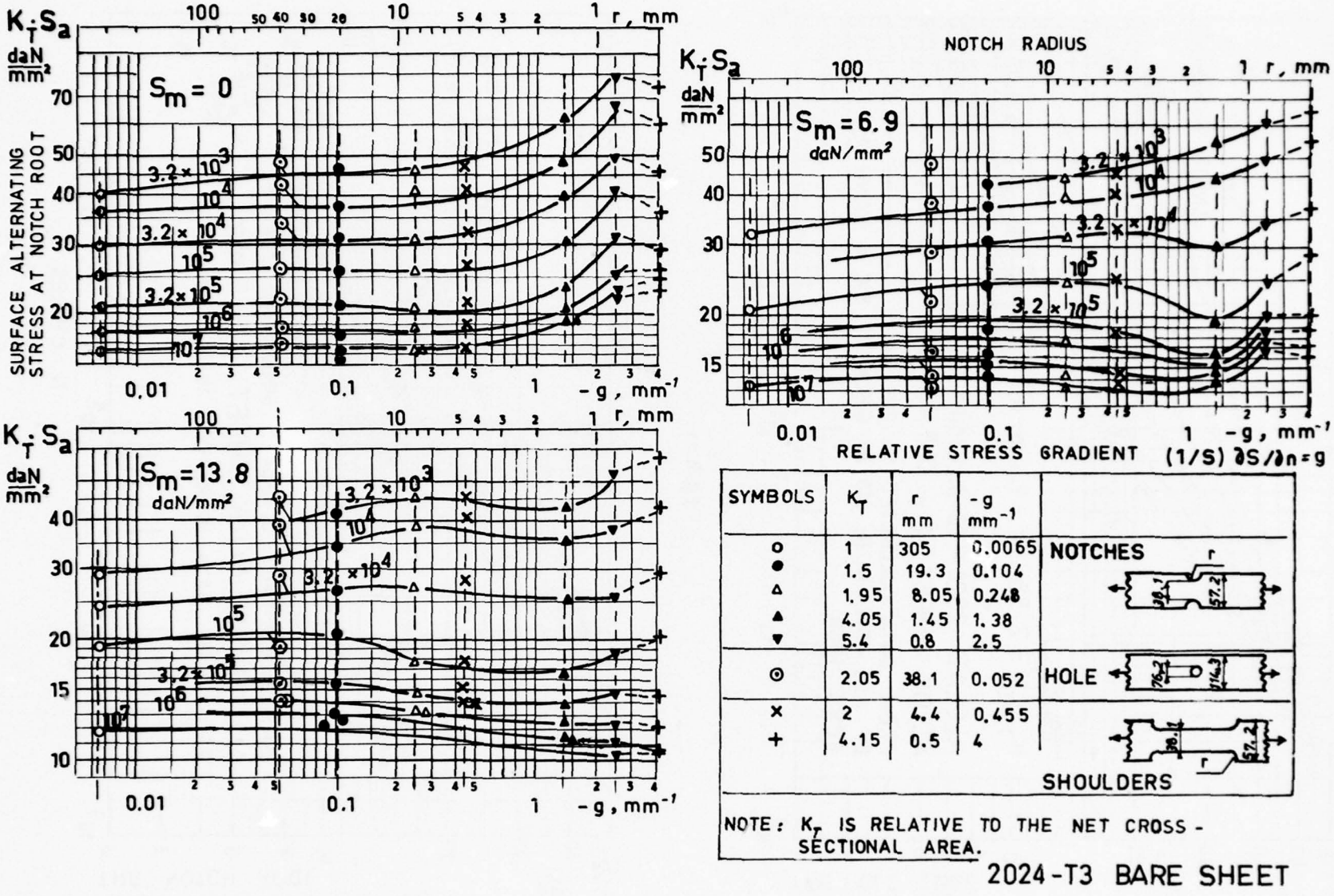

Fig.13 Master S–N curves drawn from fatigue test results reported in NACA TN 2639

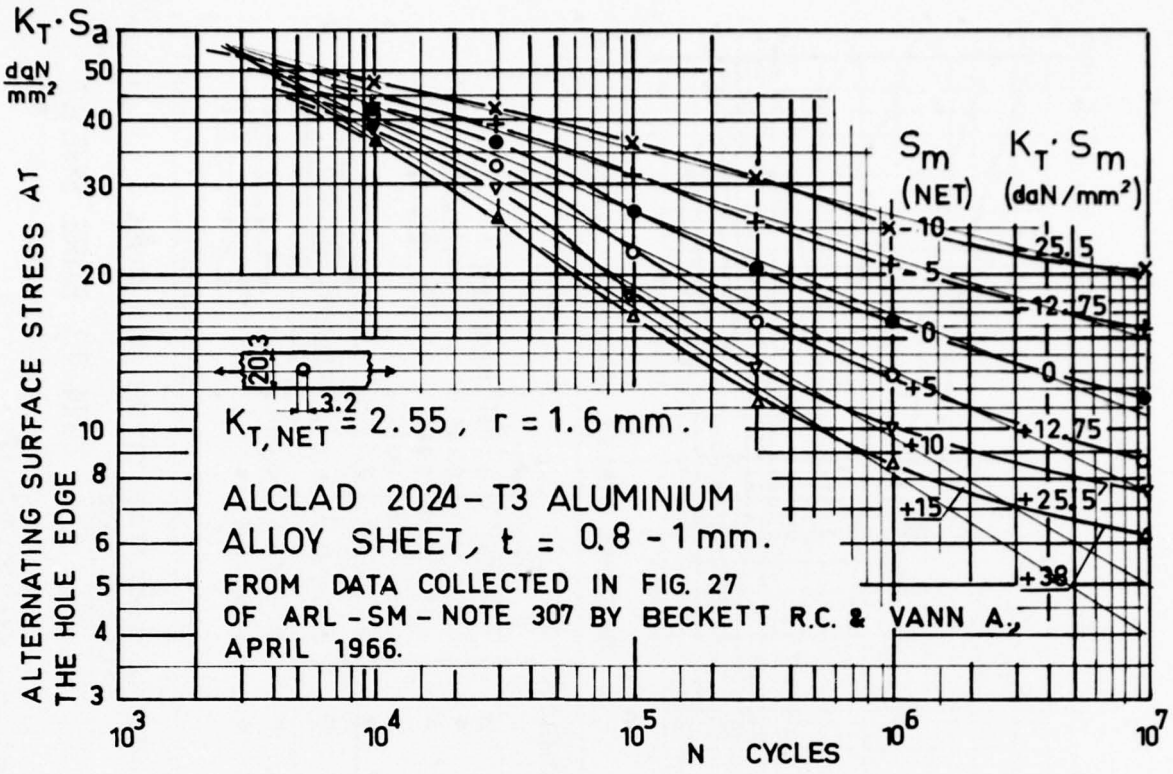

Figure 14

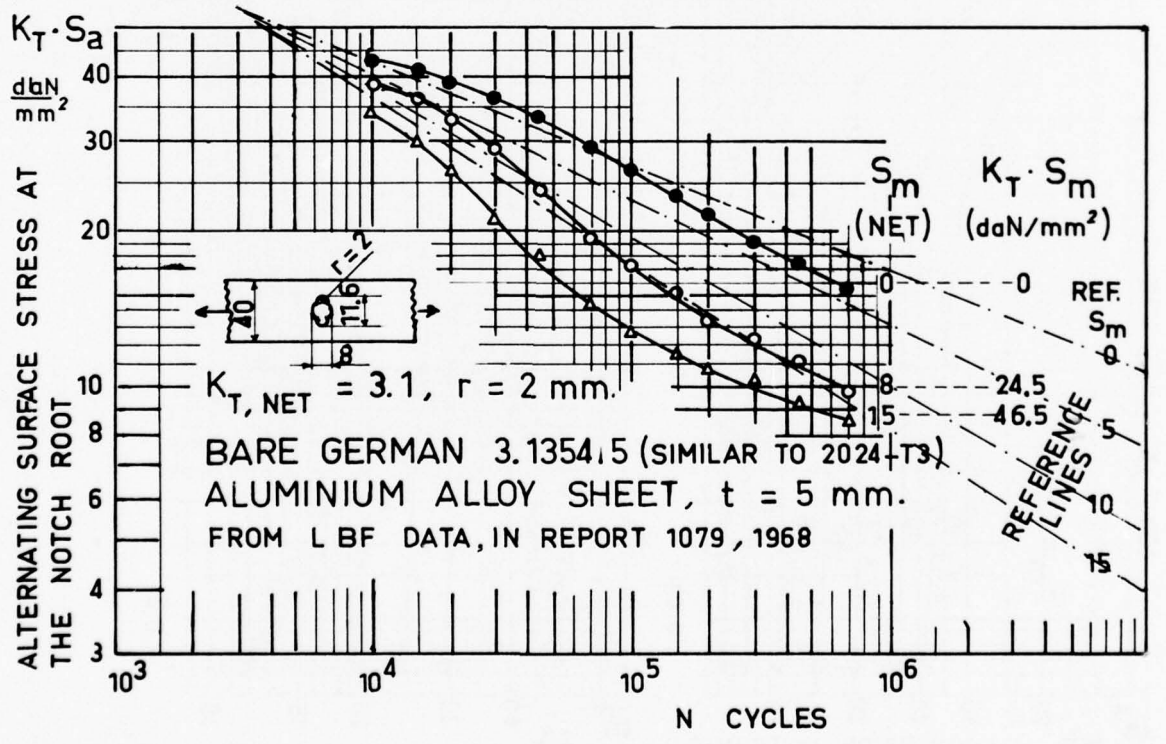

Figure 15

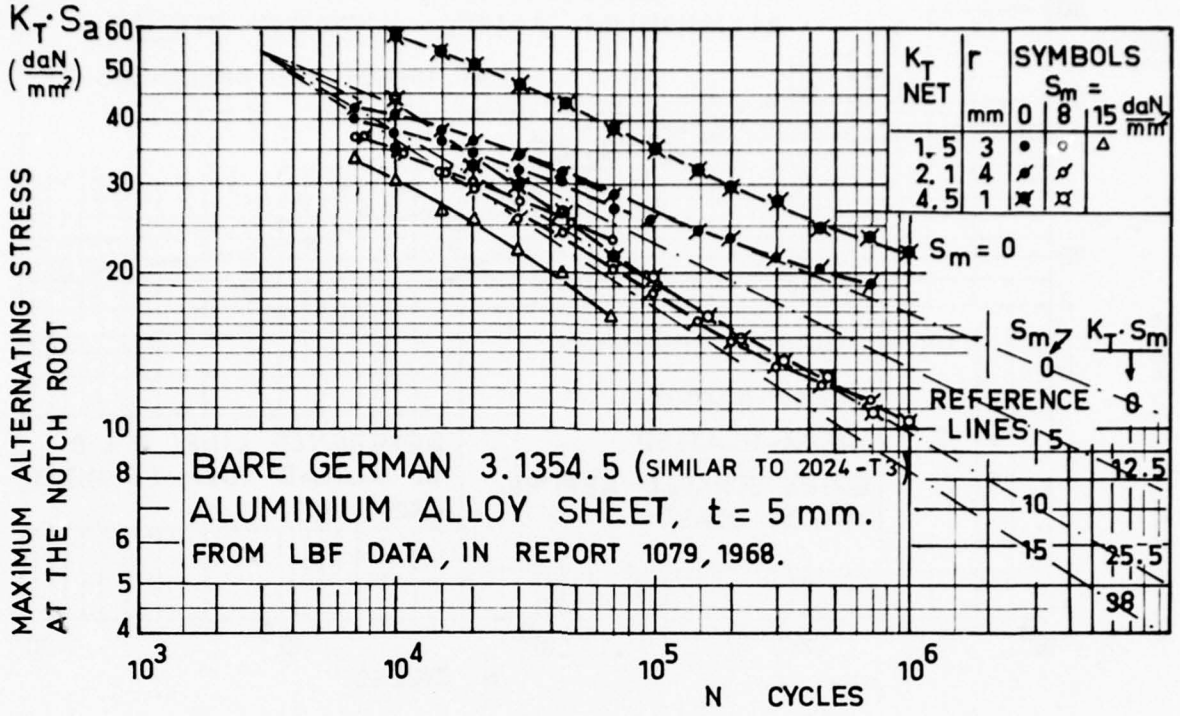

Figure 16

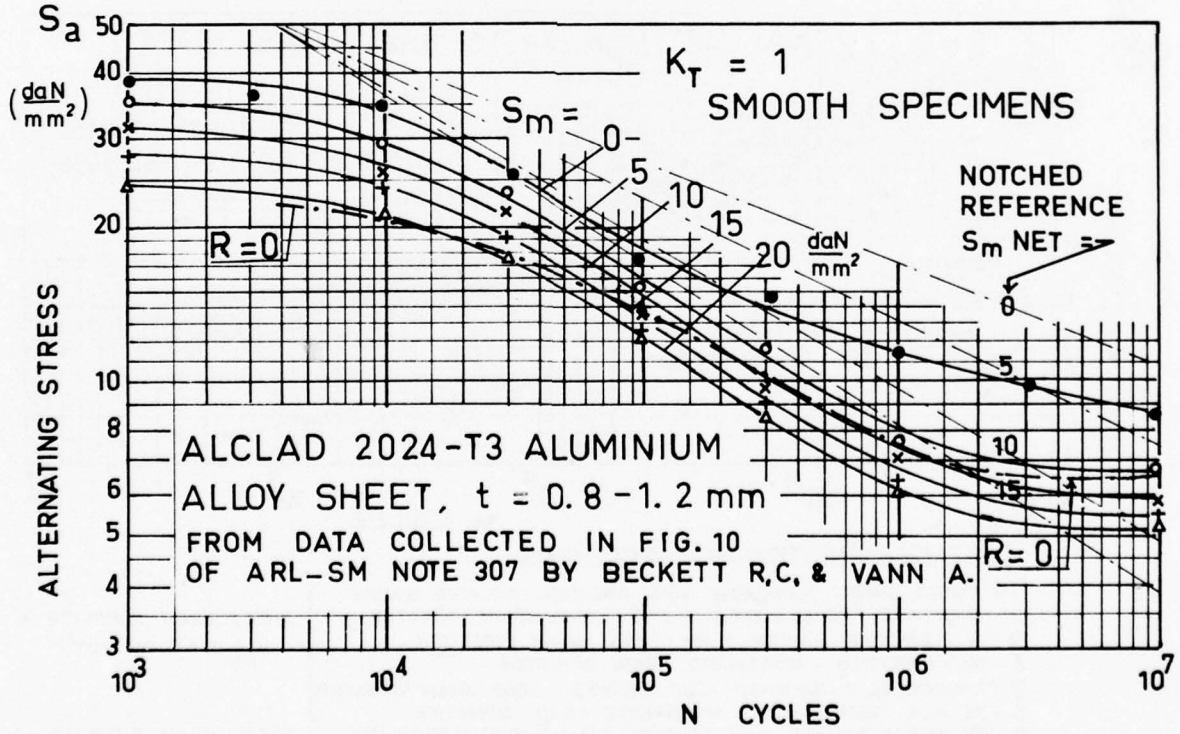

Figure 17

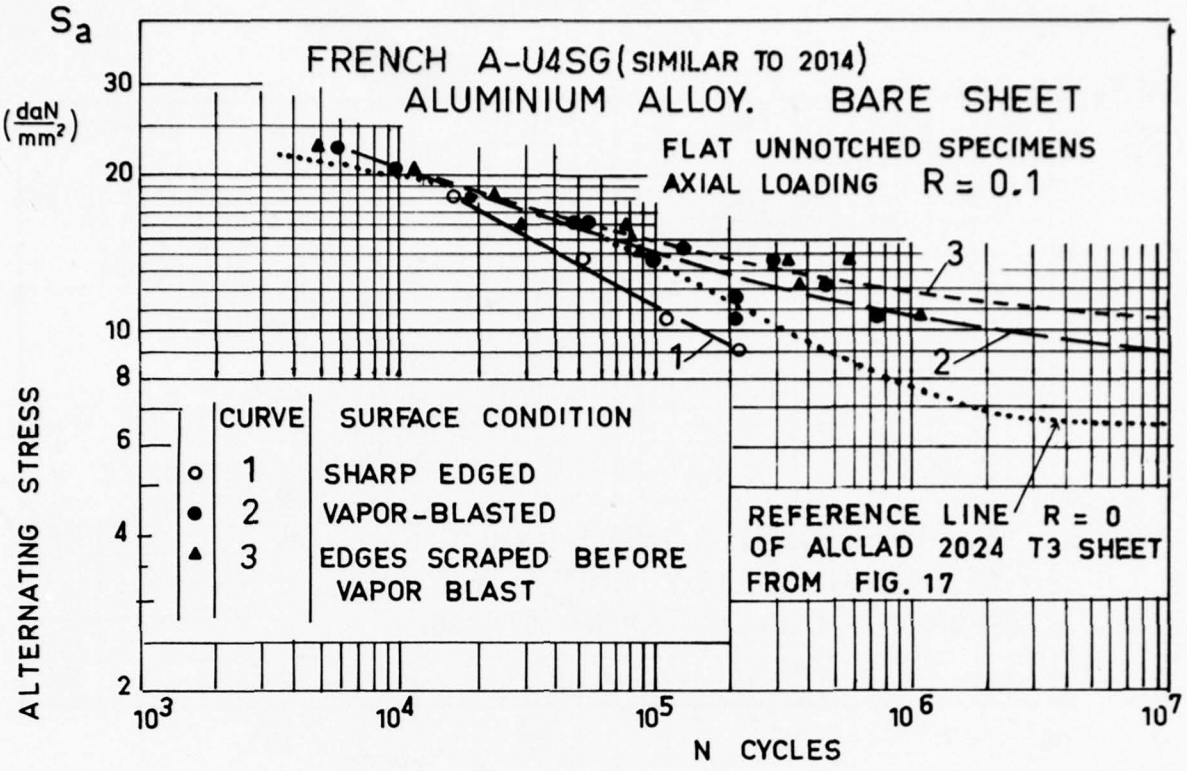

Figure 18

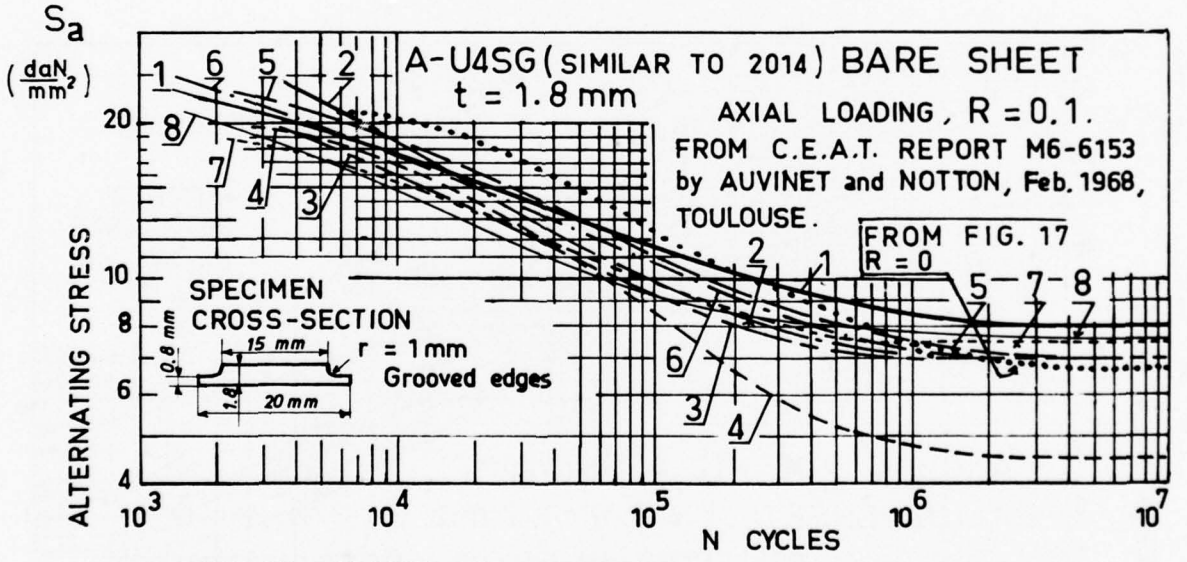

SURFACE CONDITION OF SPECIMENS

1 - VIRGIN SHEET - TRANSVERSE GRAIN DIRECTION - NO EDGE GROOVE
2 - CHEMICALLY PROVIDED EDGE GROOVES - LONG GRAIN DIRECTION
3 - No. 2 CONDITION + VAPOR BLAST - LONG GRAIN DIRECTION
4 - No. 2 CONDITION - TRANSVERSE GRAIN DIRECTION
5 - MECHANICALLY MACHINED EDGE GROOVES LONG GRAIN DIRECTION
6 - AS No. 5 CONDITION BUT TRANSVERSE GRAIN DIRECTION

} SHEET FROM SUPPLIER A $S_{ult.}$ = 48.5 daN/mm²

7 - CHEMICALLY PROVIDED EDGE GROOVES TRANSVERSE DIRECTION
8 - AS No 7 CONDITION + VAPOR BLAST TRANSVERSE DIRECTION

} SHEET FROM SUPPLIER B $S_{ult.}$ = 45.8 daN/mm²

Figure 19

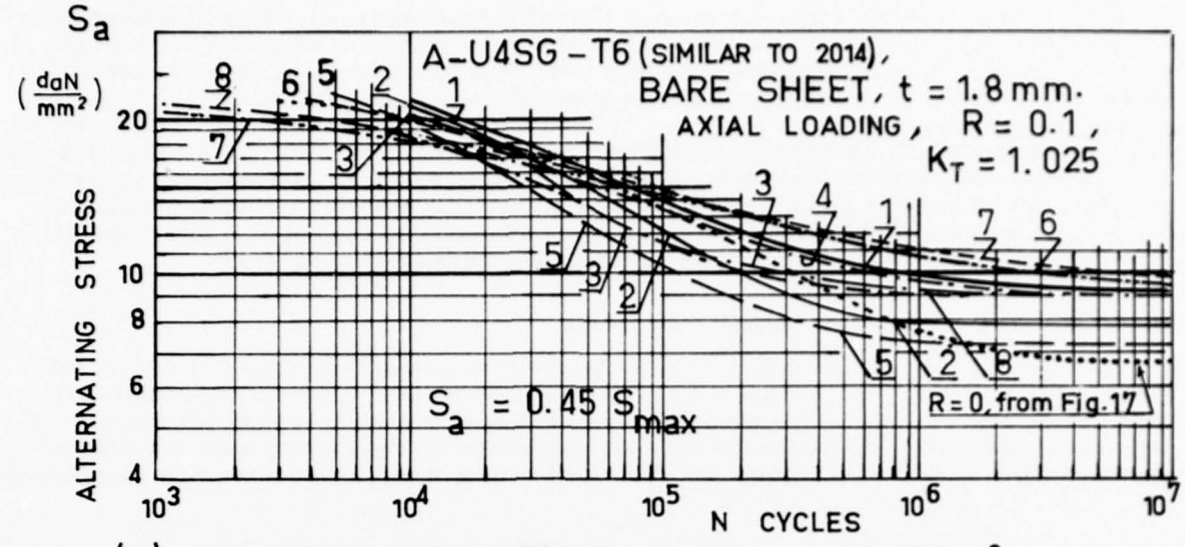

(a) ONE SHEET FROM SUPPLIER A, $S_{ult.}$ = 49 daN/mm².

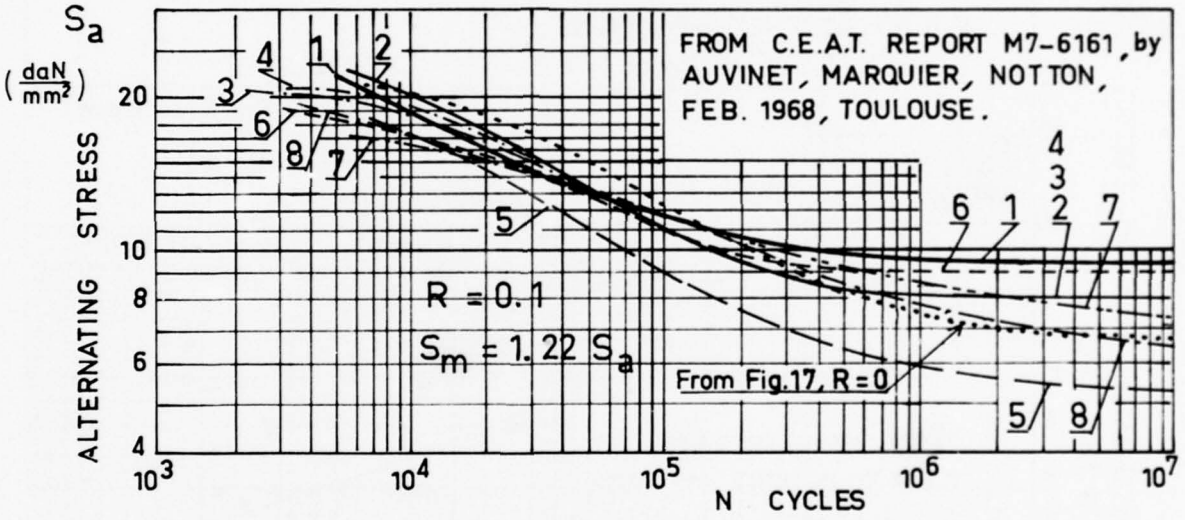

(b) ONE SHEET FROM SUPPLIER B, $S_{ult.}$ = 45 daN/mm².

SURFACE CONDITION OF SPECIMENS

1 – T6 TREATMENT BY THE SUPPLIER - VIRGIN SPECIMEN
2 – ONE FACE CHEMICALLY MACHINED BEFORE A NEW HEAT TREATMENT TO T6 CONDITION
3 – ONE FACE CHEMICALLY MACHINED FROM INITIAL T6 CONDITION
4 – No. 3 CONDITION + VAPOR BLAST ON TWO FACES
5 – No. 3 CONDITION + CHROMIC ANODIZING
6 – No. 4 CONDITION + CHROMIC ANODIZING
7 – VIRGIN SPECIMEN + ONE 4 mm-DIAMETER RIVET } STRESSES ARE FOR NET AREAS
8 – AS No. 7 BUT SULPHURIC ANODIZING OF FACES }

Figure 20

no significant effect was observed in the B-material (compare curves 3 and 4). Chromic anodizing lessens the fatigue strength of both materials but more so in the B-material (compare curves 3 and 5). After a vapour-blast operation, chromic anodizing slightly improves the fatigue strength of the A and B materials (compare curves 4 and 6). This might imply the existence of opposing effects of etching during anodizing and of the further protection against corrosion provided by anodizing. In this context, vapour-blasting before anodizing creates residual compressive stresses over a small depth below the sheet surfaces. These residual compressive stresses are not sufficiently stable to cause a strong improvement in fatigue (compare curves 3 and 4), but their effect in counteracting the possible detrimental effect of etching corrosion during anodizing might be important. This led us to assume the possibility of initial corrosion damage during anodizing in the case of the A-U4SG-T6 aluminium alloy, which is known to be susceptible to intergranular stress corrosion. The protection afforded by compressive residual stresses would be lower for the B-material which is less susceptible to stress corrosion. The sulphuric anodizing of the sheet surfaces before inserting a 4 mm-diameter rivet lessens the fatigue strength slightly. The sulphuric anodized film is thick and brittle, and may be cracked during riveting. Comparison with the A-U4G1 S–N reference line evaluated from Figure 17 for $R = 0.1$ shows improved behaviour of the A-material in the N-range from 10^4 to 10^5, and of the B-material from 10^6 to 10^7.

3.4 Specimens Machined from Thick Aluminium Alloy Plates

Systematic fatigue tests of axially loaded, round-notched specimens machined from 35 mm-thick A-U2GN-T651 aluminium alloy plates have been undertaken by the CEAT fatigue test laboratory[15]. Figure 21 shows experimental points corresponding to $1.7-K_T$ notched specimens machined from plates, in either the longitudinal or transverse direction, and axially loaded. Unfortunately, no test result is available for the fatigue strength in the short transverse direction, owing to the difficulty of machining specimens capable of being stressed in the direction of the plate thickness.

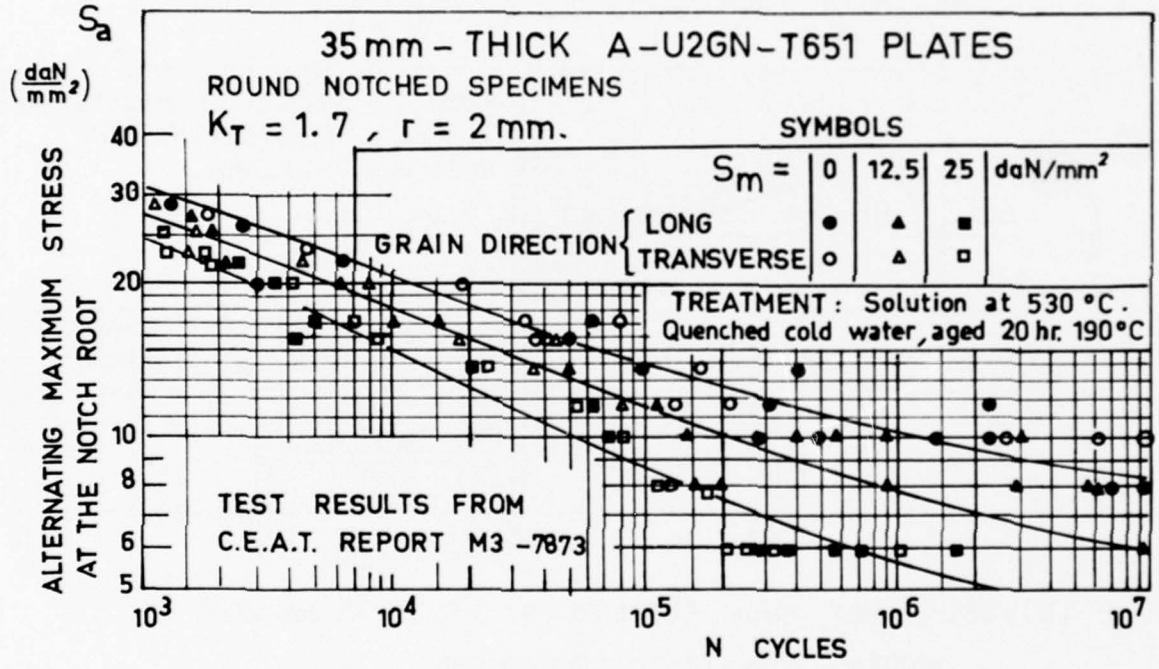

Figure 21

For the case $K_T = 1.7$ (see Figure 21) and for K_T-values equal to 1.035, 1.3, 2.3 and 3.3, fatigue test results in both the longitudinal and transverse directions may be combined and, by interpolating between S_m-values, $(K_T S_a - N) - K_T S_m$ curves were obtained, as illustrated in Figures 22 and 23 for K_T equal to 1.3 and 3.3 respectively.

For these A-U2GN-T651 aluminium alloy plates, Figure 24 shows the master $(K_T S_a - N - S_m - g)$ curves where the relative stress gradient in the direction n normal to the notch root surface is defined as

$$g = \frac{1}{S}(\partial S/\partial n)$$

and equals approximately $-2/r$ in tension and $-2(1/r + 1/d)$ in bending, where r is the notch root radius and d is the diameter of the specimen at the neck of round-waisted specimens. By interpolating for other values of the relative

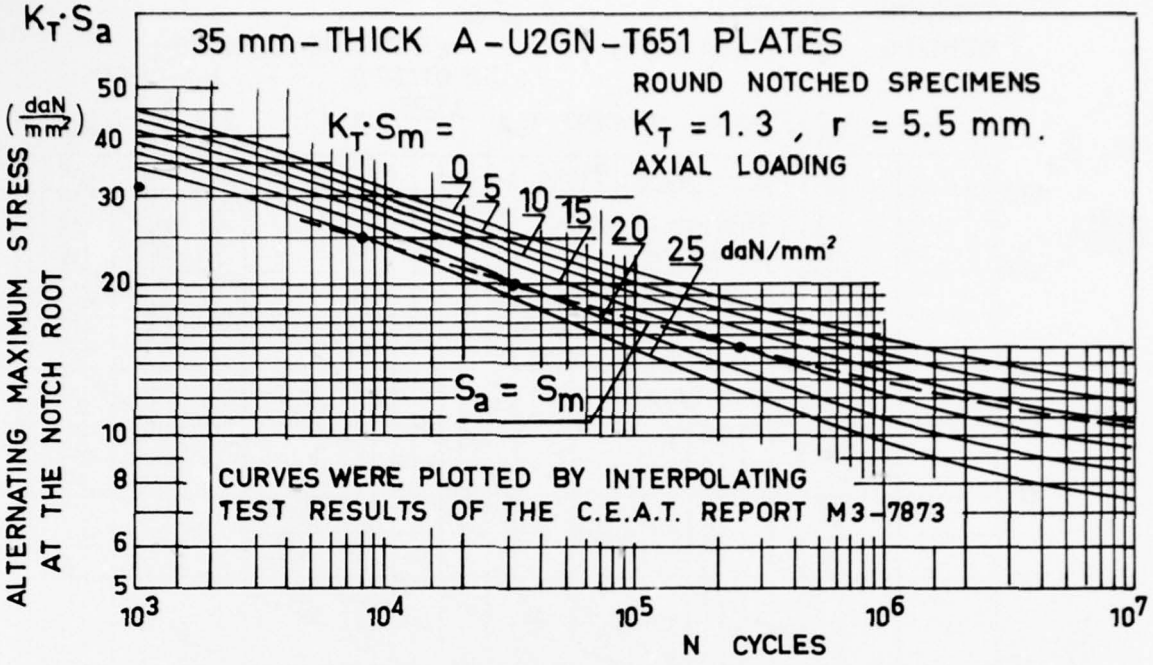

Figure 22

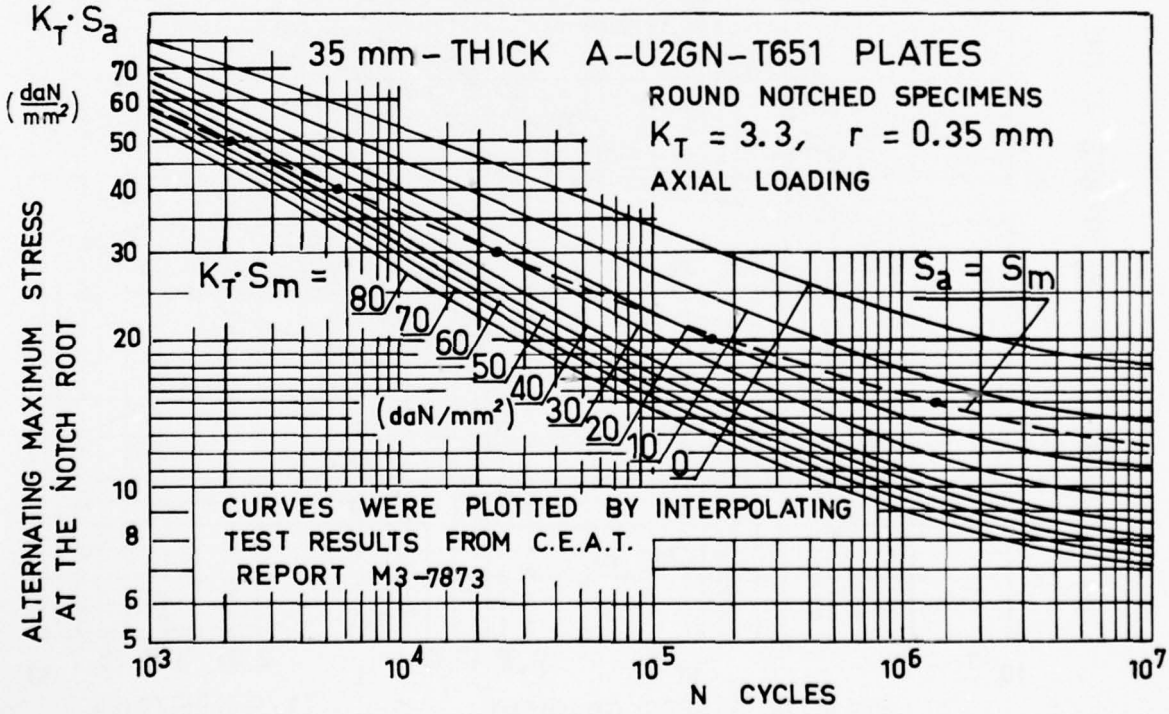

Figure 23

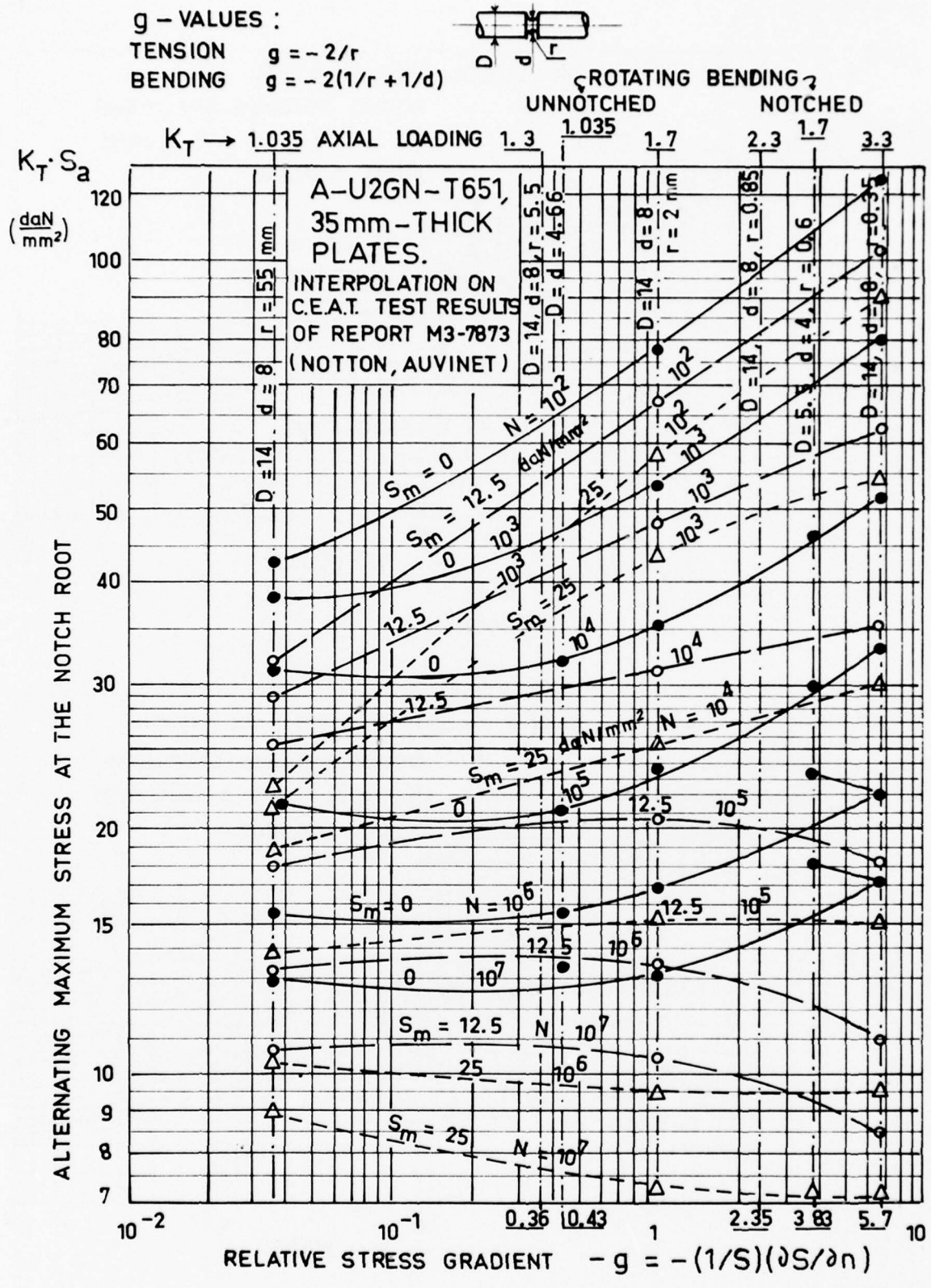
g – VALUES :
TENSION g = – 2/r
BENDING g = – 2(1/r + 1/d)
D
d
r
ROTATING BENDING
UNNOTCHED
NOTCHED
K_T → 1.035 AXIAL LOADING 1.3 1.035 1.7 2.3 1.7 3.3
$K_T \cdot S_a$
$(\frac{daN}{mm^2})$
A–U2GN–T651, 35mm–THICK PLATES.
INTERPOLATION ON C.E.A.T. TEST RESULTS OF REPORT M3-7873 (NOTTON, AUVINET)
D ±14 d = 8 r = 55 mm
D = 14, d = 8, r = 5.5
D = d = 4.66
D = 14 d = 8 r = 2 mm
D = 14 d = 8, r = 0.85
D = 5.5, d = 4, r = 0.6
D = 14, d = 8, r = 0.35
S_m = 0
S_m = 12.5 daN/mm²
S_m = 25
N = 10^2
10^3
10^4
10^5
10^6
10^7
ALTERNATING MAXIMUM STRESS AT THE NOTCH ROOT
120 100 80 70 60 50 40 30 20 15 10 9 8 7
10^{-2} 10^{-1} 0.36 0.43 1 2.35 3.83 5.7 10
RELATIVE STRESS GRADIENT – g = – (1/S)(∂S/∂n)

Figure 24

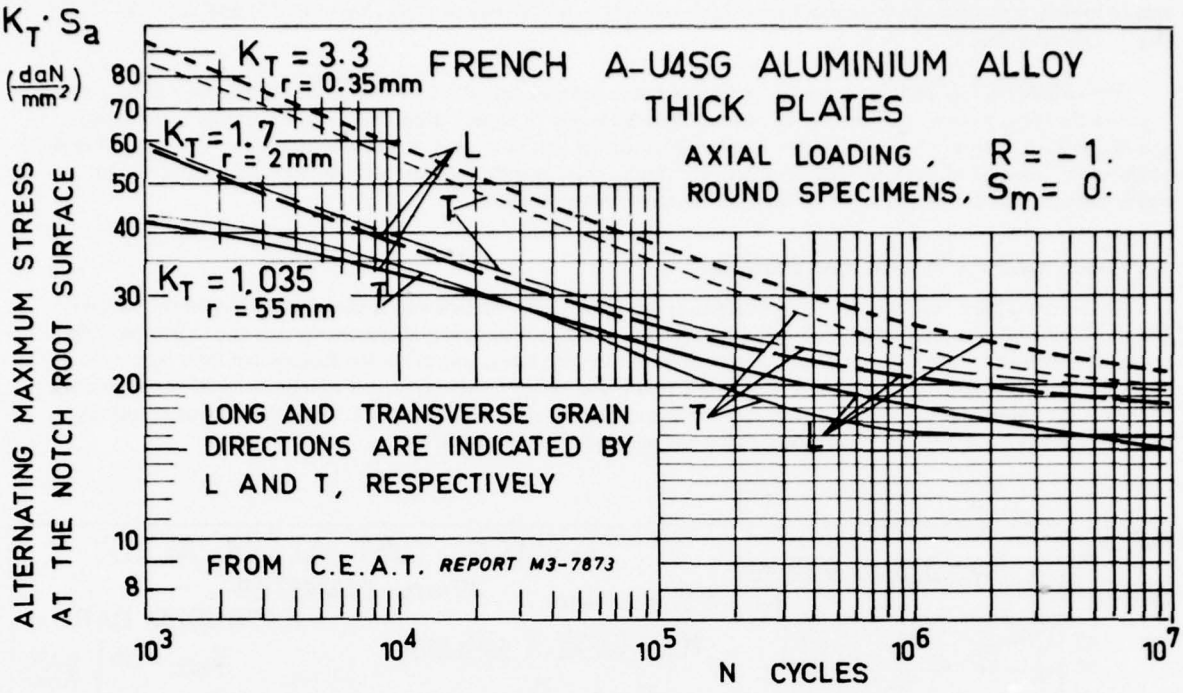

Figure 25

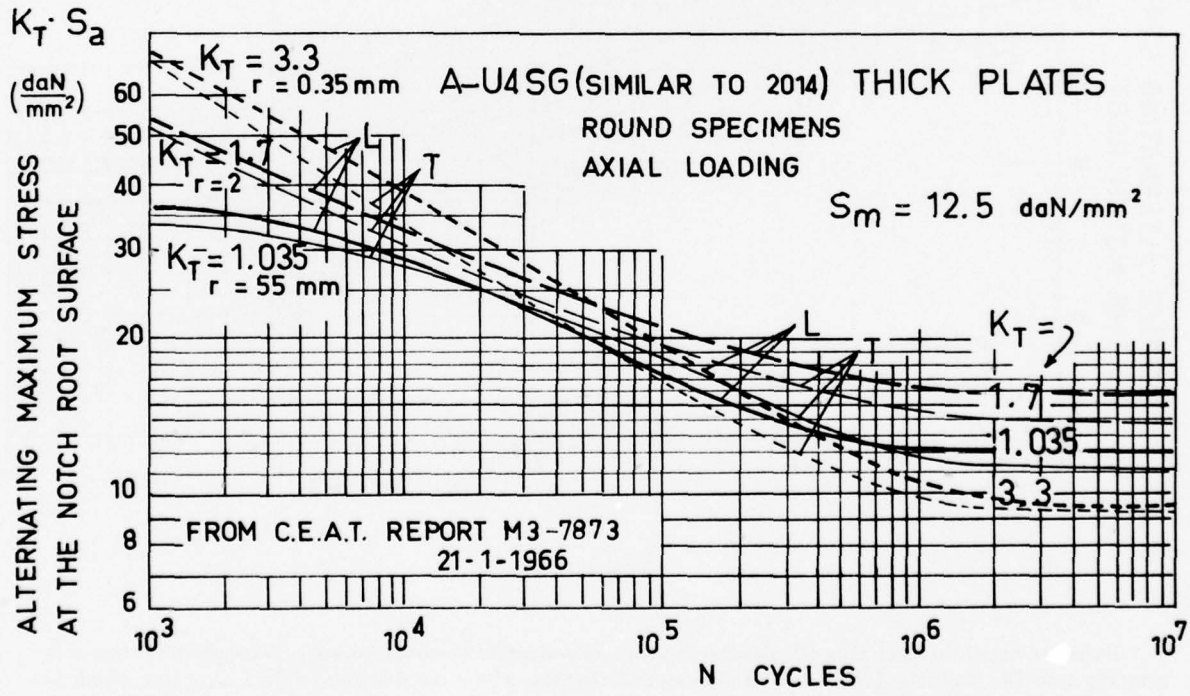

Figure 26

stress gradient, or of the notch radius, for round-waisted specimens, $(K_T S_a - N) - K_T S_m$ curves may be plotted. However, it must be emphasized that such curves are only valid for areas of the structural assembly where the tensile stress in the short transverse direction is low enough not to be dangerous. Points have been obtained from tests of axially loaded, round-notched specimens and from rotating bending tests of plain ($K_T = 1.035$) and notched ($K_T = 1.7$) specimens.

For axially loaded, plain or notched specimens taken from 32 mm-thick A-U4SG-T651 aluminium alloy plates, in either the longitudinal or transverse direction, Figures 25 and 26 show fatigue test results corresponding to $S_m = 0$ and $S_m = 12.5$ daN/mm², respectively. The direction of the specimen axis, in the longitudinal or transverse direction of the plate, has a significant, though small, effect. Again, these results illustrate well the beneficial effect of the plastic accommodation of the stress-strain cycle on stress concentration.

3.5 Axially-Loaded Specimens from Extrusions

In extruded bars, the short transverse direction is normal to the surface and is therefore radial for round bars. The machining of circumferential grooved notches in the axially stressed, round specimens cuts the extrusion grain layers, resulting in relatively lower fatigue strength levels for high stress concentration factors and high S_m-levels, as may be seen in Figure 27, which shows fatigue test results for axially-loaded specimens taken from 35 mm-diameter A-U4SG-T651 aluminium alloy bars. The treatment was carried out on bars by the laboratory and was as follows: solution for 1 hr at 502°C, cold water quenching and ageing for 16 hr at 160°C.

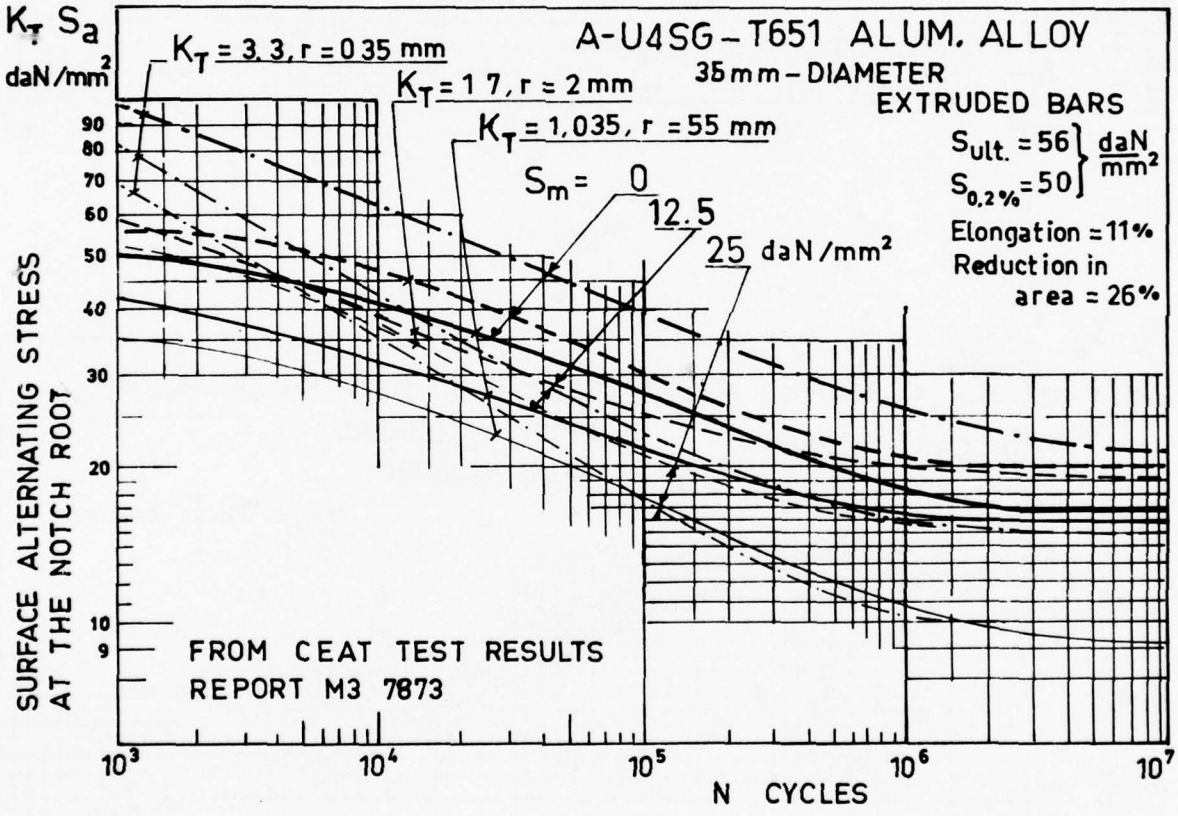

Figure 27

It may be noted that high strength aluminium alloys treated in the T6-condition are generally brittler than in the naturally aged T4-condition. Figure 28 illustrates a similar behaviour[16] of the A-U4G1-T6 aluminium alloy (similar to the 2024-T6) as compared to that of A-U4G1-T4: as far as fatigue tests in the laboratory are concerned, the ageing treatment improves the fatigue life under high stress levels, but shortens it under low stress levels.

This tendency would probably be aggravated for parts of the aircraft structure in the service environment owing to water condensation and the stress-corrosion sensibility of certain aluminium alloys such as A-Z5GU-T6 (7075-T6) and A-U4SG-T6 (similar to 2014-T6), even when treated in the T651-condition with stretching of 1 to 2% interspersed between quenching and ageing.

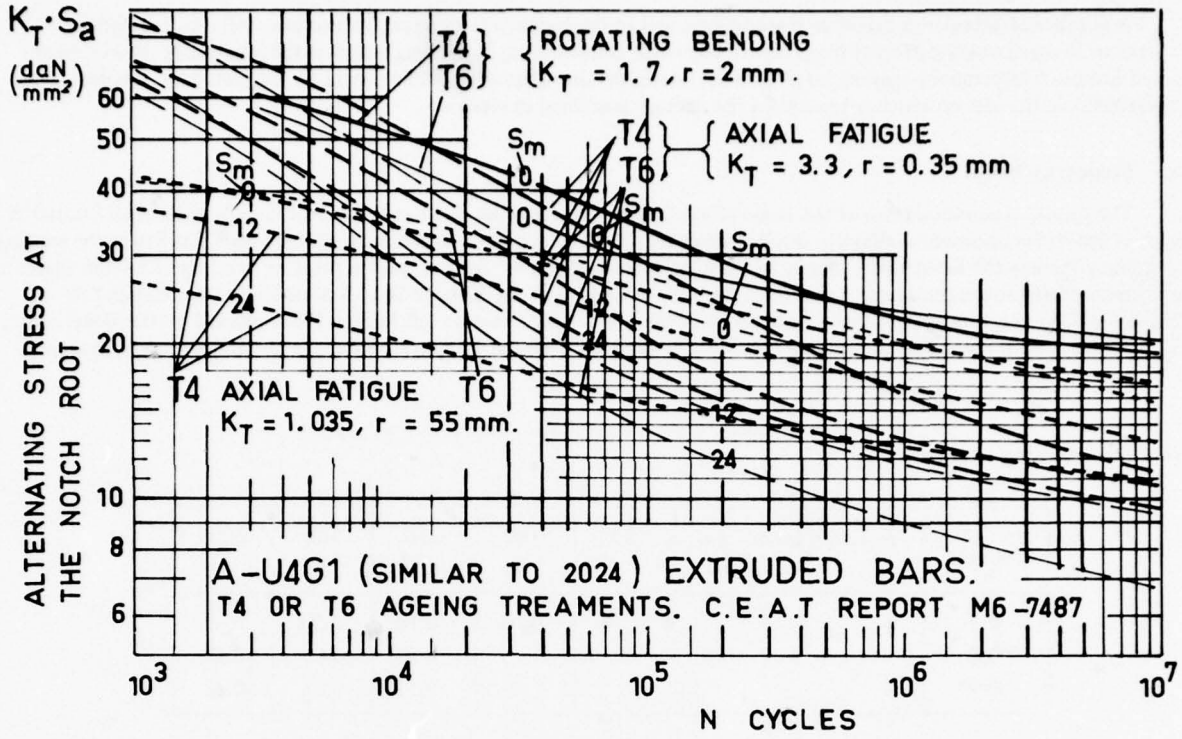

Figure 28

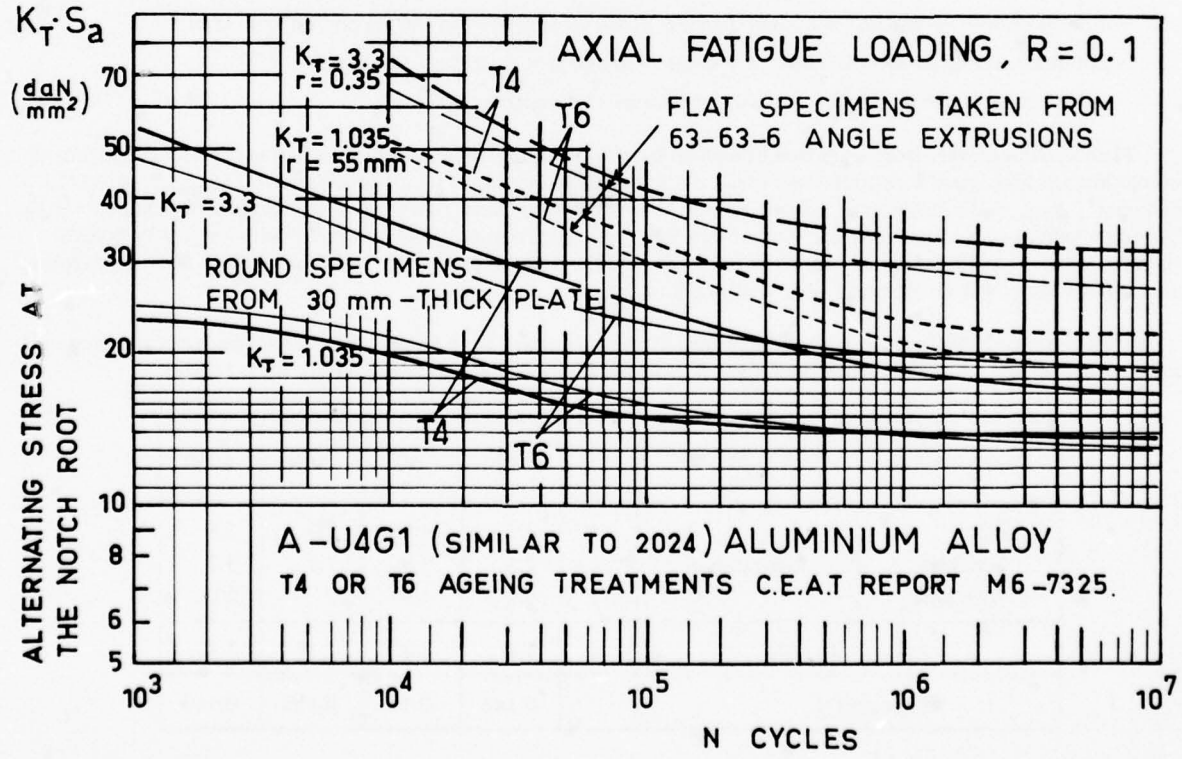

Figure 29

4. REPRESENTATIVENESS OF INDOOR FATIGUE TESTS

A number of actual conditions in manufacture and in the service use of aircraft structures will result in fatigue behaviour in service very different from that of the small conventional specimens tested in the laboratory environment. Some causes of discrepancy may be inferred from laboratory investigations, while others are suggested by detailed investigations, the aim of which is to explain the damage sustained in service.

4.1 Frequency Effect

The plastic accommodation of the stress-strain fatigue cycle may be facilitated by local metallurgical transformations such as ageing for aluminium alloys or austenite-martensite transformation in steels. In fatigue tests, the lower the loading frequency the less the fatigue life, as may be concluded from Marin's[18] fatigue tests in rotating bending of 14 mm-diameter specimens containing a transverse 2 mm-diameter hole and made of the Russian D-16-T aluminium alloy (similar to 2024-T4). The rotation speed ranged from 15 to 2000 rpm and its effect on the fatigue life depended on the stress ratio $S_a/S_{ult} = k$. With respect to the fatigue life, N_{15}, associated with the 15 rpm rotation speed, fatigue durations were

$$N = N_{15}(f/f_{15})^n$$

with the following n-values:

S_a/S_{ult}	*Rotation speed, rpm* / *Speed ratio*	15 / 1	100 / 6.7	250 / 16.7	500 / 33	2000 / 133
0.5	n =		0.10	0.18	0.30	0.35
0.6				0.13	0.18	0.18
0.7				0.11	0.13	0.12

Leleu and Notton[19] have investigated the frequency effect in the same way, using small specimens machined from one 22 mm-thick A-U2GN-T351 aluminium alloy plate. This alloy is metallurgically stable and its ageing condition is not significantly modified by fatigue or by a moderate increase in temperature. Test frequencies were 50, 500 and 6000 rpm. The specimen dimensions were:

- conical smooth specimens: 4.66 mm-diameter at the cross section of the maximum stress level,
- notched specimens: D = 5.5 mm , d = 4 mm , circular groove radius = 0.6 mm,
- cylindrical specimens, d = 5.5 mm , with transverse 2 mm-diameter hole.

Plain specimens were lathe-machined using high-speed steel tools, whereas in the machining of notched specimens overcarburized high-speed steel tools were used. Static tensile properties of the plate alloy were: $S_{proportional} = 30.3$ daN/mm² , $S_{0.2\%} = 32.7$ daN/mm² , $S_{ult} = 43.8$ daN/mm² , elongation at rupture = 21% and reduction in area = 30%. Surface roughness was about 30 RMS. From 50 to 6000 rpm, the fatigue lives of specimens with notches or holes at the stress level $S_a = 13$ daN/mm² were little affected. On the contrary, under the higher stress level $S_a = 18$ daN/mm² , a significant effect was obtained, as illustrated in Figure 30.

If the test series of the three types of specimen at the stress level $S_a = 18$ daN/mm² are considered, the life ratios may be computed, using as reference the fatigue lives at the rotation speed of 1 rpm. They are as follows:

Specimen type	*Rotational speed (rpm)*	1	10	50	500	6000
Plain	Life ratios	1	1	1.65	2.4	3.8
Notched		1	2.1	1.9	2.1	3.3
With hole		1	1.2	1.9	2	3.5
Average life ratios		1	1.4	1.8	2.17	3.53
Exponent n			0.146	0.15	0.124	0.144

It may be recalled from Maurin and Barrois[20] that the results of fatigue tests on plane specimens with a central hole and small riveted joints made from A-Z1 clad A-U2GN-T6 aluminium alloy sheet yielded n-values from 0.07 to 0.12.

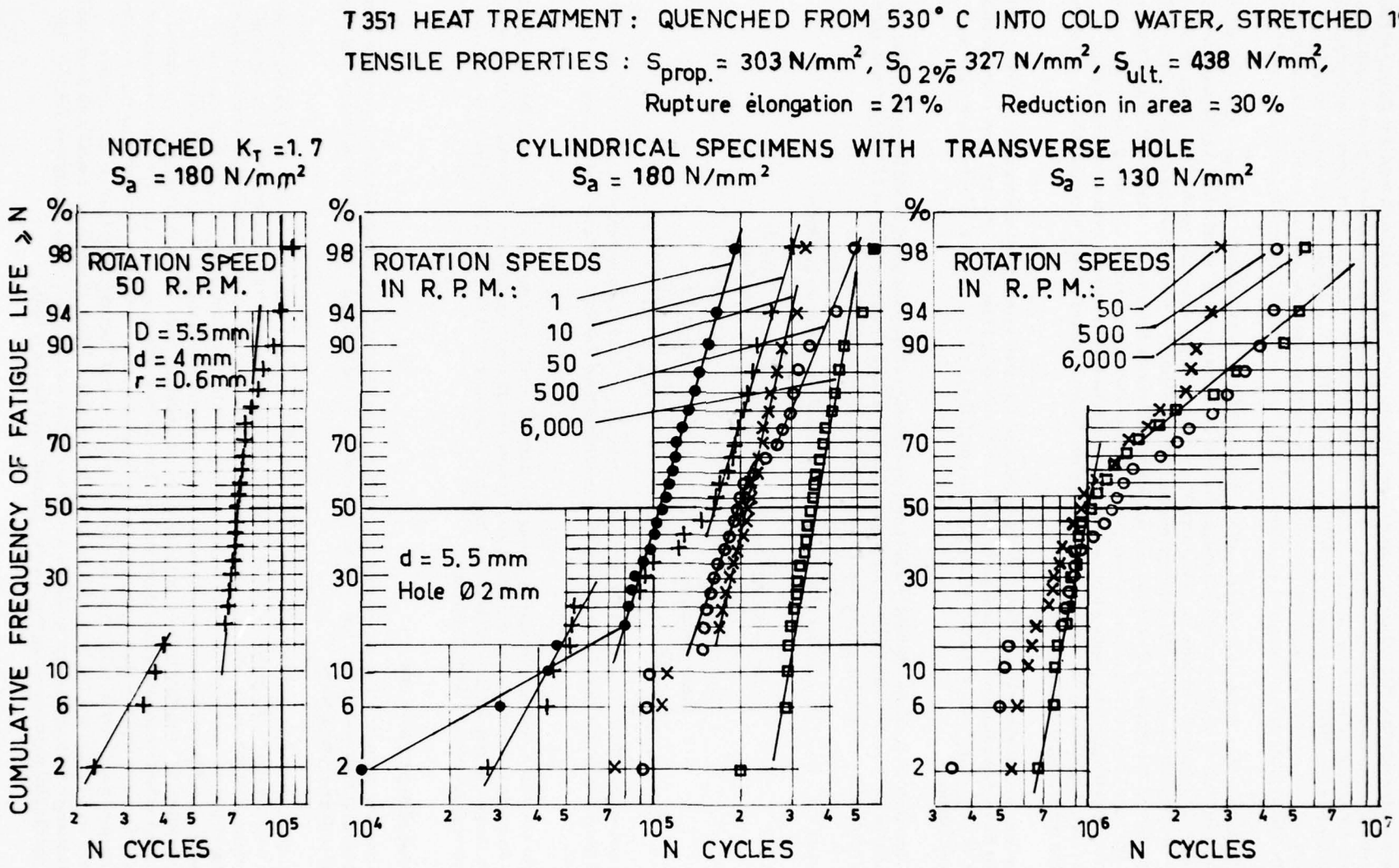

Fig.30 Bimodal statistical distributions of fatigue life of A-U2GN-T351 aluminium alloy specimens for several rotational speeds from 1 to 6000 rpm

The existence of multimodal distributions of the fatigue lives reveals the effects of several phenomena at various levels. At the level of slip barriers which have various degrees of stability with respect to the loading – barriers such as inclusions, coherent precipitates, dislocation knots, etc. – residual stresses due to heat-treatment and to the cold-working during manufacture diminish with successive fatigue cycles. The less stable slip barriers, with respect to fatigue stressing, are overcome, and stresses which balance the external loading are applied to a reduced number of points of resistance, from which microcracks and vacancies originate and may combine into crack initiation. At the grain level the residual stresses produced by cold-working during manufacture are reduced. The accommodation of the fatigue stress-strain cycle which has been observed at the geometrical notch level is likely to exist at the grain level, and both accommodations which soften the initially hardened material will lower the local tensile stresses and improve the fatigue strength[21].

Let us consider the cumulative frequency curves in Figure 30 for $S_a = 13$ daN/mm^2 ($S_a/S_{ult} = 0.3$). The curvature towards high numbers of cycles is well known and is related to the "understressing" effect which may be explained by the mechanism of fatigue accommodation of the stress-strain cycle at the grain level and on the stress concentration areas. For $S_a = 18$ daN/mm^2 ($S_a/S_{ult} = 0.41$), the accommodation improvement is not complete for certain specimens before the combination of microcracks and vacancies into dangerous small cracks, the growth of which results in final fatigue fracture. Owing to the local temperature increase in the neighbourhood of surmounted slip barriers, the accommodation phenomena within the grain may become more accentuated at high loading frequencies, even if the mean surface temperature is not significantly increased. That would explain the displacement towards high numbers of cycles of the curves when the loading frequency is increased.

The existence of multimodal distribution of the fatigue lives for various stress levels was revealed in 1958 by both Finney and Mann[22] and Shabalin[23]. A number of papers were reviewed by Finney[24] in 1967 and more recent investigations were made by Luther and Williams[25] in 1973 for mild steel, then by Korbacher[26] in 1974 for oxygen-free high-conductivity copper.

For aluminium alloys alone, Shabalin[23] and Mori[27] are reported to have investigated on the frequency effect. Most of the investigations reported correspond to rotating bending tests at high frequencies (300 to 12,000 rpm) with plain specimens; the stress concentration is related only to the bending stress distribution.

In practice, the loading frequencies to be considered for aircraft structures are as follows:

ground-air-ground loads:	0.1 to 10 cycles per hour, or 0.000027 to 0.0027 c/s
manoeuvre and gust loads:	0.1 to 10 c/s
engine vibrations:	20 to 200 c/s
jet noise:	100 to 1000 c/s

It is evident that, if any frequency effect exists, the dominant part of the fatigue damage, related to the so-called ground-air-ground or peak-to-peak load variation, will be underestimated if laboratory fatigue tests are used in the evaluation.

On the other hand, corrosion damage by pitting will drastically shorten the period of fatigue-crack initiation, and water condensation in assembly gaps and recesses may increase the crack propagation rate. Therefore the absolute time elapsed on the ground may well be a parameter as significant as the number of loading cycles in relation to the actual fatigue-corrosion behaviour of aircraft structures.

4.2 Corrosion-Fatigue Interaction

In a corrosive environment, that most generally present in aircraft structures being condensed water resulting from the ground-high altitude-ground variation of the air temperature, corrosion damage may act alone or may interact with the fatigue damage in several ways.

Corrosion damage may exist before the application of fatigue loading. For materials such as 2024-T4 extrusions which are very sensitive to *exfoliating corrosion*, corrosion damage may create irregular scores at rivet hole edges and become origins of fatigue cracks. *Pitting corrosion* creates numerous local pits, causing a drastic lowering of the fatigue strength for high numbers of cycles which correspond to long periods of exposure to corrosion, by creating a multi-notched surface condition and by relieving the beneficial compressive residual stresses, due to cold-working during manufacture within a thin surface layer of the material. In the laboratory, most *corrosion-fatigue tests* were carried out with simultaneous surface corrosion and fatigue loading. The lowering of fatigue strength in a corrosive environment is illustrated in Figure 31 for three aluminium alloys and one magnesium alloy[28]. While S–N curves from the specimens tested in air show a tendency to fatigue limit thresholds, the S–N curves from specimens tested in the sea-water environment seem to have absolute limits of the duration before failure. Figure 32 shows also a significant decrease of the fatigue strength for maraging steel specimens wetted by distilled water[29] at pH-values ranging from 6.8 to 7. In this case, the distilled water appears as a sufficiently harmful agent for use in tests.

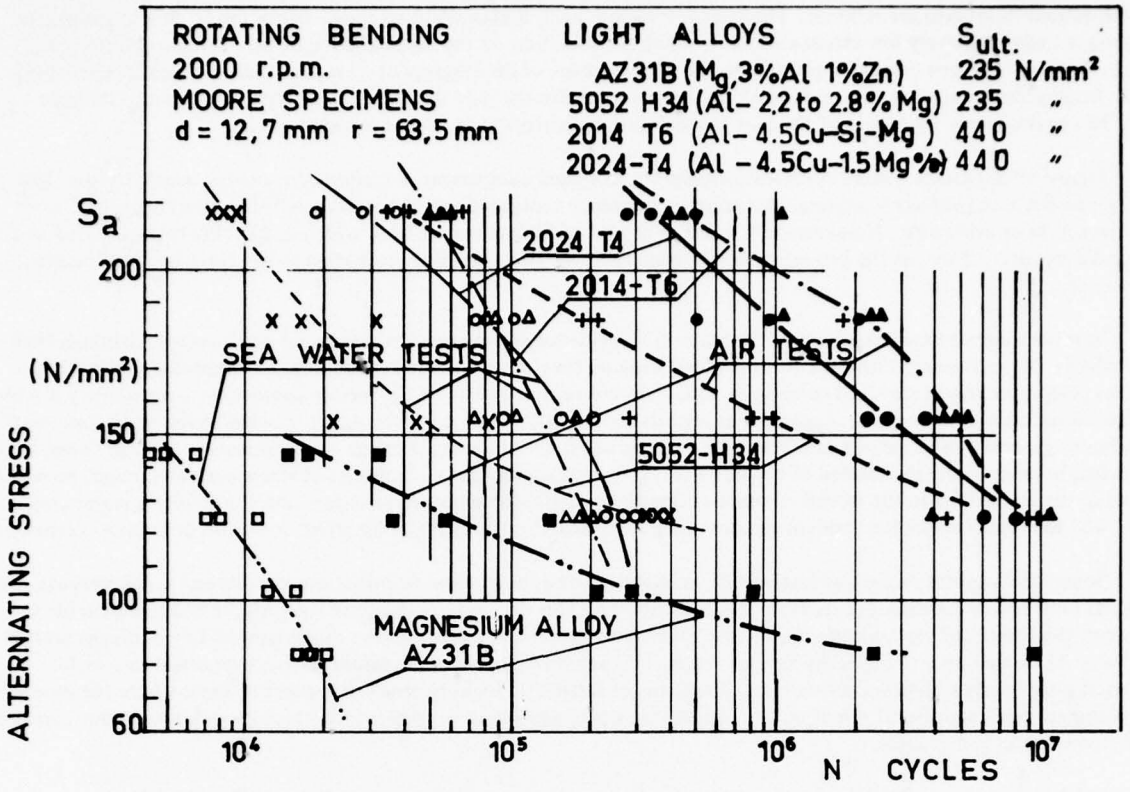

Figure 31

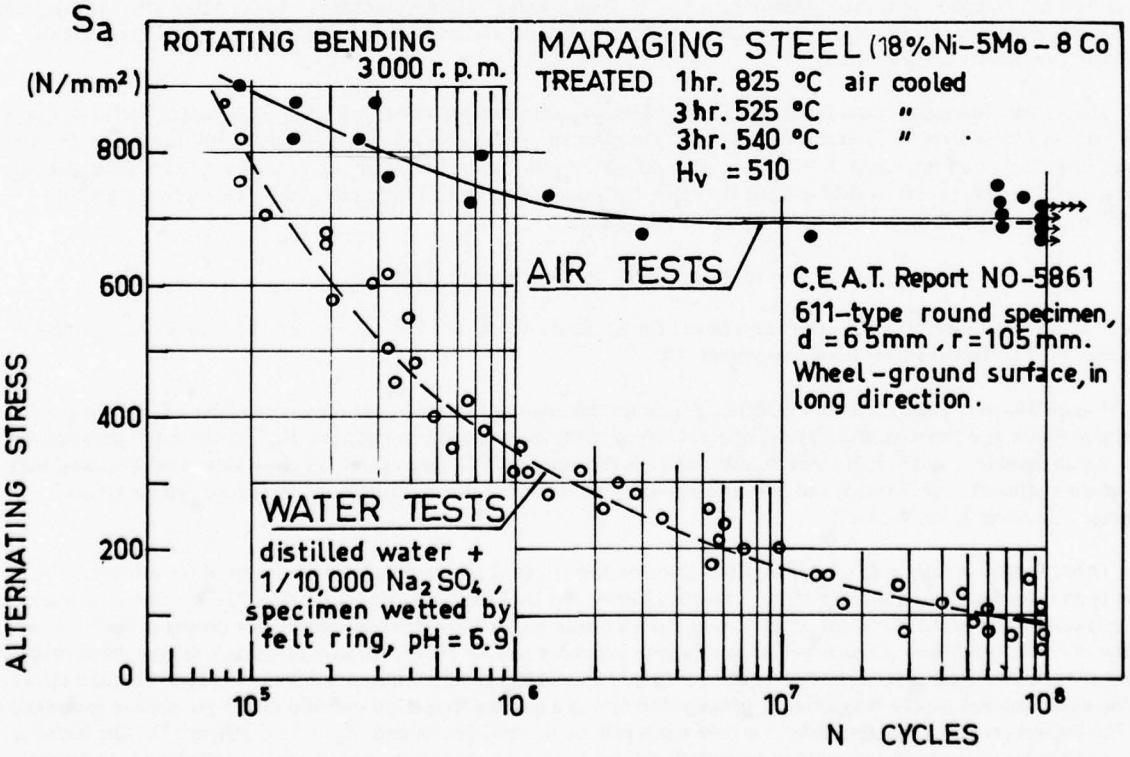

Figure 32

In forgings, *stress corrosion* may create a surface crack, the propagation of which stops when the residual stresses which caused its growth are relieved. The stress-corrosion crack is equivalent to a very sharp notch, able to propagate in fatigue under relatively low stresses which would have no action on the unnotched material. Stress corrosion may originate from only one corrosion pit near to the parting plane of die forgings or to some other emergent plane arising from forging flow, and may then extend along this plane within the part thickness. This type of dangerous damage may be apparent only by failure of the part through fatigue corrosion or stress corrosion alone.

Figure 33 illustrates a more complex problem[30]. In a steel component, a surface area existed where friction had destroyed the zinc protective coating; this region was poorly ventilated and there was a felt ring retaining water, from condensation or otherwise. Numerous pits acted as origins of fatigue cracks from which cracks slowly propagated under fatigue-corrosion. Then, as the propagation rate increased, the part played by corrosion in the crack growth became negligible.

In-service damage sometimes arises from a rare coincidence of adverse circumstances. Such events, although their probability of occurrence is low, are to be avoided because they govern the in-service safety. Laboratory tests provide results corresponding to standard conditions which are not representative of the service conditions, because they are too simple in nature and often too exaggerated as regards the activity of the corrosive agent. Owing to the small number of specimens generally used, results of laboratory tests are often near to average values, whereas service damage, when first revealed, belongs to the low lifetail of the unknown statistical distribution. Problems of stress corrosion might be investigated in the laboratory to the extent of representing the periodic temperature variation, and the resulting water condensation, and the reduction of the residual stresses when the crack front propagates by stress corrosion or fatigue corrosion.

Sometimes reports on fatigue tests divide fatigue lives into incubation, or initiation, periods and crack propagation periods until finally fracture occurs from static instability. This division is somewhat arbitrary, it being impossible to measure the lengths of very minute cracks. At the beginning the crack propagation rate is subject to significant scatter and may be slowed up or delayed by surface residual compressive stresses. Therefore fatigue properties cannot be inferred only from crack propagation tests. Problems of fatigue under corrosion correspond to cases where the corrosive environment has a significant effect on the fatigue crack propagation rate, whereas the crack growth rate under corrosion and steady stress is negligible.

In laboratory tests, the time unit for corrosion damage depends on the nature of the corrosive action. For continued wetting by an active solution, the unit will be that of the real time when the corrosion damage is predominant at very low fatigue stresses; this will be the fatigue cycle at high stress and short fatigue lives for which the corrosive agent has had no time to cause significant damage. In the service use of aircraft structures, the time unit for fatigue without corrosion is the flight, owing to the major influence of the ground-air-ground, peak-to-peak stress variations, while the time unit for corrosion alone would be intermediate between the flight, which causes water vapour to condense into assemply gaps and cracks, and the day, for periods of which corrosion activity persists and may be reinforced by daily temperature variation for aircraft parked outside.

Despite the foregoing reservations, fatigue crack propagation tests in laboratory conditions supply useful comparative information. Most tests on sheet materials use w-wide sheet specimens containing a 2a-long central through crack under a loading giving a uniform stress $S = S_m \pm S_a$ far enough from the crack to remain uniform during crack propagation. Assuming elasticity, the stress field around the crack tip is defined within an infinitely small domain by a standard distribution multiplied by a stress intensity factor K such as

$$K = S\sqrt{(\pi a)}c_w \quad \text{with} \quad c_w = 1/\sqrt{[1-(2a/w)^2]}$$

where c_w, from Dixon[31], is the correction factor for the finite width w. Like S, K may be divided into a steady component K_m and an alternating component K_a.

Figure 34, from Donaldson and Anderson[32], shows the major influence of the alternating term K_a of the stress intensity factor and the small, though significant, effect of the mean steady component K_m on the crack propagation rate da/dn, where a is the half-crack length and n is the number of fatigue cycles. These results were obtained with specimen widths of over 300 mm and have been used by the author in the interpretation of indoor fatigue tests of fuselage skin made from 2024-T3.

Other results of fatigue crack propagation tests, on the effect of the loading frequency and of the environment, have been investigated by Hartman et al.[33], and by Schijve and De Rijk[34] for 2024-T3 and 7075-T6 aluminium alloys, using smaller specimens. For 1 mm-thick Alclad 2024-T3 aluminium alloy sheet specimens, for testing in both *dry air* (water content lower than 20 parts per million) and in *saturated wet air* (100% relative humidity), fatigue crack propagation has been investigated for loading frequencies from 24 to 3400 cycles per minute. Figure 35 shows that the effect of the water content on the fatigue crack propagation rate at a loading frequency of 3400 cycles per minute is negligible for the highest crack propagation rate (3×10^{-3} mm/cycle or 0.2 mm per second, $K_a = 13.5$ MN/m$^{1.5}$). The harmful effect of the water is very small, even in saturated air: the time between two successive crack extensions is too short, or the crack growth velocity is too high. On the contrary, with the 24 cycles/min loading frequency, the damage due to water vapour occurs at the very low water content of 20 ppm and is not significantly increased in saturated air. At crack propagation velocities lower than 4×10^{-5} mm/s, the duration of one crack extension is sufficient to produce damage at the lowest values of water content.

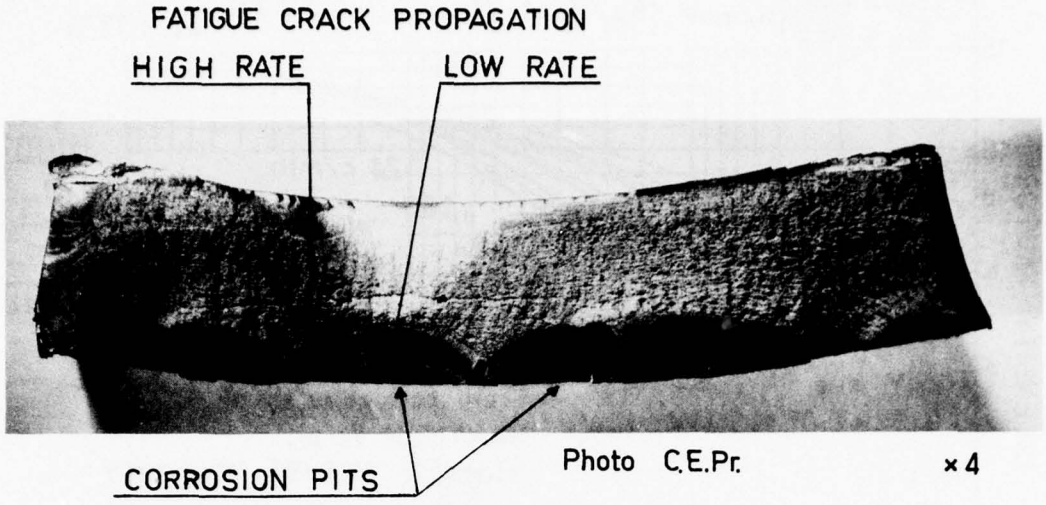

Fig.33 Cracks initiated in fatigue corrosion from corrosion pits

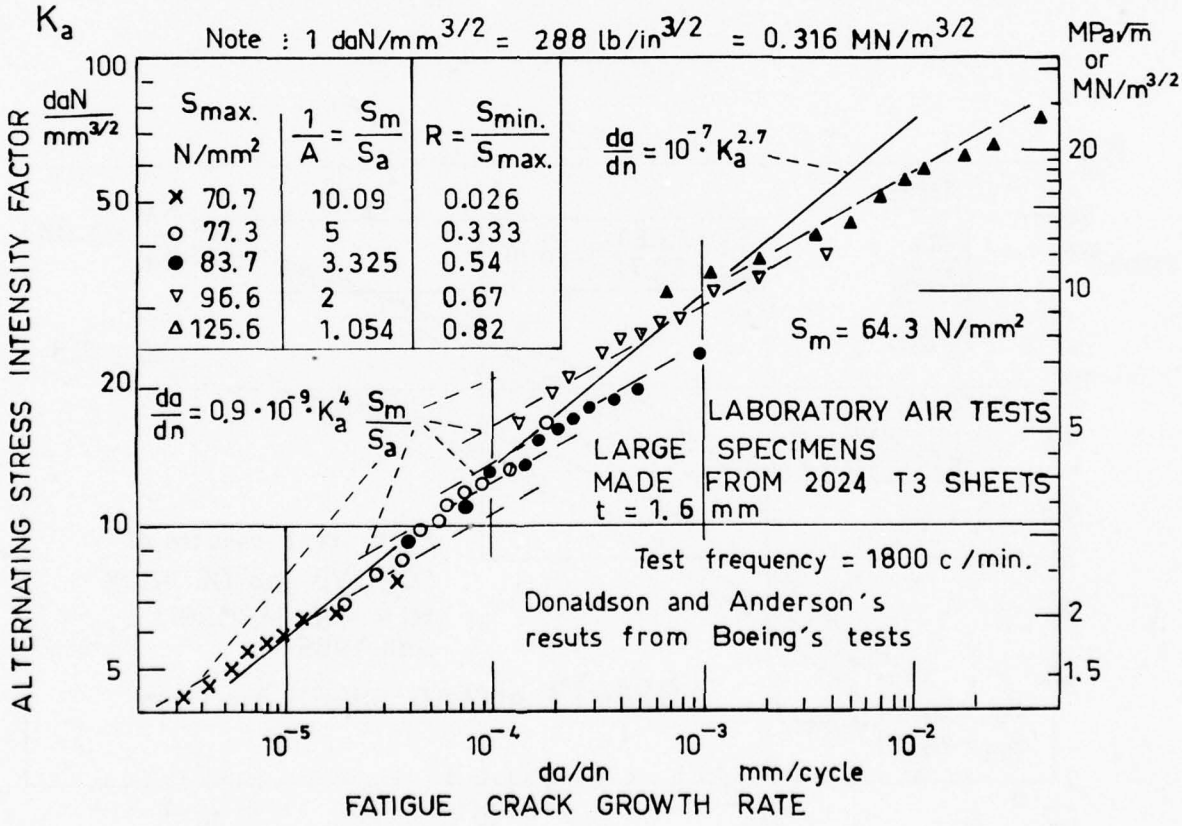

Figure 34

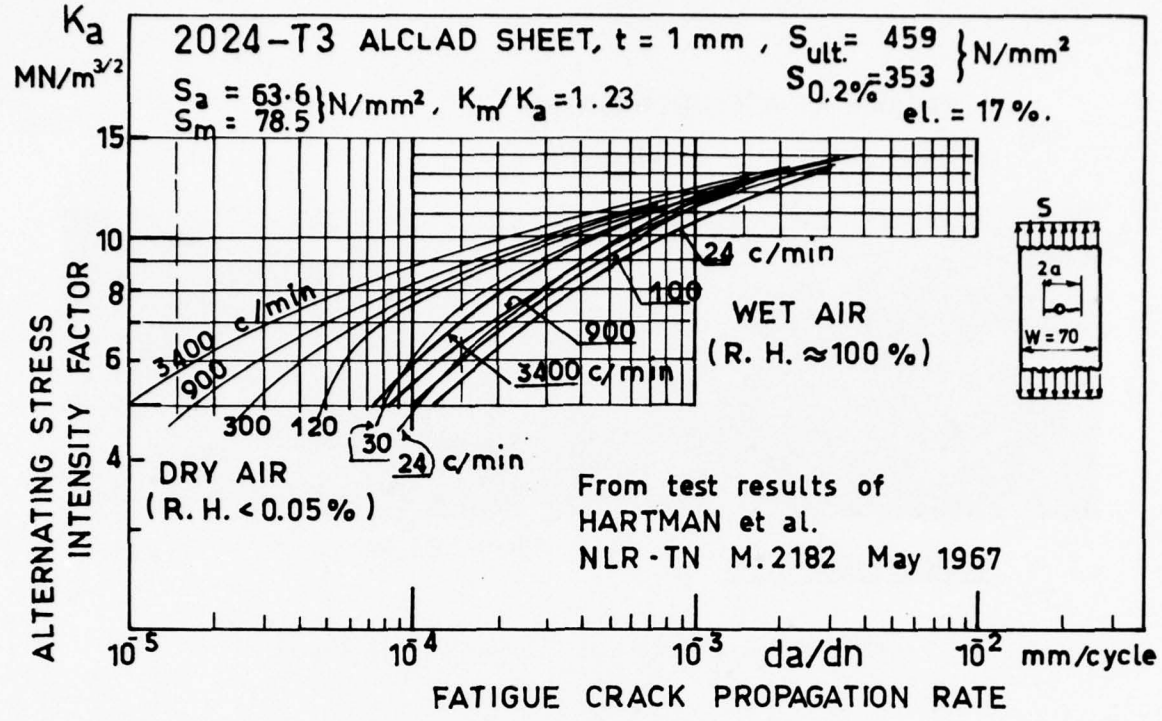

Figure 35

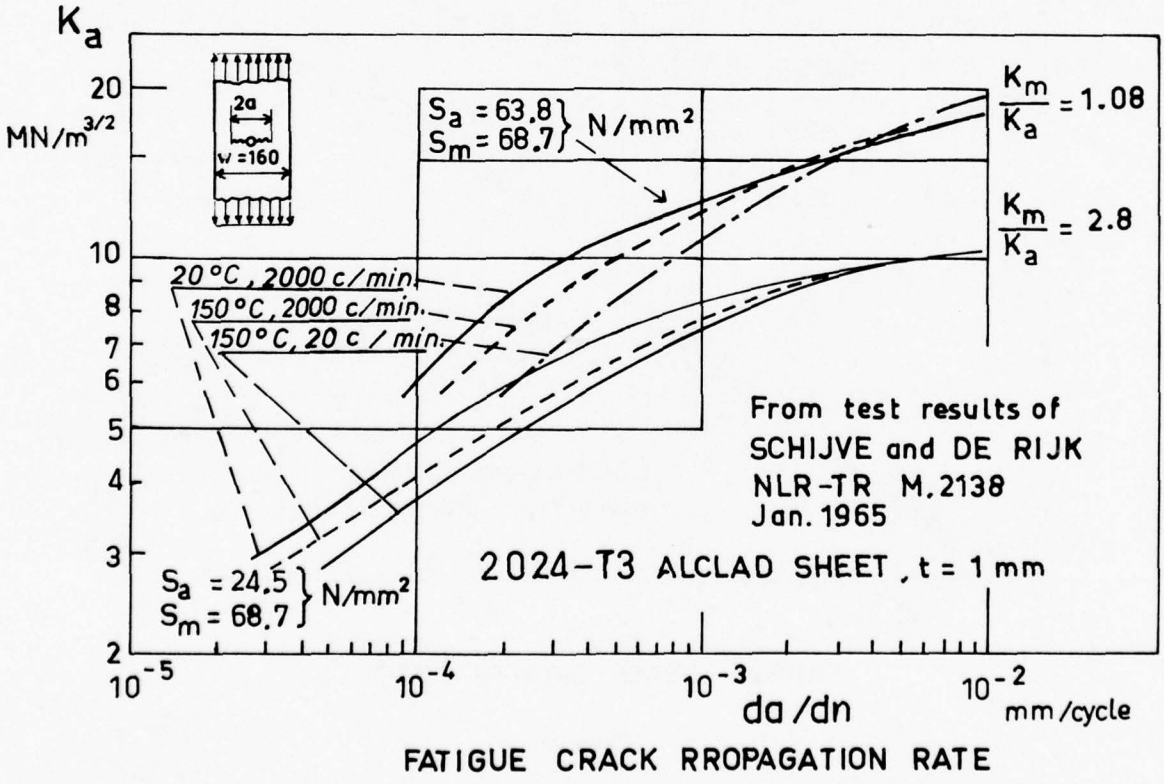

Figure 36

Figure 36 shows that temperature effects and low-loading frequency effects may be compared: the water action is enhanced by the temperature level. It may be noted that these effects are reduced for higher values of the K_m/K_a ratio, i.e., when a relatively higher level of the steady stress, S_m, favours the accommodation of the stress-strain cycle.

Figure 37, from Hartman et al.[33], shows the effect of water content on the fatigue crack propagation rate at room temperature and 3400 cycles/min loading frequency in 70 mm-wide, 1 mm-thick centre-cracked specimens made from clad 7075-T6 aluminium alloy sheet. The crack propagation velocity, da/dt, at which the effect of the water content in air is negligible is of the same order of magnitude as for the 2024 aluminium alloy: 0.11 mm/s instead of 0.2 mm/s.

Similar behaviour occurs *in high-strength, low-alloy steels*. For example, Figure 38 shows results of an investigation on the fatigue-corrosion strength of D6AC steel by Kemsley et al.[35]. Under repeated loadings in tension ($R < 0.1$), compact ASTM-T2 specimens had the same value of fatigue crack propagation rate in dry air and distilled water for $\Delta K = 70\ MN/m^{1.5}$ and 1 Hz frequency loading. The corresponding crack propagation velocity for which the distilled water caused no significant damage was $da/dt = 0.0015$ mm/s. Note that this steel is less susceptible to fatigue-corrosion damage than the very high-strength low-alloy steel 4340M investigated by Speidel[36], the results of which are shown in Figure 39. In this case, the damaging effect of the non-aerated, distilled water is negligible with respect to the behaviour in a vacuum for $da/dn = 10^{-1}$ mm/cycle, $\Delta K = 70\ MN/m^{1.5}$, $f = 0.1$ Hz and therefore for values of crack growth velocity $da/dt \geqslant 0.01$ mm/s.

In the early use of *titanium alloys*, their excellent resistance to corrosion led to the assumption that no stress-corrosion trouble would occur in environments known to be harmful to steels and aluminium alloys. Using smooth or moderately notched specimens, this hope was partially verified for some environments, except that stress-corrosion cases occurred in various other environments, such as chloro-solvents like trichloroethylene in trace quantities, freon, methanol, nitrogen tetraoxide, etc. Moreover, parts that were pre-cracked by other causes, such as forging flaws, sharp notches or fatigue cracks, have shown stress-corrosion susceptibility in sea water, distilled water and hydrogen gas at sustained stress levels which would not otherwise cause failure[37,38]. Also, fatigue crack growth is encouraged by corrosion. Some test results from a thorough evaluation of the mechanical properties of IMI 685 titanium alloy by Ryder et al.[39] are shown in Figure 40. As in the preceding cases of aluminium alloys and low-alloy high-strength steels, the damaging effect of the water environment with respect to test results obtained in laboratory air (about 50% relative humidity) is significant at low ΔK-levels and low fatigue crack propagation rates. For crack growth velocities higher than 0.001 mm/s, which corresponds to $da/dn = 0.01$ mm/cycle, the behaviour in fatigue becomes independent of water content.

The foregoing examples of corrosion-fatigue crack propagation tests in laboratory conditions indicate behaviour in the presence of water vapour common to several metals, which should be explained by a predominant common mechanism. This suggests the following comments.

(i) On the macroscopic scale, it is not unusual to find actual cases of fatigue corrosion such as that shown in the photograph of Figure 33 relating to a cracked steel component. It may be assumed that cracks may be initiated in surface corrosion pitting, stress corrosion or corrosion fatigue, propagating first in corrosion fatigue, and then in fatigue until final fracture depending on the ΔK-levels. Moreover, in considering aircraft components in service conditions, rest periods between flights may result in stress corrosion in areas where residual stresses have arisen during manufacture or assembly. Speidel[40], investigating the behaviour of 2.5 cm-thick 7079-T651 aluminium alloy plates stressed in the short transverse direction by using DCB specimens, has shown a significant effect of corrosion on fatigue crack propagation. He established a distinction between two types of corrosion fatigue: "True corrosion fatigue is almost exclusively transgranular in aluminium alloys. In contrast, stress corrosion under cyclic loads is almost exclusively intergranular in aluminium alloys." We think that this distinction is of the same kind as the distinction between true fatigue for $N > 10^5$ cycles and low-cycle fatigue for $2 < N < 10^4$ cycles. Only the magnitude of the effect is different, being higher with stressing in the short transverse direction owing to grain flattening and the associated brittleness in the perpendicular direction. As far as possible, scientific progress tends towards the explanation of analogous phenomena by a common predominant cause, as well as by secondary factors.

(ii) The important action of the hydrogen ion and molecule in stress corrosion and therefore in the intermediate stage of corrosion fatigue during crack propagation, was first established for high-strength steels, so completing earlier theories on cracking by preferential attack of the metal next to grain boundaries and of the stress rupture of the oxide film. Now there are numerous investigations on titanium alloys and the predominant action of hydrogen is confirmed. Some authors have suggested an analogous hydrogen action in high-strength aluminium alloys. Since Hartman[41] and Van Leeuwen et al.[42] have investigated the contribution of corrosion to the stress-corrosion cracking of Al-Zn-Mg alloys and have proposed considering the preferential grain boundary attack only as initiating a crack, whereas crack propagation may often be controlled by a different factor, alone or in conjunction with other factors.

(iii) In all the tests reported, the crack propagation rate depends only slightly on the water content, from the usual laboratory test value to 100% relative humidity. It might appear that laboratory tests may be considered representative of the actual service environment. However, no test result is available to establish a correlation between the usual laboratory conditions and the service condition most frequently found damaging, i.e., the presence of water condensation in recesses, assembly gaps, deep corrosion pits, fatigue cracks, etc., where

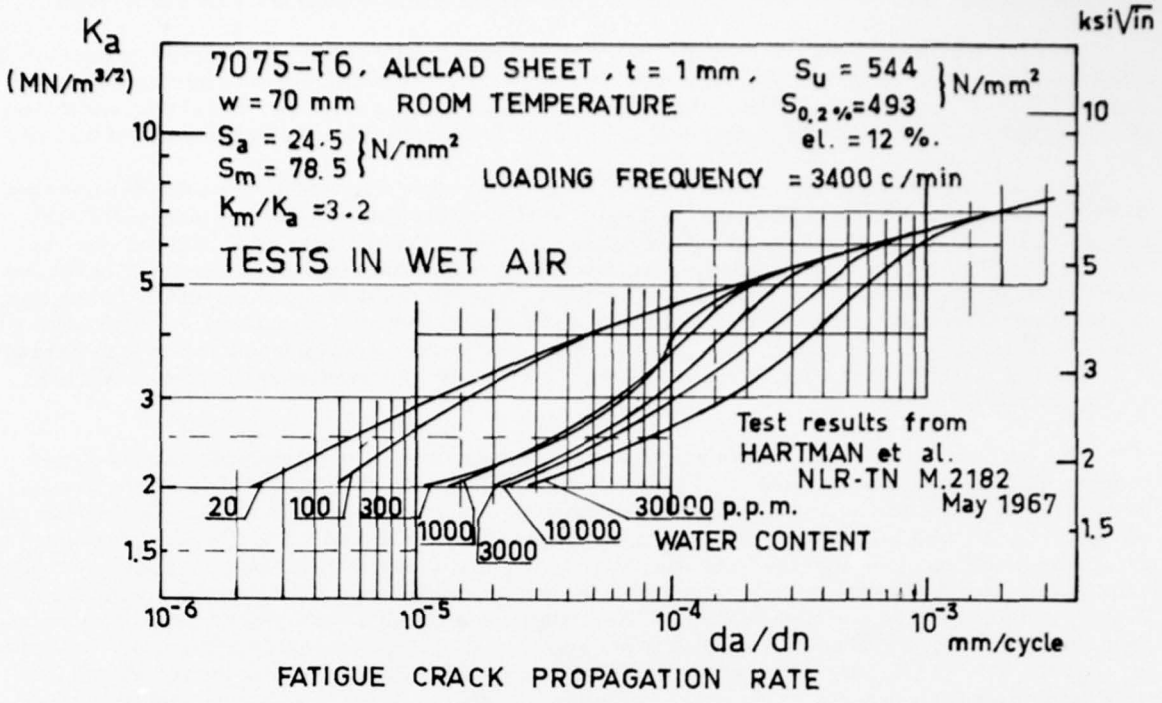

Figure 37

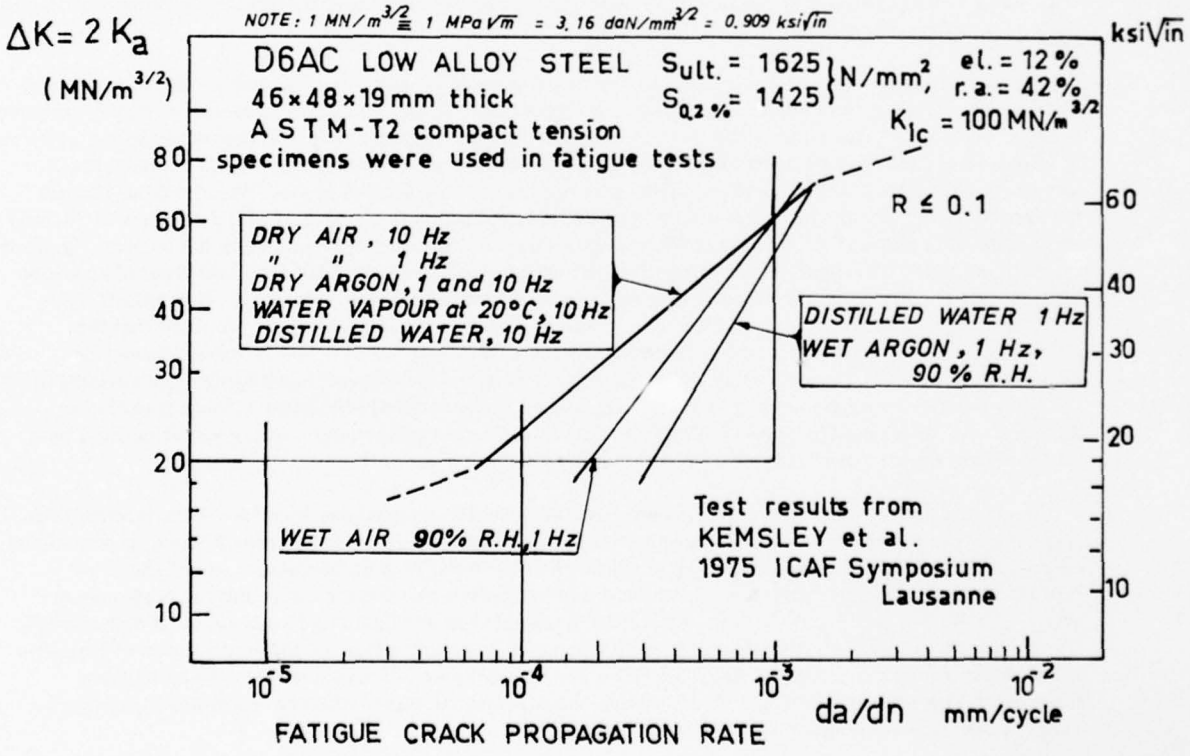

Figure 38

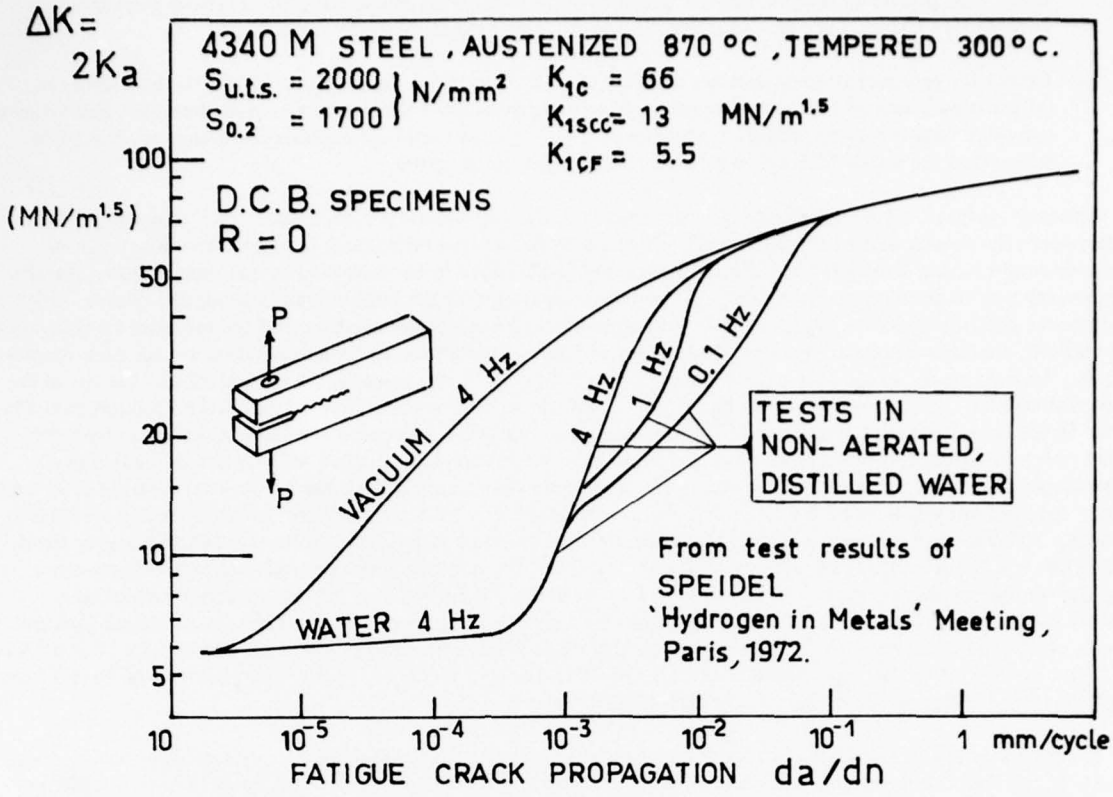

Figure 39

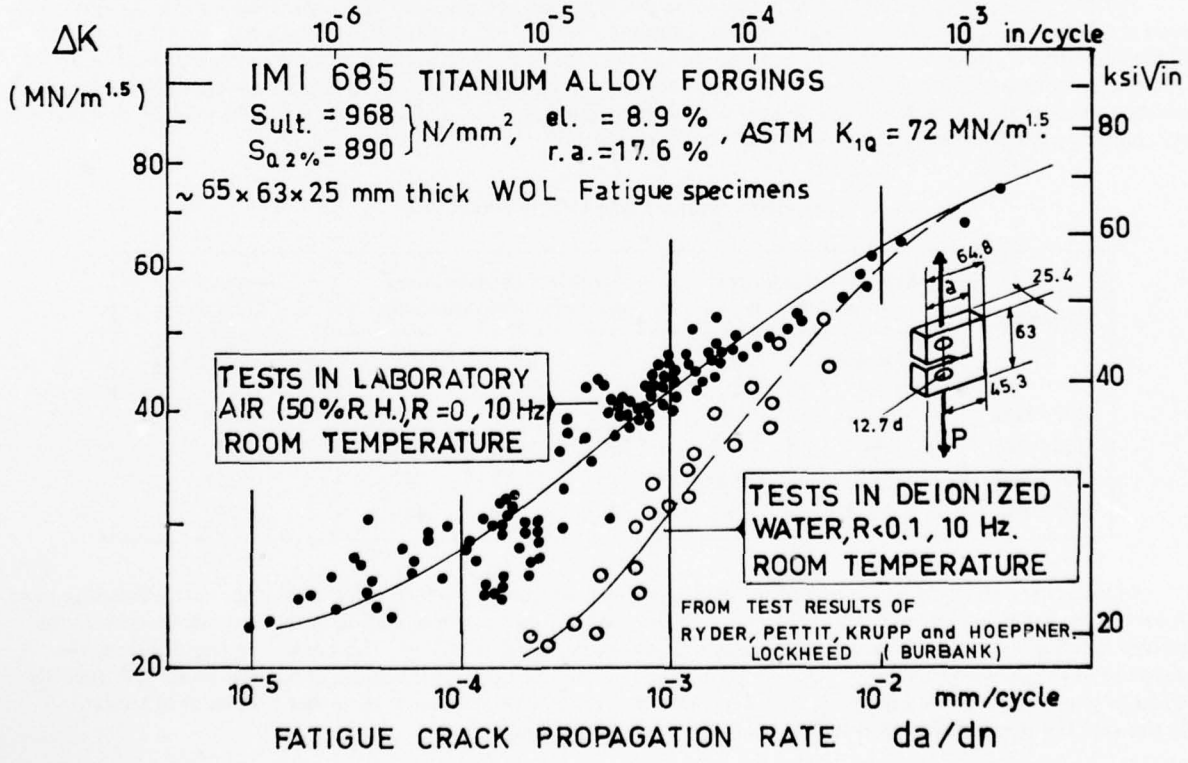

Figure 40

water, even if initially neutral, quickly becomes acid owing to the mechanism called crevice corrosion by differential aeration, hydrogen ions penetrating into the material from the crack front.

(iv) Except for very recent investigations, of which that of Speidel[40] is the only one known to the author, no information exists on the corrosion fatigue of material stressed in the short transverse direction. From stress-corrosion data it may be inferred that this would be the most useful information for designers. It is to be hoped that the use of DCB specimens may become general in future.

Although useful in fail-safe studies of aircraft structures, the corrosion effect on fatigue crack propagation rate concerns only the shorter part of the fatigue life, it being understood that microcrack propagation until a crack of detectable length occurs is included in the initiation period and is likely to be controlled by the same factors. Results of *systematic tests in an outdoor environment* do not allow separation of the initiation and propagation stages, which are moreover difficult to define. Outdoor tests with night-to-day temperature variation, and the associated water vapour condensation, are fairly representative of altitude-to-ground service variations in specimens containing recesses, assembly gaps, etc. Unfortunately, in the only available test, by Leybold et al.[43], the specimens had no crack-like feature in the failed cross section. Specimens were machined from 1.3 mm-thick, clad or bare, 2024-T3 and 7075-T6 aluminium alloy sheets. In the cross section of maximum bending stresses, 25.4 mm wide, specimens contained a 6.35 mm-diameter reamed hole. At a frequency of about 430 cycles per minute, a vibrating table applied 4000 cycles of loading in a 10-minute period each working day, while specimens were subjected to atmospheric conditions over a period of several months. Applied stresses were 82.8 ± 172.5 N/mm^2 in bare specimens, 82.8 ± 100 N/mm^2 in 7075-T6 clad specimens, and 82.8 ± 103.5 N/mm^2 in tests on clad 2024-T3 specimens. The meteorological conditions at NASA Langley Field, which is close to the Atlantic coast, were rainy for about 50% of the days when the tests were done and there was a heavy dew on the specimens nearly every morning. This, with the salt air, represented test conditions which were probably severe by comparison with average conditions for aircraft (except for local conditions in structural gaps and recesses, etc.). The tests showed that atmospheric conditions shortened the average life of specimens tested out of doors by a factor of about 3 for bare specimens of 2024-T3 or 7075-T6, by a factor of 1.5 for clad specimens of 7075-T6 and has no significant effect on the average life of clad 2024-T3 specimens.

The scatter of results on fatigue life for outdoor tests is much less than that of laboratory tested specimens. An estimate of the standard deviation of the logarithm of the fatigue life within the 10%–90% limits showed a reduction by a factor of 3 for bare specimens and by a factor of 2 for clad 2024-T3 specimens for which the lowest values of fatigue life are 417,000 cycles in the open air and only 227,000 cycles in the laboratory, although the average lives were comparable. This reduction in scatter can not, however, be used in the interpretation of tests on larger structures in outside conditions, because there is no information on the behaviour of a representative structural assembly.

Further research by Leybold[44] used the same type of specimen and the same batch of material. First the specimens were statically loaded and exposed to atmospheric conditions for ½, 1, 2, 3 and 4 years; they were then fatigue-loaded in the laboratory. The adverse effect of exposure to the elements was partial after six months and complete after a year. The clad specimens were not affected. Again, the results cannot be utilised because, in aircraft fatigue tests, most of the damage occurs at rivet or bolt holes, with load transfer by bearing pressure, and a possible effect, not visible, of fretting. By comparing the effect of cladding, we obtain the following table.

Geometric Mean Fatigue Life, in 1000 Cycles

Specimen	*Exposure and fatigue together*		*Fatigue in the laboratory after exposure outside of*			*Storage for 4 years and then fatigue in the laboratory*
	Laboratory	*Outside*	*½*	*1*	*4 years*	
2024 bare	464	146	137	153	90	269
2024 clad	590	550	220	3000	3000	1540
7075 bare	277	920	83	77	61	251
7075 clad	430	283	506	890	467	739

In these tests, the beneficial effect of the plating is well confirmed, even for indoor tests of specimens stored indoors. A part of the beneficial effect, if not the whole, is to be ascribed to the accommodation of the stress-strain cycle in the surface cladding layer material owing to the relative stress gradients, $g_t = -2/t = -1.54$ mm^{-1} in bending along the direction of the thickness and $g_r = -2/r = -0.315$ mm^{-1} in the direction of the radius at the hole edge. The opposite effect of plating is shown in Figure 11, for CEAT tests of bare and clad aluminium alloy sheets under axial tension. In this case the stress gradient was zero in the direction of the thickness.

This comparison emphasizes the designer's difficulties if his decision in structural design matters is to be based on such information alone. The NACA outdoor tests were not representative of the behaviour of structural elements because of the absence of assembly gaps and the bending stressing of a thin sheet with holes, which is not the most

critical type of loading in actual aircraft structures made of thin sheet panels and extrusions. The CEAT tests were not representative of the water condensation and only partially representative of the stresses.

In simultaneous indoor and outdoor testing using identical specimens, identically loaded by means of hydraulic jacks, the pressure of which is controlled, as with other jacks used in fatigue tests of wing centre sections, Schijve and De Rijk[45] have investigated the effect of the outdoor atmospheric environment on fatigue crack propagation rates in 2 mm-thick 2024-T3 Alclad and 7075-T6 clad aluminium alloy sheet specimens. Five cracks produced by prior low stress fatigue loading were initiated from centre notches, distant 230 mm apart in the 100 mm-wide specimens. Loads of various levels were applied at frequencies from 6 to 45 cycles per minute, either in random sequences or in programmed low-high-low sequences, with or without intervening batches of ground-to-air cycles in each type of sequence. The outdoor environment considered was country air and innocuous. Fatigue loads were applied during the daytime only. The duration of test for each specimen ranged from 16 to 106 days during the period from March to August. The indoor relative humidity was equal to or somewhat lower than the outdoor humidity. Frequently, outdoor specimens were wettish, owing to residual rain or dew. Test results yielded the following main conclusions:

- in 2024-T3 Alclad specimens, fatigue cracks propagate at about the same rate outdoors as indoors,
- in 7075-T6 clad specimens, fatigue cracks propagate outdoors about 1.5 to 2 times faster than indoors, this being tentatively attributed to stress corrosion.

The duration of full-scale fatigue tests is often longer than a year and may result in a more severe atmospheric action during the crack initiation period when the test is carried out in the open air with the fuselage immersed in a water tank. The comparison between laboratory and service behaviour is mainly the shortening effect of the service environment on the crack initiation period until detectable cracks occur, entailing some risk or implying repair. In the NASA outdoor bending fatigue tests of specimens with holes, the stress level is very high at the hole edge intersection with the cladding-core interface. The role of the cladding is sacrificial, the corrosion damage extending into the cladding layer before it enters the core material. However, the surface and interface geometric roughnesses are modified by corrosion pitting and cause premature crack initiation. In the NLR outdoor tension tests of pre-cracked specimens, the corrosion had insufficient time to damage the cladding-core interface during the relatively brief fatigue crack propagation tests. With the 7075-T6 clad specimens, the effect of the environment is to be attributed only to some corrosion or hydrogen action within the metal round the crack tip. These tests show that indoor conditions are not very different from outdoor conditions as long as only rapid crack propagation is considered.

In aircraft structures, during full-scale fatigue tests or in service, most cracks start from riveted and bolted joints, most often from fastener holes at the most heavily loaded end, that is, stressed by the highest direct tension and by the highest tension due to the load transferred to the fastener. Fretting-corrosion damage occurs between assembled components and between fastener shanks and holes. The problem of the corresponding stress concentration is the subject of Section 5 of this paper.

From the information available, it is not possible to answer the very important question: Does the fretting-corrosion period of fatigue damage in aircraft structures depend, significantly or otherwise, on the outdoor service environment? The answer would justify full-scale fatigue tests, either indoors if the effect is low or outdoors if it is not. It might be useful to investigate this problem, using riveted or bolted specimens at various ratios of transferred to bypassed load, in tests of short and long duration, in indoor or outdoor environments.

In a comprehensive survey Anderson[46] noted that, from statistical data on damage incurred during full-scale fatigue tests and during service "no one of the laboratory full-scale test defects could be identified as environmental-related, whereas most of the identified damage initiators in service were, or were suspected to be, corrosion related. Furthermore, the tenor of airlines' replies indicated that corrosion-related problems were of major concern. The conclusion seems inescapable that probably the most important element in 'scatter factor' between service experience and full-scale test experience is traceable to environmental influences."

In relation to the reasons proposed by Anderson[46,48] for the differences between the service and test behaviour of aircraft structures, Harpur and Troughton[47] noted the absence of some structural elements and of some types of loading in the tests. Recent experience has led us to emphasize that many small fatigue cracks are not revealed when using X-ray inspection or other, more sophisticated, means, except when the exact location of a possible crack is known. Cracks have been known to escape several X-ray inspections in open air on the full-scale structure. Later, specimens were cut from the structure tested, after failure elsewhere; the aim was to evaluate maintenance and repair procedures by complementary fatigue tests. Most of the cracks escaped the additional inspection and were finally revealed as being origins of cracks propagating to fracture. Further dismantling of attachment fittings in another region, where a small number of cracks was visible, revealed a further number of incipient cracks escaping X-ray detection. The lessons from this were: (a) even with several load paths, structures are not fail-safe when their components are subjected to the same stress level and are simultaneously damaged, (b) most of the cracks originating at holes occur at the end-fastener holes of fastener rows overloaded locally owing to the load transferred to an attachment fitting or to a reinforcement or additional material stretched by the stresses and strains of the structure below, and (c) a fatigue test is completed and has provided all possible information only when the complete damage is known. This last item of research is particularly rewarding when an analysis is made to establish a correlation between the computed stress concentration factors and the

"fatigue equivalent" stress concentration factors by means of a damage adjustment coefficient, as proposed in the following section. Then perhaps full-scale fatigue tests would no longer be judged as were laboratory fatigue tests about 40 years ago: the means of obtaining minimum information for maximum cost.

5. INTERPRETATION OF FATIGUE DAMAGE INCURRED DURING FULL-SCALE FATIGUE TESTS OR IN SERVICE

5.1 General

In the earlier sections, a critical study of fatigue data has proved beyond doubt that no standardized figures of any material property can be used as a basis for life evaluation. Too many factors, not represented in tests and of unknown value, have a significant effect on the fatigue behaviour of actual structures. Only two problems can be treated to an approximation adequate in practice. They are as follows:

(i) From knowledge of the loading programme applied during a full-scale fatigue test in a known environment during the period which elapsed until the particular local damage occurred, to predict for the same degree of damage, the test duration which would correspond to another loading programme. It is possible to extend the prediction to in-service behaviour if the service loading is known or may be evaluated and, to be on the safe side, either by using an arbitrary high scatter factor or, with a moderate reserve factor, from knowledge of similar damage in actual service under a different, statistically known, flight loading.

(ii) For the same local structure, when only minor modifications are being considered in order to extend the fatigue life, to predict the probable increase in life. Moreover, interpretation of damage may determine the values of some parameters which might be used in prediction analysis applied to a different size of structure of the same general type as the structural detail considered. Naturally the prediction accuracy would decrease as the differences from the structure tested increased.

Assessments of fatigue lives are essentially comparisons of the structure area considered with a reference structure, the fatigue behaviour of which is known from previous tests. The reference structure may be a plain or notched specimen, an assembly or another structure containing the local detail to be considered, subjected to the same type of loading. The earlier method of fatigue life assessment of a notched component was based, for comparison, on the higher surface fatigue stress in the notch, so that the favourable effect of the stress gradient with depth was disregarded. This method is conservative if the data used are from axial fatigue tests on plain specimens; it is simple and may be used to check whether or not the fatigue strength can definitely be considered sufficient. However, fatigue strength may be overestimated when using rotating bending results on small-diameter plain specimens. This method fails with corrosion, fretting or superimposition of undefined stress raisers.

An improvement on this method was made by taking stress gradients into account and by using fatigue test results of a set of notched specimens with several notch factor values. This enabled us to plot a set of S–N curves in the form $(K_T S_a - N) - K_T S_m$, like those presented in Sections 2 and 3.

When the fatigue loading no longer consists of constant amplitude load cycles but is a random or programmed loading, consisting of numerous loads of various degree, S–N curves are used in conjunction with a *cumulative damage rule*. Despite a number of rules proposed for computing a parameter related to such an abstract quantity as "damage", each rule being checked against the author's test results but not against all the rest, it is advisable to use the simplest, but not the most simplistic, Miner's rule. It gives less extreme errors, although it is questionable, and its use cannot result in false confidence. The *Miner-Palmgren cumulative damage rule* is:

$$D = \Sigma n_i/N_i ,$$

where n_i is the number of cycles applied at stress level S_i, while N_i is the number of cycles at failure under the same stress level. D would equal 1 at failure if the Miner formula were exact. In most cases D ranges from 0.5 to 2 for plain specimens under various programmed loadings. For structural assemblies the range of variation may be larger, owing to premature failure of a brittle part under the highest load level of the programme or, on the contrary, owing to the improvement due to the application of higher loads when no crack exists.

Generally, it is possible to compute or to measure the *nominal stresses* applied to the structure in the damaged area, far enough from the damage to be not seriously affected by the stress concentration at the origins of damage. A value is assumed for the *stress concentration factor* K_T at the stress raiser from which the fatigue damage originates.

Using S–N reference curves of notched specimens corresponding to the K_T-value assumed, the Miner damage d_1 for one loading programme will be multiplied by the number n_1 of loading programmes applied until the damage occurs and the Miner damage will be $D_1 = n_1 d_1$.

Another loading programme will give a partial damage d_2 per programme and the number of loading programmes likely to have been applied when damage occurred would be

$$n_2 = n_1 d_1 / d_2 .$$

Then, because of the scatter in fatigue life and the need for a reserve, the resulting life is divided by a *reserve factor*, k_r, ranging from 3 to 5, and the safe flight life during which the damage considered is not likely to occur may be assumed as

$$N_2 = (n_2 f_2)/k_r ,$$

where n_2 is the number of flight load programmes, each associated with f_2 flights, and k_r is the reserve factor.

With this early method of life assessment based on the *relative Miner damage*, the S–N values used were often situated in a poorly representative region of the S–N curve, when the computed Miner damage of the test, D_1, differed considerably from unity, owing to wrongly assumed values of the local nominal stress level or of the stress concentration factor.

This is the reason for the concept of "*equivalent notch factor*", K_{Teq}, introduced by Hayes[49]. Fatigue test results of notched specimens with several values of notch stress concentration factor were used to define by interpolation the equivalent notch factor from a fatigue test of the component being tested under constant amplitude loading. Then interpolation of S–N curves according to this equivalent notch factor enabled an assessment to be made of the component fatigue behaviour under any loading programme.

Recently[50], using a set of $(S_a–N)–S_m$ curves representative of the sheet material and the notch radius, the author made a modification to the S–N values derived from the S–N curves by using a *multiplying factor*, c, applied to the nominal stress levels in order to obtain a value of unity for the computed Miner damage D_1 corresponding to the actual test damage. This multiplying factor can also be defined as a multiplier for bending moments, axial loads, load factors or any quantity proportional to the load level.

Now, we propose to apply this method by defining two quantities, namely the *damage equivalent notch factor*, K_{DE}, and the *damage adjustment factor*, k_{DA}, such that

$$K_{DE} = K_T k_{DA}$$

may be used in conjunction with the set of $(K_T S_a–N)–K_T S_m$ curves described in Sections 2 and 3. The particular set of curves used would correspond to the material and the actual notch radius. The theoretical surface stress levels at the notch root would be

$$S = K_{DE} \times S_{nominal} = (K_T S_{nominal}) k_{DA} .$$

Interest in the definitions of K_{DE} and k_{DA} centres around the hope of obtaining similar values of k_{DA} for similar design features.

In general, interpretation of fatigue tests would consist of two stages:

(a) the theoretical elasticity analysis of the state of stress at the crack origin, and

(b) the damage computation, using an appropriate set of S–N curves, assumed to be representative of the local fatigue conditions.

Interpretation of fatigue damage in service would involve two other types of data:

(c) statistical evaluation of the flight loads, and

(d) evaluation of the damage adjustment factor, from the full-scale fatigue tests or from previous full-scale fatigue tests of structures which have sustained similar damage; after some evaluation of analogous local structural designs in this way, the corresponding damage adjustment factors could probably be corrected to account for the service environment.

The theoretical elasticity calculations relate to the essential parts, but not the whole, of the evaluation sequence that transforms external load levels into surface stress levels and relative stress gradients at notch roots, through the computation of nominal stress levels within large regions of the structure, then nominal stress levels in the neighbourhood of stress raisers such as fasteners in assemblies, and finally any stress concentration factors which may be superimposed.

5.2 Stress Concentrations at the Edges of Fastener Holes in Assemblies

In aircraft structures most of the fatigue cracks originate from fastener holes, and the problem of the corresponding stress concentration has been considered very important for several decades. In 1962 Deneff[51] computed local stresses in a multi-rivet statically-redundant assembly, each assembly sheet being idealized by a system of rectangular meshes in a network, the nodes of which were at the hole centres. The lines of the network were assumed to be axially loaded bars transferring shear loads to rectangular sheet elements. Deformations due to bearing stresses in holes and to rivet bending were evaluated from static tests. Computation, restricted to the elastic range, yielded nominal stresses applied

near each hole and local loads transferred by each rivet. Allowable values of these loads and stresses were derived from fatigue tests on elementary elements. In 1969 Jarfall[52] made a further investigation on the fatigue assessment of a joint by determining the quality of a fastener installation from an analysis of a set of four sheet strip or assembly specimens, namely: a specimen with a plain hole, with a fastener without load transfer, with a fastener with low load transfer and a two-row lap joint specimen with equal transfer per row.

The problem of computing the load distribution between fasteners was discussed in the years between 1938 and 1950 by Vogt[53], who used an empirical formula in an attempt to summarize the experimental results of Volkersen[54], and by Rosenfeld[55]. Theoretical aspects of the stiffness in a loaded hole and in the joining of two strips by one fastener have been reviewed more recently by Harris et al.[56] Although no definitive data are available and computations of the stresses in riveted assemblies depend on too many parameters, most of which are not known well enough to permit more than an order-of-magnitude assessment, an attempt has been made to gather available data and to determine the unknown points[57]. A short description of the method is given and is followed by an example of its application to the interpretation of full-scale fatigue damage.

5.2.1 The Loaded Hole – Analysis of the Displacements by Integration of Theocaris Stress Distributions for a Strip of Finite Width[58]

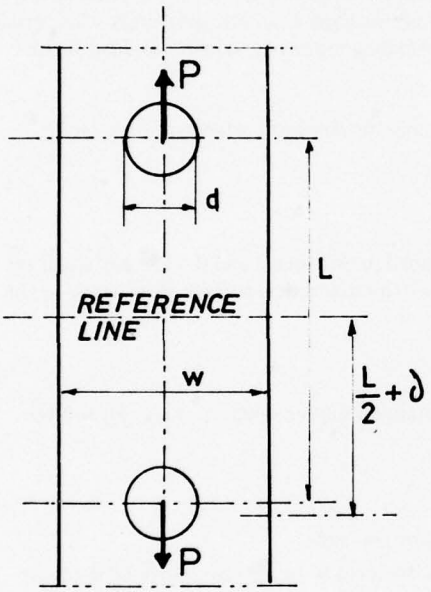

Figure 41

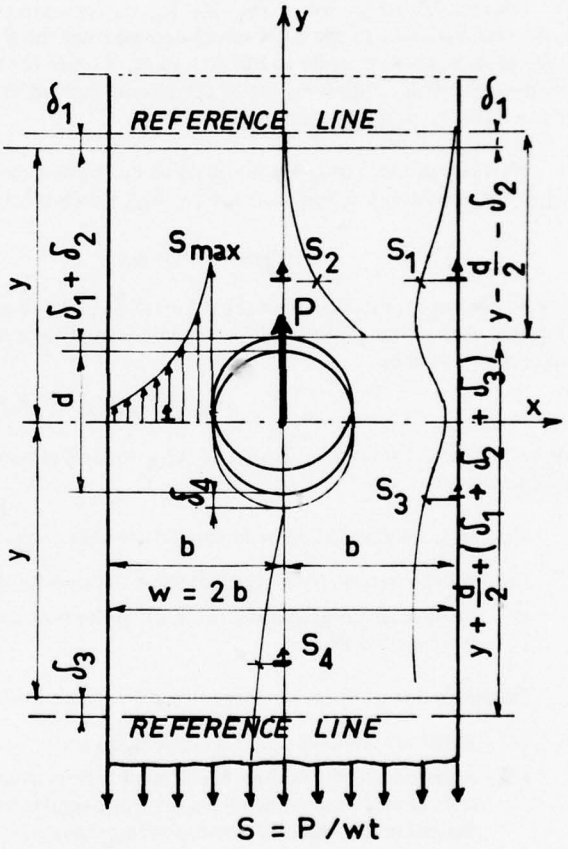

Figure 42

The expression in the form of equations of the problem of the hyperstatical joint of two strips by shear fasteners introduces the elementary problem of the strains in a plate with a hole loaded by means of a pin. This elementary problem is poorly defined since there is no reference point from which to measure the displacements. This difficulty can be avoided by considering the symmetric loading of a plate by two loads, of the same amplitude but opposite sign, each being applied to one of the two holes (see Figure 41). The axis of symmetry perpendicular to the load direction may be selected as the reference axis of displacements. For a plate large enough by comparison with the distance L between the hole centres, the stresses will be negligible except in the hole region. In an infinite plate, the displacement of each hole with respect to the reference line will depend only on P/Et and on Poisson's ratio if the distance L between the hole centres is large enough for the stresses on the reference line to be ignored.

Applying S[t] Venant's principle on the fading of local disturbances of zero resultant force, the displacement reference may be chosen at a strip cross section where the stress distribution is uniform, to an acceptable degree of approximation. Figure 42 shows the procedure used to evaluate the relative displacement of the contact point of the pin with the hole edge, with respect to the initial location of the hole centre, that is to say, $\delta_1 + \delta_2$, from the summation of strain integrals in the direction of the y-axis at the strip edges and at the middle axis. In the same way, the displacement of the hole centre with respect to a reference line located at $-y$ will be given by the strain integral at the strip edge along the negative half of the y-axis. In order to obtain convergent integrals, the difference between the mean elongation of the strip without the hole to the elongation of the strip with the hole is calculated. The overall relative displacement of the pin-plate contact point with respect to the reference line is given by

$$\delta = (\delta)_y - (S/E)y = \delta_1 + \delta_2 + \delta_3 - (S/E)y .$$

An attempt to obtain empirical relationships that permit interpolation between λ-values and extrapolation towards $\lambda = 0$ gives

$$\delta = 0.8\, wS/E(1-\lambda) . \qquad (1)$$

The stress at the hole edge has its highest value at the ends of the diameter perpendicular to the load direction. From values of the stresses computed by Theocaris[59] for the values 0.2, 0.3, 0.4 and 0.5 of $\lambda = d/w$, the author has proposed the following empirical relationship for the maximum stress and the stress concentration factor K_T with respect to the net cross-sectional area:

$$S_{max} = K_T S_{Net} \quad \text{with} \quad S_{Net} = S/(1-\lambda)$$

$$K_T = \lambda + 1/\lambda . \qquad (2)$$

Figure 43 compares this empirical relationship with the Theocaris values, marked T, and with measured values in tests on aluminium panels or in photoelasticity tests[59,60].

It will be useful to know the ratio, K_b, of the maximum stress to the average bearing pressure, $p = P/td$:

$$S_{max} = \frac{P}{td} K_b , \quad \text{with} \quad K_b = \frac{1+\lambda^2}{1-\lambda} . \qquad (3)$$

From Bickley[61], the limiting value of K_b is 1 when λ reaches zero. This shows that the maximum stress, S_{max}, tends to the average bearing pressure when the net stress tends to zero for strip width increasing to infinity.

From the discussion in Reference 57, the limiting result of Howland[62] for the open hole is still right for the loaded hole: when λ tends to 1, K_T tends to 2.

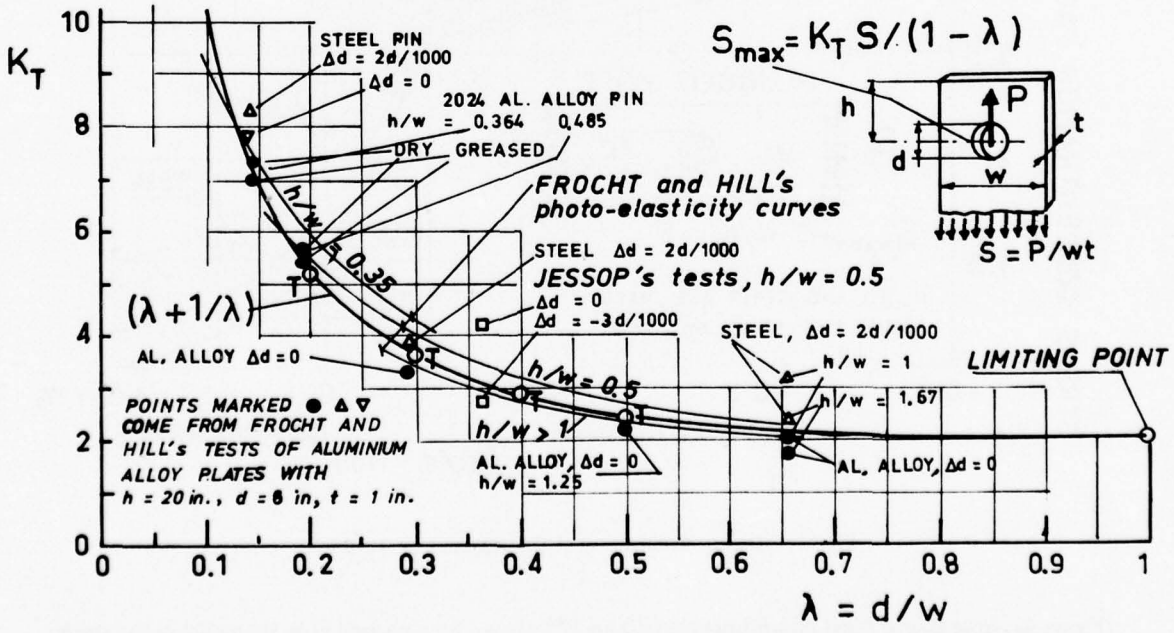

Fig.43 Net stress concentration factor in loaded holes

5.2.2 Elongation of a Strip Containing a Circular Hole Under Tension – Stress Concentration Factor for Direct Tension Stresses

As illustrated in Figure 44, stress concentrations at hole edges in bolted joints result from the superimposition of two stress systems. They are (i) the stresses due to the load R transferred from the bolt to the strip and (ii) the stresses due to the residual tensile load not yet transferred and bypassing the hole, P − R.

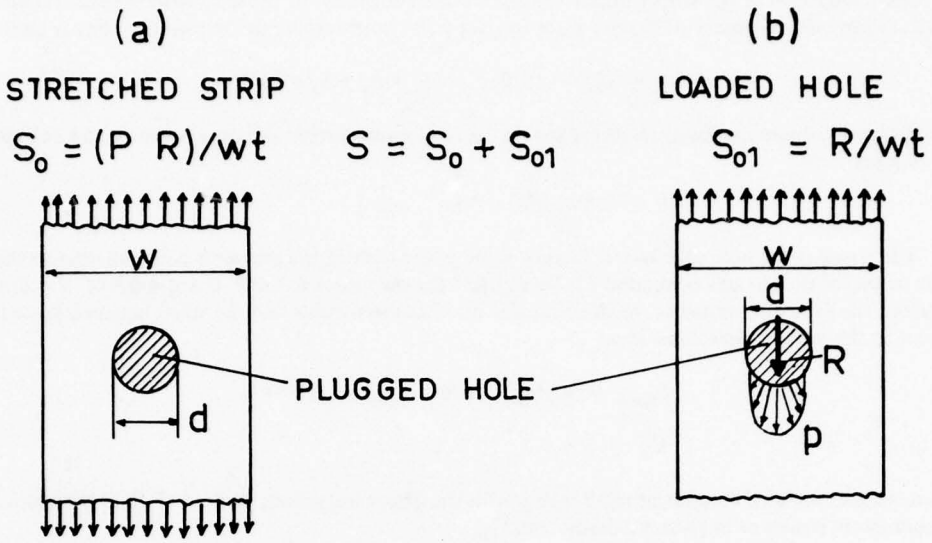

Fig.44 Breakdown of the strip loading into direct and transferred loads

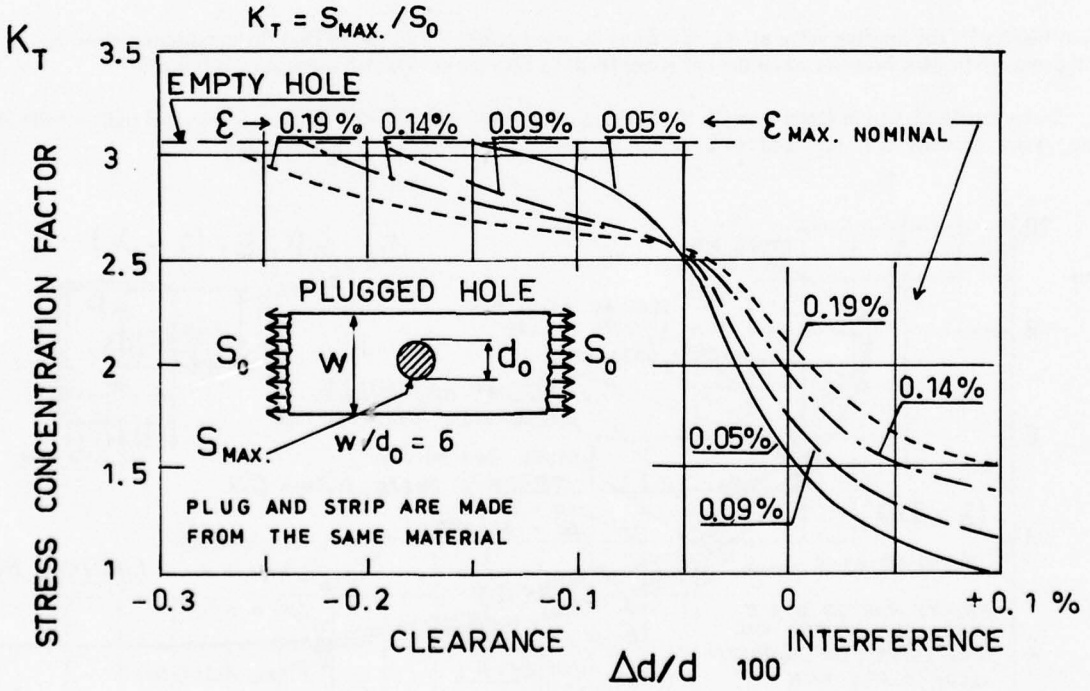

Fig.45 Stress concentration at the edge of a plugged hole

Figure 45, from Elsner[63] and drawn from Hertel's book[64], shows, for a plugged hole, the values of the stress concentration factor, K_T, that defines the maximum stress at the hole edge, taking as reference the gross area of the strip cross section. The plug is assumed to be of the same material as the strip and K_T-values depend on the clearance or interference between the plug and the hole edge as well as on the highest nominal strain, $\epsilon_{nom} = S_0/E = (S_m + S_a)/E$,

the nominal stress being $S_0 = P/wt$. It may be seen that an interference of about $\Delta d/d = 1/1000$ is sufficient to annul the stress concentration if the applied nominal stress is lower than 0.0005E, that is to say, 35 N/mm² for aluminium alloys. The interference obtained in practice by severe crushing of rivet heads is higher than 1 per cent. However, this interference will be easily annulled under nominal tensile stresses higher than the yield strength. Under fatigue loading, it may be observed with loaded holes that the improvement due to interference is significant only for interference ranging from 0.3 to 0.4 per cent of the diameter, i.e., higher than that for which the yield stress is reached.

We recall that, for an empty hole, the stress concentration factor is, from Heywood's approximation[65] of Howland's calculations[62]:

$$S_{max}/S_{net} = K_{T\,net} = 3\left[1 - \frac{d}{w} + \left(\frac{d}{w}\right)^2 - \frac{1}{3}\left(\frac{d}{w}\right)^3\right], \tag{4}$$

or, with $d/w \leqslant 0.3$,

$$S_{max}/S_{net} = \frac{3}{1 + d/w}, \tag{5}$$

where $S_{net} = S_0/(1 - d/w)$.

The problem of the elongation of a strip between the centres of two holes in the median line of the strip, under tension loads applied far from the hole centres, may be treated empirically by using the numerical results of some computations done by Harris et al., using a finite-element method, and the numerical results of Howland's calculations of stresses, and then integrating them, as done previously with the Theocaris results. The distance L between two hole centres is increased under a tensile stress S by the elementary elongation, LS/E, and a supplementary elongation ΔL, for which the approximation proposed is

$$\Delta L = \frac{P}{Et}\left[\lambda\left(\frac{1.3}{1 - \lambda} - 1\right) + \frac{L}{w}\right], \tag{6}$$

where $\lambda = d/w$.

5.2.3 General Equation and Solution for the Deflection of Tight Pins on an Elastic Foundation

No clearance is assumed between the pin and the elastic foundation. Figure 46 shows the sign convention used in the equations. The shear load, Q, causes warping of the initially plane cross section of the pin, the S-shaped surface of which remains perpendicular to the lower and upper fibres. The inclination of the pin, β, depends on the surface element taken as reference. The variation of the cross-section warping is not free but is modified by axial stresses of zero resultant; the plane whose intersection with the warped surface defines deflection vectors of zero resultant and zero resultant moment has been taken as reference for the inclination due to the shear load. For a circular cross section, Cowper[66] has proposed

$$\beta = \frac{Q}{\mu GA} \quad \text{with} \quad \mu = \frac{5(1 + \nu)}{7 + 6\nu}, \tag{7}$$

where A is the cross-sectional area and

G is Coulomb's modulus, $G = E/2(1 + \nu)$.

The bending moment M creates a curvature of the pin axis with an angular difference $d\psi$, such that

$$-d\psi = \frac{M}{E_f I_f}\,dx, \tag{8}$$

where E_f is the modulus of elasticity of the pin and $I_f = \pi d^4/64$. The slope of the lower and the upper fibres of the pin results from the summation of β and ψ:

$$dy/dx = \beta + \psi. \tag{9}$$

Finally, it is assumed that the reaction of the material of the strip under the pin pressure equals that of an elastic foundation made from parallel springs[56] or of numerous thin sheets and therefore does not depend on x.

The differential equation is

$$\frac{d^4y}{dx^4} - \frac{k}{\mu G_f A_f}\frac{d^2y}{dx^2} + \frac{k}{E_f I_f}y = 0, \tag{10}$$

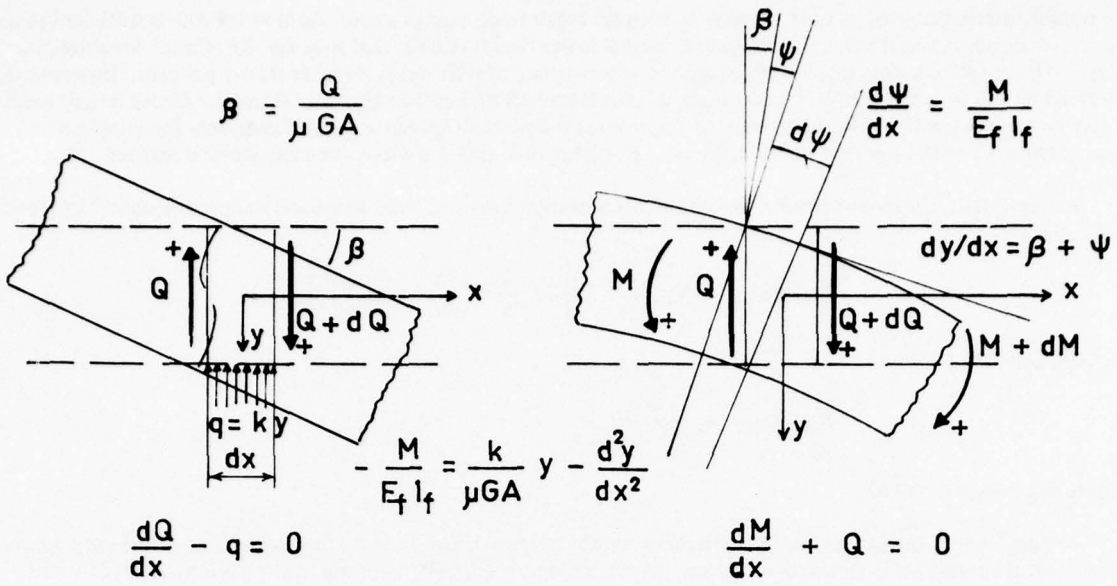

Fig.46 Deformation of a beam on an elastic foundation

where the foundation modulus may be deduced from relationship (3), proposed previously, such that

$$k = E(1-\lambda)/0.8\,. \tag{11}$$

With the notation

$$m = k/\mu G_f A_f \quad \text{and} \quad n = k/E_f I_f\,,$$

the general solution of the differential equation is

$$y = A \sin \omega x \, \mathrm{sh}\varphi x + B \sin \omega x \, \mathrm{ch}\varphi x + C \cos \omega x \, \mathrm{sh}\varphi x + D \cos \omega x \, \mathrm{ch}\varphi x\,,$$

where

$$\omega^2 = \frac{\sqrt{n}}{2}\left(1 - \frac{m}{2\sqrt{n}}\right) \quad \text{and} \quad \varphi^2 = \frac{\sqrt{n}}{2}\left(1 + \frac{m}{2\sqrt{n}}\right). \tag{12}$$

Finally, t being the thickness of the strip, the following expressions for ωt and φt are obtained:

$$\begin{aligned} \omega t &= (t/d)2\left(\frac{k}{\pi E_f}\right)^{1/4}\left[1 - 0.75\left(\frac{k}{\pi E_f}\right)^{1/2}\right]^{1/2} \\ \varphi t &= (t/d)2\left(\frac{k}{\pi E_f}\right)^{1/4}\left[1 + 0.75\left(\frac{k}{\pi E_f}\right)^{1/2}\right]^{1/2}. \end{aligned} \tag{13}$$

In the case of single asymmetric shear, the shank bending deflection is adding to that of the general inclination of the shank as a body. This inclination is resisted by the bearing reactions of the assembled strips and by the partial clamping effect of the rivet or bolt heads. In single shear, the simplified reference case is no longer the uniform distribution of the bearing load but is the inclination as a body of the fastener shank, assumed to be absolutely rigid. It is still assumed that each strip is composed of separate thin laminae or, equally, that the foundation modulus k is constant through the strip thickness, the distributions of the bearing loads being linear, as illustrated in Figure 47.

Let q_o, q_a, q_{1b} and q_{1o} be unit bearing loads along the fastener shank at the strip surfaces. The equilibrium conditions of the shank yield the solution[57]

$$\begin{aligned} q_a &= (P/a)\frac{1 + 3\epsilon^2 + 4\epsilon^3}{1 + \epsilon^3}\,, \quad q_{1b} = (P/b)\frac{4 + 3\epsilon + \epsilon^3}{1 + \epsilon^3}\,, \\ q_o &= (P/a)\frac{1 - 3\epsilon^2 - 2\epsilon^3}{1 + \epsilon^3}\,, \quad q_{1o} = (P/a)\frac{\epsilon^3 - 3\epsilon - 2}{1 + \epsilon^3}\,, \end{aligned} \tag{14}$$

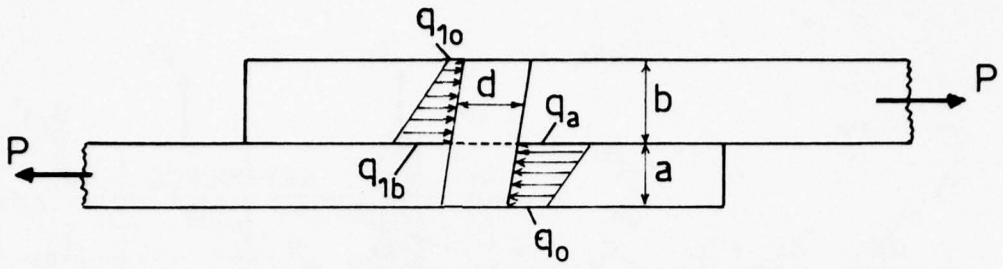

Fig.47 Inclination of a rigid pin

where $\epsilon = a/b$. When ϵ varies from 0 to 1, the numerical values of the bearing *load concentration factors* $K_{q_a} = q_{a\,max}/q_{a\,mean} = q_a a/P$, $K_{q_b} = q_{1b} b/P$, and of the coefficients $C_o = q_o a/P$ and $C_{1o} = q_{1o} b/P$ are as follows:

$\epsilon = a/b$	0	0.1	0.2	0.3	0.4	0.5	0.6	0.7	0.8	0.9	1
K_{q_a}	1	1.033	1.143	1.342	1.632	2	2.421	2.861	3.286	3.67	4
C_o	1	0.967	0.857	0.658	0.308	0	−0.421	−0.861	−1.286	−1.67	−2
K_{q_b}	4	4.297	4.571	4.797	4.947	5	4.947	4.797	4.571	4.297	4
C_{1o}	−2	−2.297	−2.571	−2.797	−2.947	−3	−2.947	−2.797	−2.571	−2.297	−2

The secondary bending moments on the pin with free ends are

$$\left.\begin{aligned} &\text{– strip (a):} \qquad \Delta M = (q_a - q_o)\frac{a^2}{12} = \frac{Pa}{2}\epsilon^2\left(\frac{1+\epsilon}{1+\epsilon^3}\right), \\ &\text{– strip (b):} \qquad \Delta M_1 = (q_{1b} - q_{1o})\frac{b^2}{12} = \frac{Pb}{2}\left(\frac{1+\epsilon}{1+\epsilon^3}\right). \end{aligned}\right\} \tag{15}$$

The secondary stresses due to the bearing concentration do not depend on the hinge or clamping conditions of the strip ends at the points where the external load is applied, as is the case, on the contrary, with secondary bending stresses considered generally as aggravating fatigue damage in single shear assemblies. The distinction between these two causes of secondary stresses is not easy, each of them belonging to a simplified representation of actual features.

In the case where the fastener is a bolt, tightening the strips through two oversize washers ensuring good clamping of the bolt head and nut with respect to the outer surfaces of the strip, secondary stresses due to bearing are very low and the bending moment due to the inclination of the bolt shank is resisted by bending bearing pressures under the head and nut of the bolt. However, apart from the bearing surfaces of the head and nut, the load eccentricity creates bending moments[68,69], depending on the eccentricity and the magnitude of the load, the bending under tension giving deflections that are not proportional to the load, and secondary stresses which increase at a rate lower than that of the load. Moreover, these stresses will not be a maximum at the hole edge, if the clamping effect of the bolt is sufficient.

Considering now the flexibility of the actual fasteners, the problem of the bearing load distribution, no longer linear, is treated by using the notation and coordinates defined in Figure 48.

In general, the two strips have different thicknesses and 8 unknown integration constants are to be computed from the set of linear equations representing the equilibrium and boundary conditions as follows:

– two equilibrium conditions of the pin segments:

$$\int_0^a k y dx = P \tag{16}$$

and

$$\int_0^b k y_1 dx_1 = P, \tag{17}$$

– two interface continuity conditions:

$$(dy/dx)_{x=a} = (dy_1/dx_1)_{x_1=b} \tag{18}$$

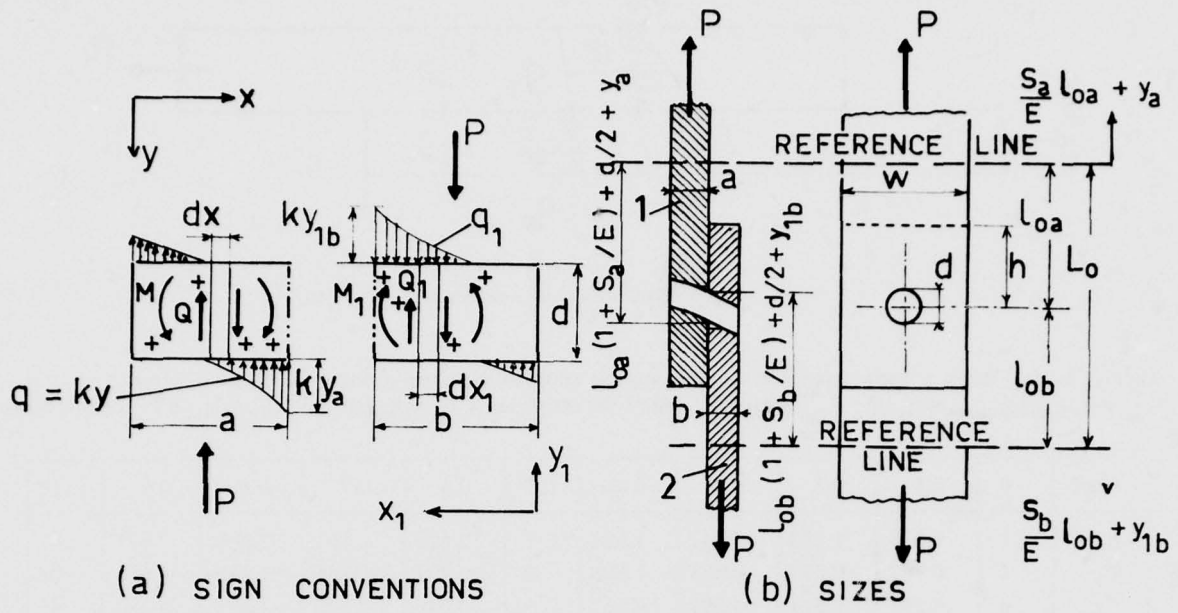

Fig.48 Loaded hole – single shear of the fastener

$$(M)_{x=a} + (M_1)_{x_1=b} = 0 \quad \text{or} \quad \left(\frac{d^2y}{dx^2} - my\right)_{x=a} + \left(\frac{d^2y_1}{dx_1^2} - my_1\right)_{x_1=b} = 0\,, \tag{19}$$

– two boundary conditions of zero shear load at the pin ends:

$$(Q)_{x=0} = 0\,, \quad \text{that is to say,} \quad \left(\frac{d^3y}{dx^3} - m\frac{dy}{dx}\right)_{x=0} = 0\,, \tag{20}$$

and

$$(Q_1)_{x_1=0} = 0\,, \quad \text{i.e.,} \quad \left(\frac{d^3y_1}{dx_1^3} - m\frac{dy_1}{dx_1}\right)_{x_1=0} = 0\,. \tag{21}$$

– Finally, the remaining two conditions both depend on the axial pressure:

For pins with *free ends*, the two conditions of zero bending moment are

$$(M)_{x=0} = \left(\frac{d^2y}{dx^2} - my\right)_{x=0} = 0\,, \tag{22}$$

and

$$(M_1)_{x_1=0} = \left(\frac{d^2y_1}{dx_1^2} - my_1\right)_{x_1=0} = 0\,. \tag{23}$$

In the case of *tight-fitting bolts and assuming perfect clamping of* the shank ends onto the outside strip surfaces, the two conditions of zero slope are

$$(dy/dx)_{x=0} = 0 \tag{24}$$

and

$$(dy_1/dx_1)_{x_1=0} = 0\,. \tag{25}$$

These conditions have been developed in Reference 57 and have yielded the coefficients and second members of the set of linear equations which determine the values of the constants $A, B, C, D, A_1, B_1, C_1$ and D_1 of the two general solutions relating to the two pin segments:

$$y = A \sin \omega x \, \mathrm{sh}\varphi x + B \sin \omega x \, \mathrm{ch}\varphi x + C \cos \omega x \, \mathrm{sh}\varphi x + D \cos \omega x \, \mathrm{ch}\varphi x\,, \tag{26}$$

$$y_1 = A_1 \sin \omega x_1 \, \mathrm{sh}\varphi x_1 + B_1 \sin \omega x_1 \, \mathrm{ch}\varphi x_1 + C_1 \cos \omega x_1 \, \mathrm{sh}\varphi x_1 + D_1 \cos \omega x_1 \, \mathrm{ch}\varphi x_1\,. \tag{27}$$

When conditions (20) and (21) hold, conditions (24) and (25) become $B = C = 0$ and $B_1 = C_1 = 0$. The coefficients are shown in detail in Figure 49.

$\lambda = \frac{d}{w}$, $m = k/\mu GA = \frac{15}{\pi d^2}(1-\lambda)\frac{E}{E_f}$, $n = k/E_f l = \frac{80}{\pi d^4}(1-\lambda)\frac{E}{E_f}$, $\varphi^2 = (1+\frac{m}{2\sqrt{n}})\sqrt{(n/4)}$, $\omega^2 = (1-\frac{m}{2\sqrt{n}})\sqrt{(n/4)}$,
$k = (1-\lambda)E/0.8$

$r_1 = \sin\omega a \cdot \mathrm{sh}\,\varphi a$, $s_1 = \sin\omega b \cdot \mathrm{sh}\,\varphi b$,
$r_2 = \sin\omega a \cdot \mathrm{ch}\,\varphi a$, $s_2 = \sin\omega b \cdot \mathrm{ch}\,\varphi b$,
$r_3 = \cos\omega a \cdot \mathrm{sh}\,\varphi a$, $s_3 = \cos\omega b \cdot \mathrm{sh}\,\varphi b$,
$r_4 = \cos\omega a \cdot \mathrm{ch}\,\varphi a$, $s_4 = \cos\omega b \cdot \mathrm{ch}\,\varphi b$.

$\frac{m}{2}d^2 = (\varphi^2 - \omega^2)d^2$, $d^2\sqrt{n} = (\varphi^2+\omega^2)d^2$,
$v = \frac{4\varphi\omega}{m} = \frac{2\varphi\omega}{(\varphi^2-\omega^2)} = \frac{1}{m}\sqrt{(n-\frac{m^2}{4})}$.

	COEFFICIENTS								
	A	B	C	D	A_1	B_1	C_1	D_1	SECOND MEMBER
22	$g_{11} = 1$	0	0	$g_{14} = -1/v$	0	0	0	0	0
20	0	$g_{22} = 1$	$g_{23} = -\varphi/\omega$	0	0	0	0	0	0
16	g_{31} $\varphi a r_2 - \omega a r_3$	$g_{32} = \varphi a r_1 - \omega a(r_4-1)$	$g_{33} = \varphi a(r_4-1) + \omega a r_1$	$g_{34} = \varphi a r_3 + \omega a r_2$	0	0	0	0	$\frac{a}{d}\cdot\frac{P}{kd}(\varphi^2+\omega^2)d^2$
18	$g_{41} = \varphi d r_2 + \omega d r_3$	$g_{42} = \varphi d r_1 + \omega d r_4$	$g_{43} = \varphi d r_4 - \omega d r_1$	$g_{44} = \varphi d r_3 - \omega d r_2$	$g_{45} = -(\varphi d s_2 + \omega d s_3)$	$g_{46} = -(\varphi d s_1 + \omega d s_4)$	$g_{47} = -(\varphi d s_4 - \omega d s_1)$	$g_{48} = -(\varphi d s_3 - \omega d s_2)$	0
19	$g_{51} = r_1 - v r_4$	$g_{52} = r_2 - v r_3$	$g_{53} = r_3 + v r_2$	$g_{54} = r_4 + v r_1$	$g_{55} = s_1 - v s_4$	$g_{56} = s_2 - v s_3$	$g_{57} = s_3 + v s_2$	$g_{58} = s_4 + v s_1$	0
17	0	0	0	0	$g_{65} = \varphi b s_2 - \omega b s_3$	$g_{66} = \varphi b s_1 - \omega b(s_4-1)$	$g_{67} = \varphi b(s_4-1) + \omega b s_1$	$g_{68} = \varphi b s_3 + \omega b s_2$	$\frac{b}{d}\cdot\frac{P}{kd}(\varphi^2+\omega^2)d^2$
23	0	0	0	0	$g_{75} = 1$	0	0	$g_{78} = -1/v$	0
21	0	0	0	0	0	$g_{86} = 1$	$g_{87} = -\varphi/\omega$	0	0

Fig.49 Matrix elements of the equilibrium and boundary equation set of the deflection in single shear

With $d/w = 0.2$, $k = E$ and $k/E_f = 1$, Figure 50 shows results of numerical computations for the case $a = b$. It may be seen that the axial tightening of bolts or rivets has a fundamental influence on stresses and displacements in the single shear case. With the usual values of a/d ranging from 0.4 to 0.6, displacements and bearing load concentrations are very much increased if, owing to a manufacturing defect or to loosening in service, the axial tightening is low, thus nullifying the holding effect of the fastener heads. Moreover, very long rivets ($a/d > 0.6$) having an enclosed total strip thickness greater than 1.2 diameters tend to behave in the same way as free end pins.

The actual stressing, by shear stresses at the hypothetical interfaces of the thin laminae which are assumed to constitute the actual mass of the strips, must stiffen the strips at bearing concentration points and increase bearing load concentration factors, whereas the local flattening of the pin cross section must have the opposite effect. For lack of other information, it has been proposed[57] to apply again the correction suggested by the results of displacement tests in symmetrical assemblies under double shear, that is to say, the correction

$$(\partial)_{\text{corrected}} = (\partial)_{\text{computed}} \left(0.8 + 0.3\,\frac{E}{E_f}\right). \tag{28}$$

For the limiting case of *very tight heads*, Figures 51 and 52 give the deflection coefficients and the bearing load concentration factors. The influence of the thickness ratio, b/a, is shown better in Figure 53. For the short fastener shanks, deflections and K_q-values are comparable with those of the symmetrical double shear case, but they increase and tend towards the values of the single-shear case with the increase of a/d.

5.2.4 Evaluation of Stress Concentrations

With the two causes of stress concentration at a fastener hole edge, either by the external loading of the sheet or by the bearing load transferred by the fastener, the highest stresses occur at the ends of the hole diameter perpendicular to the direction of load. The fatigue crack source to be considered being at the same point at the interface of joined sheets, the stresses may be superimposed. However, there is a difference between the two causes in that the stress concentrations due to bearing are always in tension, since the bearing pressure applies to the opposite half of the hole surface when the sign of the load changes. Figure 54 illustrates this behaviour in the more frequent case of fatigue critical fasteners, where no compressive stress occurs although the external loading changes from tension to compression.

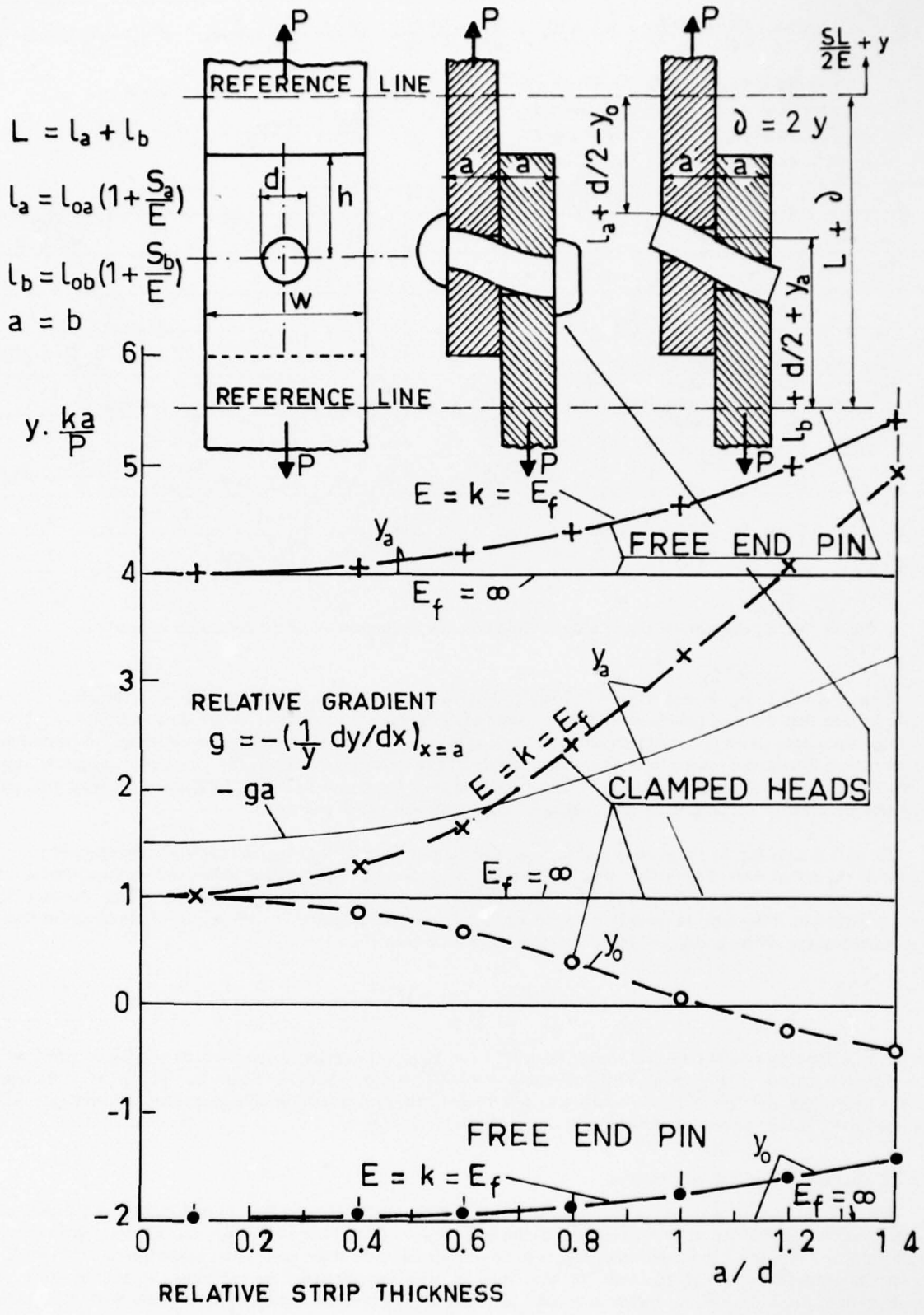

Fig.50 Bearing displacements in single shear of a fastener between two strips. d/w = 0.2

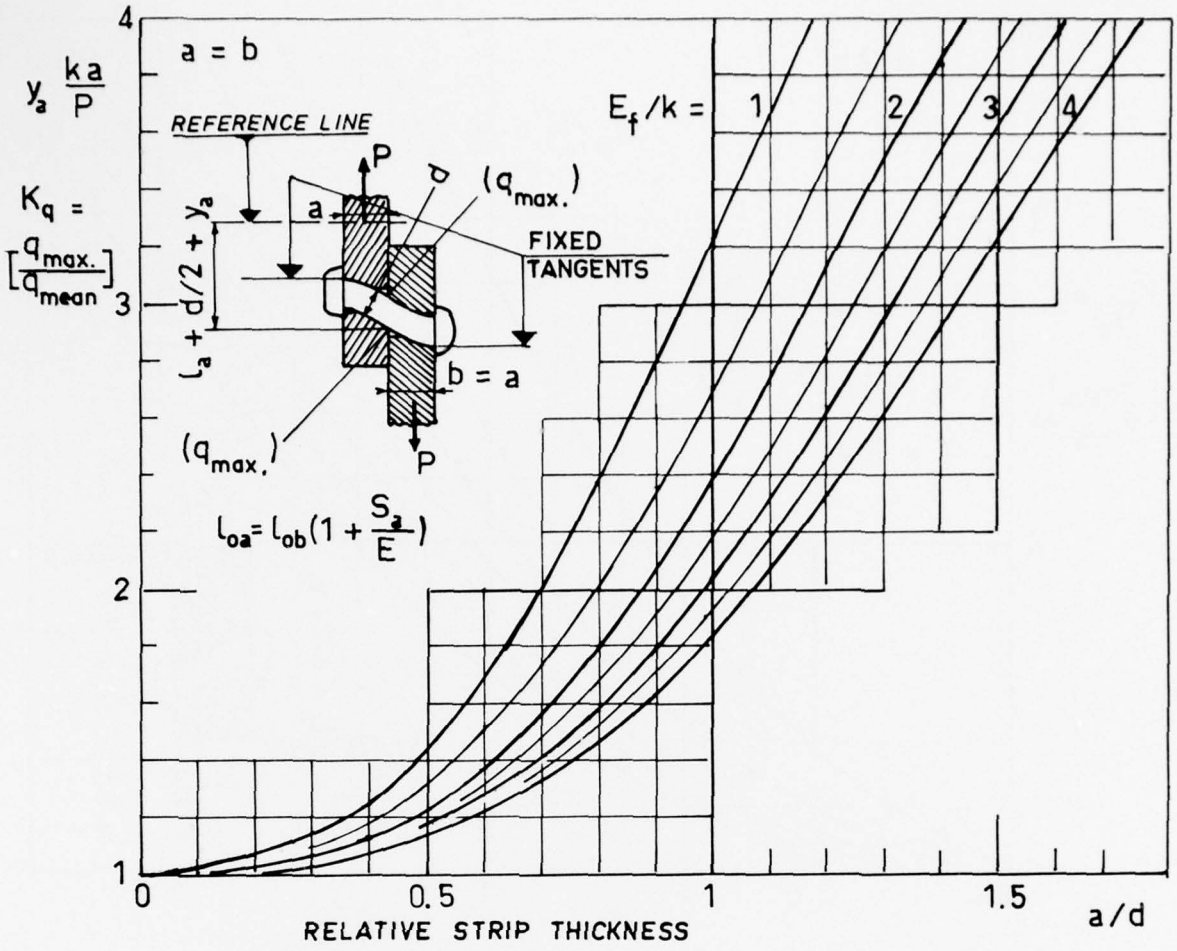

Fig.51 Bearing load concentration factor. Single shear of a fastener with clamped heads. a = b

Suppose that a strip, of width w and thickness t, is subjected to a direct tensile load and to a transferred load, P_1, applied to a hole surface by a fastener; the highest stress, S_{max}, is the sum of three terms defined as follows:

– The *direct concentration stress*, $\Delta S_{max\,1}$, due to the direct stress $(S_n - P_1/wt)$ bypassing the hole, is

$$\Delta S_{max\,1} = K_T(S_n - P_1/wt), \tag{29}$$

where K_T *is the usual stress concentration factor corresponding to the hole when plugged by the fastener shank* (see Figure 45).

– The *stress concentration due to the transferred load* consists of two terms:

– the term corresponding to the *mean bearing pressure*, $p = P_1/td = q_{mean}/d$, is

$$\Delta S_{max\,2} = \frac{q_{mean}}{d}(1 + \lambda^2)/(1 - \lambda), \tag{30}$$

where $\lambda = d/w$;

– the term corresponding to the *secondary bearing load* Δq is

$$\Delta S_{max\,3} = c\frac{\Delta q}{d}(1 + \lambda^2)/(1 - \lambda) = \Delta S_{max\,2}(K_q - 1), \tag{31}$$

where K_q is the bearing load concentration factor, and

c is a correction coefficient which should take account of the lessening of the stress concentration from the point of bearing load concentration to that of highest tensile stress, and of the possible opposite effect of the strips being composed of separate thin sheets. Until other information is available, c will be assumed equal to 1.

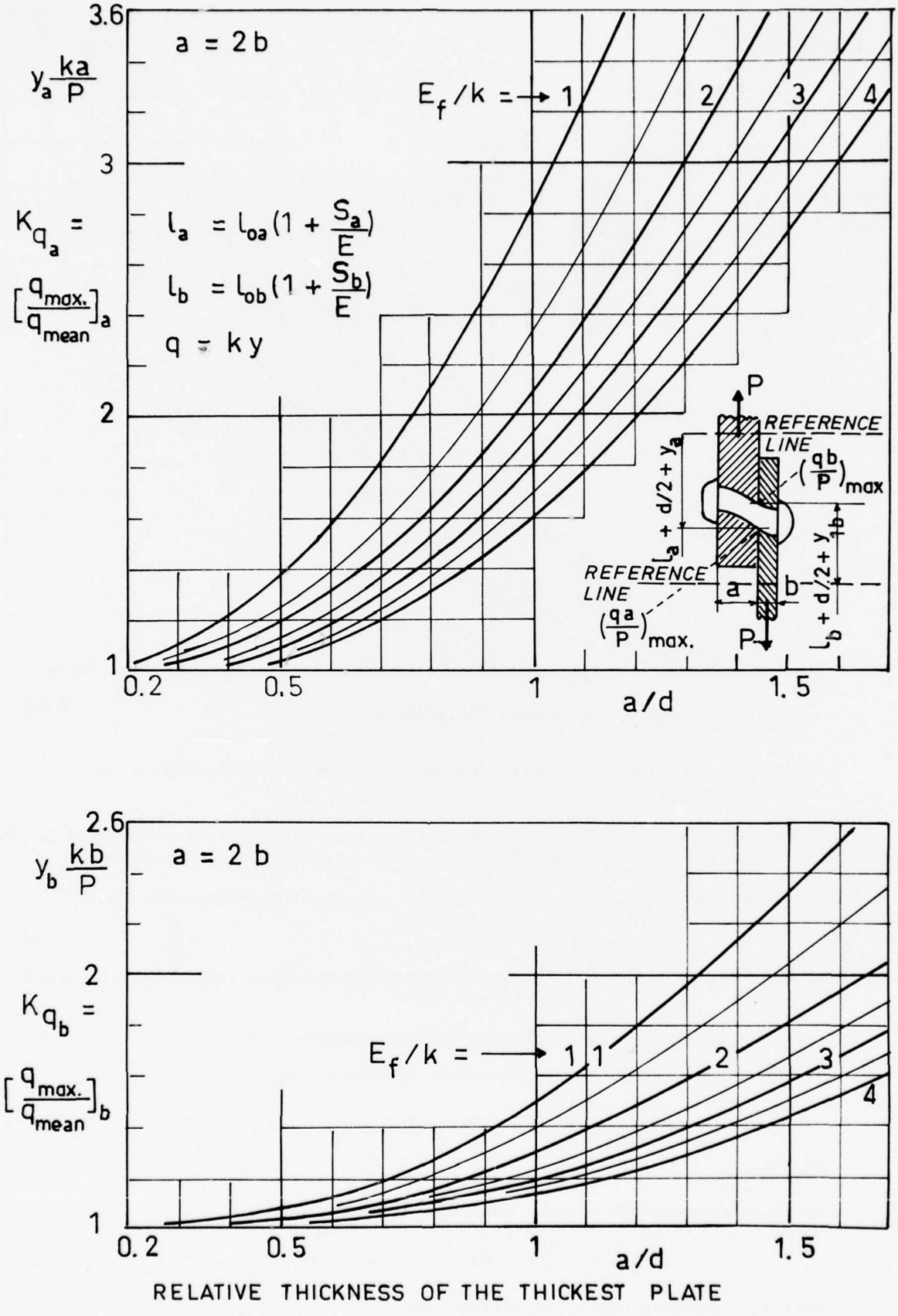

Fig.52 Bearing load concentration factor. Single shear of a fastener with clamped heads. a = 2b

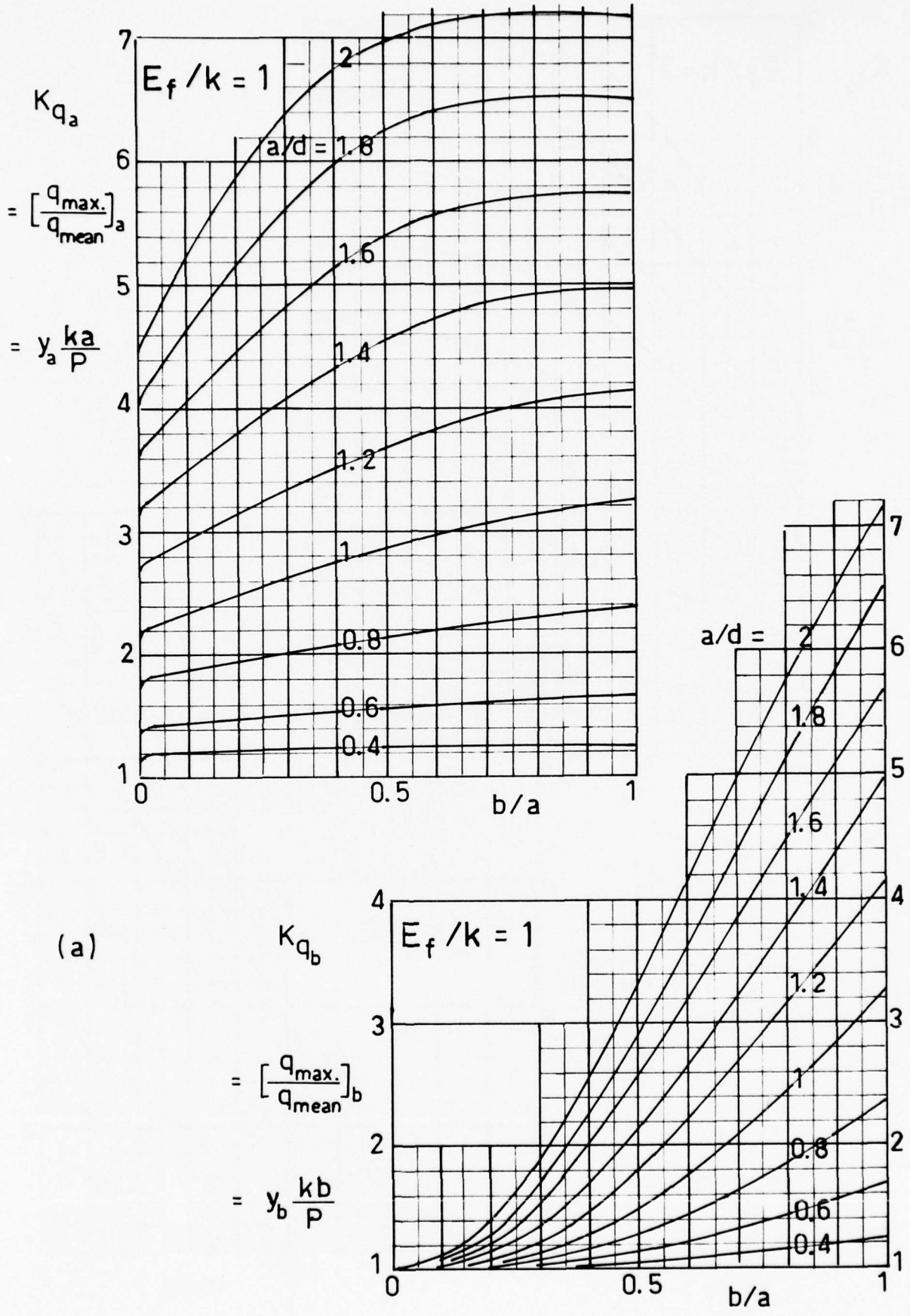
K_{q_a}
$= \left[\frac{q_{max.}}{q_{mean}}\right]_a$
$= y_a \frac{ka}{P}$
$E_f/k = 1$
a/d = 1.8
2
1.6
1.4
1.2
1
0.8
0.6
0.4
b/a
0
0.5
1
(a)
K_{q_b}
$= \left[\frac{q_{max.}}{q_{mean}}\right]_b$
$= y_b \frac{kb}{P}$
$E_f/k = 1$
a/d =
2
1.8
1.6
1.4
1.2
1
0.8
0.6
0.4
b/a

Figure 53(a)

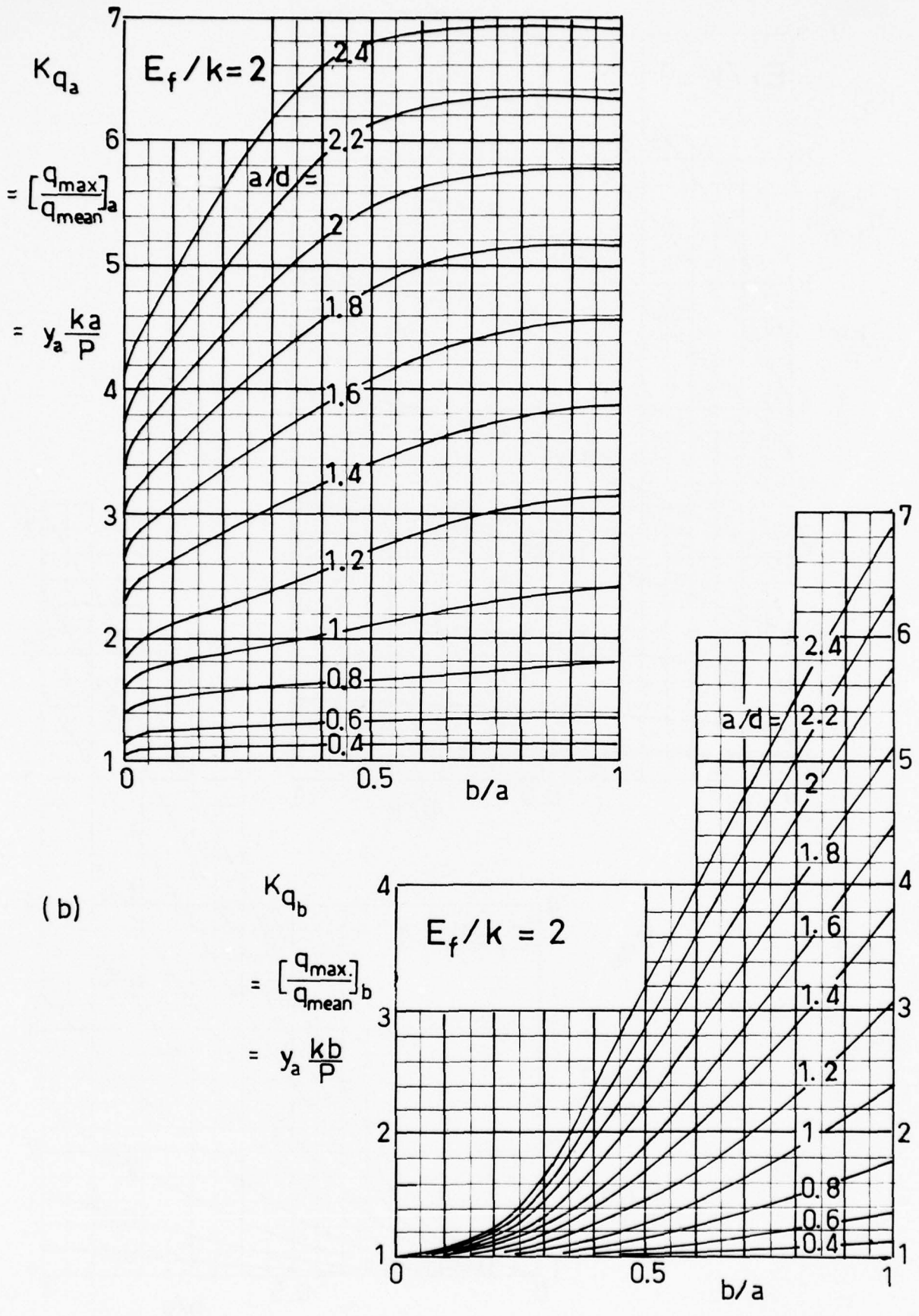
K_{q_a}
$= \left[\frac{q_{max}}{q_{mean}}\right]_a$
$= y_a \frac{ka}{P}$
$E_f / k = 2$
a/d =
2.4
2.2
2
1.8
1.6
1.4
1.2
1
0.8
0.6
0.4
b/a
0
0.5
1
1
2
3
4
5
6
7
(b)
K_{q_b}
$= \left[\frac{q_{max}}{q_{mean}}\right]_b$
$= y_a \frac{kb}{P}$
$E_f / k = 2$
a/d =
2.4
2.2
2
1.8
1.6
1.4
1.2
1
0.8
0.6
0.4
b/a
0
0.5
1
1
2
3
4
5
6
7

Figure 53(b)

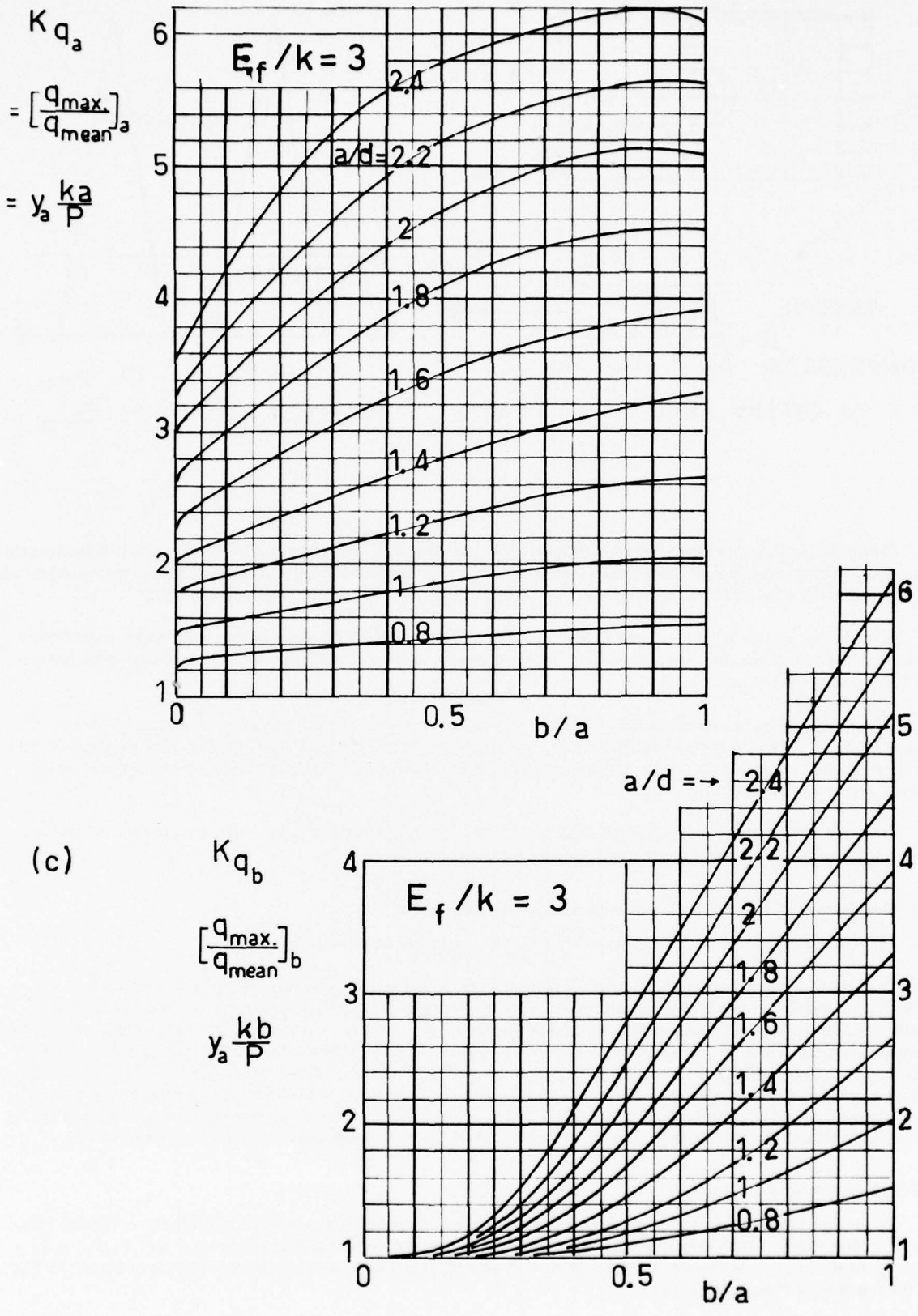
$K q_a$
$= \left[\frac{q_{max.}}{q_{mean}}\right]_a$
$= y_a \frac{ka}{P}$
$E_f / k = 3$
a/d = 2.4
2.2
2
1.8
1.6
1.4
1.2
1
0.8
b/a
(c)
$K q_b$
$\left[\frac{q_{max.}}{q_{mean}}\right]_b$
$y_a \frac{kb}{P}$
$E_f / k = 3$
a/d =→
2.4
2.2
2
1.8
1.6
1.4
1.2
1
0.8
b/a

Figure 53(c)

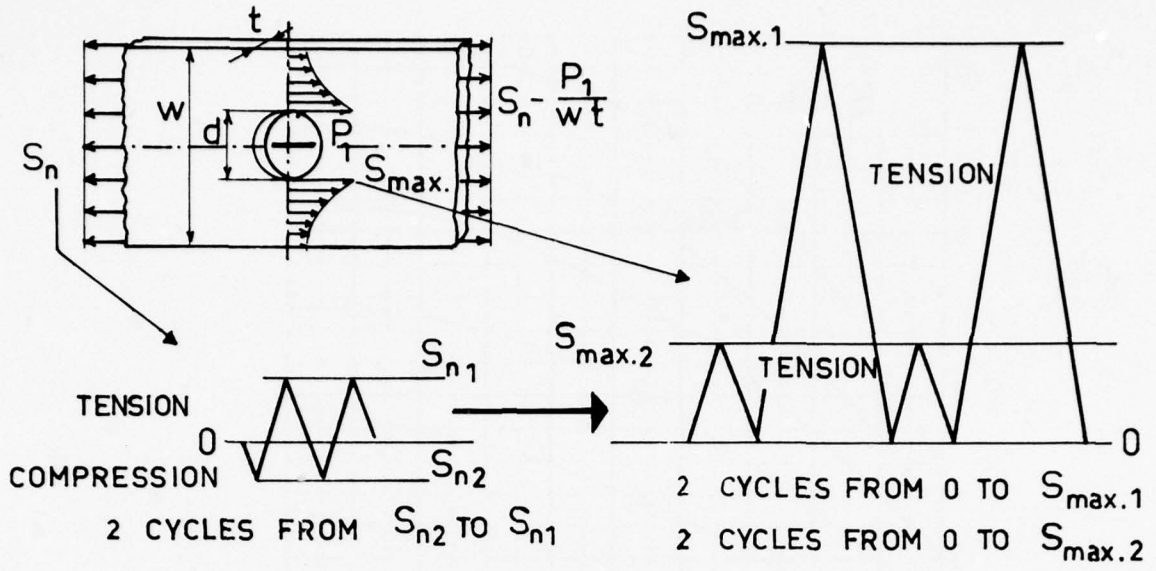

Figure 54

Critical fastener holes correspond to high values of the bearing load concentration factor K_q and it is noteworthy that, despite some incursions of the external loading into the compression domain, the highest stresses at hole edges will be tensile in most cases, if not always, for areas of aircraft structures that are stretched in level flight.

In structural regions where the nominal stresses are compressive in level flight, fatigue cracks often occur in thin sheet skin at points where the compressive skin buckling creates bending tensile stresses near the ends of stiffeners, reinforcing strips or fittings.

With heavy compressive stresses, fatigue cracks may occur at the edge of an open hole, owing to the plastic accommodation of the stress-strain fatigue cycle. From laboratory tests at CEAT (Ref.70), the crack propagation rate is very slow compared with that of the tensile-tested specimen. This mode of fatigue cracking is not possible when fasteners are without significant clearance.

However, although this is rare, fatigue cracks may originate from tensile stresses resulting from bearing stresses due to the compressive loads that are transferred by the critical fasteners.

5.3 Distribution of Transferred Loads in Strips Joined by Fasteners

From Reference 57, it is useful to recall the following summary and discussion.

In order to avoid outside protrusion or roughness, local reinforcements of aircraft wing skins and fuselage skins are often put on inside surfaces and their fasteners are stressed in single shear. The same is true for fasteners attaching ancillary equipment or its mounting onto internal members of the structure such as fuselage frames or thin webs of the wing or tail spars. These additional components are stretched, owing to the elongation of the members underneath, and their reactions overload the main members at the edges of fastener holes. Besides the higher bearing concentration factors occurring in practice for various cases of single shear, the further example considered emphasizes the practical importance of the general problem of the additional surface elements stretched by the elongation under load of the principle structural members below them, in which premature fatigue damage may occur at overstressed holes.

5.3.1 Formation of Equations

In the case of double shear, the assembly investigated and its model are represented respectively in Figures 55(a) and (b), after Vogt[53]. With the same notation, Figure 55(c) corresponds to the single shear case. Let $P_1, P_2, \ldots, P_{n-1}$ and P_n be the loads transferred by each fastener, rivet or bolt. The tensile loads in the central strip of Figure 55(b) or in the top strip of Figure 55(c) are

$$Q_1 = P_1, \quad Q_2 = P_1 + P_2, \ldots, \quad Q_i = \sum_1^i P_k, \tag{32}$$

with

$$P_i = Q_{i+1} - Q_i. \tag{33}$$

In the set of top and bottom strips of Figure 55(b) or in the lower strip of Figure 55(c), the tensile loads are

$$R_1 = P - Q_1 , \ldots\ldots , R_i = P - Q_i . \tag{34}$$

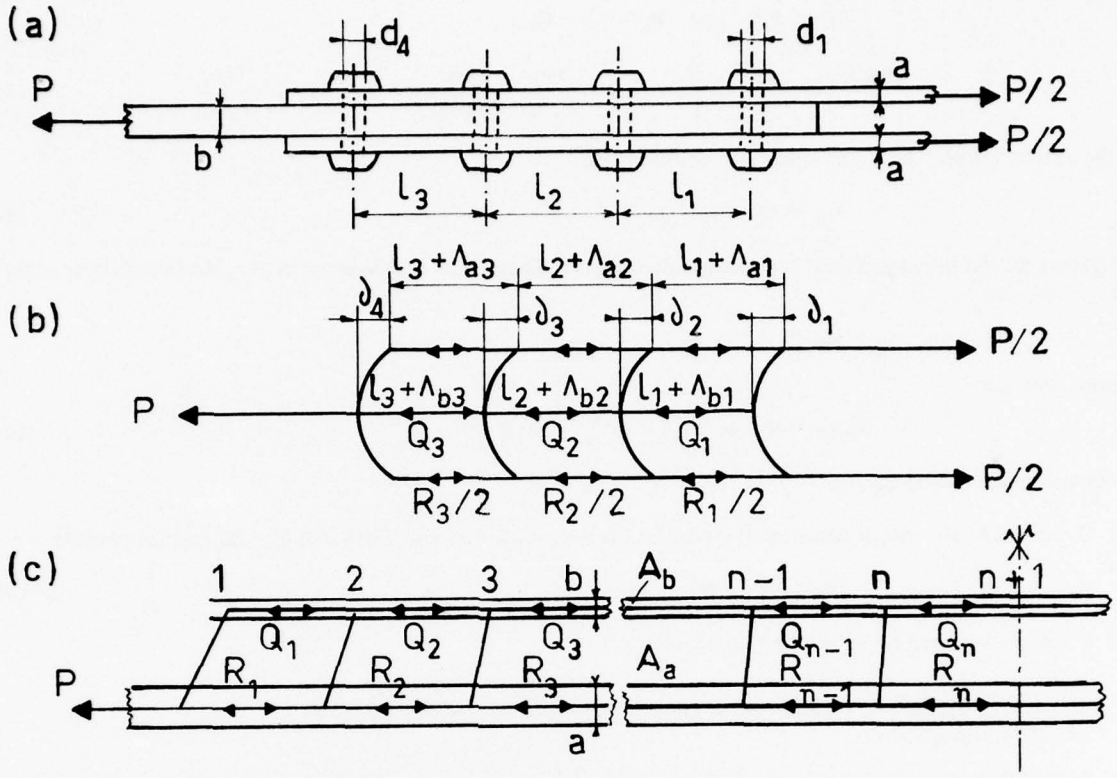

Fig.55 Models of spliced joint and of reinforced joint

The relative displacement of strips due to bearing stresses may be written as

$$\partial_i = P_i f_i , \tag{35}$$

where f_i is the coefficient of relative displacement between the strips, taking account of the local strains of rivet and strips with respect to the state of stress assumed in the calculations, i.e., the uniform distribution of the stress through the strip widths and along the strip length between two successive fasteners which are origins of transverse lines at which the tensile stress in the strip is assumed to vary in abrupt steps. With $k = (1 - \lambda)E/0.8$, where $\lambda = d/w$, d is the hole diameter, w is the strip width, E is the elastic modulus of the strip, and with the values of $y_a ka/P$ and $y_b kb/P$ given in Figures 50 to 53 as functions of E_f/k, a/d and b/a, the displacements y_{ai} and y_{bi} between each reference line and the fastener centres may be computed. Then the relative displacements are

$$\partial_i = y_{ai} + y_{bi} . \tag{36}$$

The theoretical elongations of the centre and side strips are respectively

$$\Lambda_{ai} = \alpha_i R_i l_i / E_a A_{ai} \quad \text{and} \quad \Lambda_{bi} = \beta_i Q_i l_i / E_b A_{bi} , \tag{37}$$

where l_i is the distance between the successive fasteners numbered i and i + 1,

A_{ai} and A_{bi} are respectively the cross-sectional areas of centre and side strips in the span l_i between fasteners i and i + 1,

E_a and E_b are the elastic moduli of the strips,

α_i and β_i are coefficients which take account of the effect of the holes on the elongation of the strip. From Equation (6), these coefficients are approximately $1 + (d/l)([1.3/(1 - \lambda)] - 1)$ for a plain hole; no value is available for a plugged hole and so the same value will be used provisionally.

Within the distance between two fasteners, the compatibility of displacements implies

$$\partial_i - \partial_{i+1} = \Lambda_{ai} - \Lambda_{bi} \tag{38}$$

and, with

$$\partial_i = P_i f_i \quad \text{and} \quad P_i = Q_i - Q_{i-1} ,$$

$$-Q_{i-1} f_i + Q_i \left[f_i + f_{i+1} + \frac{l_i \alpha_i}{E_a A_{ai}} + \frac{l_i \beta_i}{E_b A_{bi}} \right] - Q_{i+1} f_{i+1} = \frac{P l_i \alpha_i}{E_a A_{ai}} . \tag{39}$$

In the case of a *spliced joint*, the boundary conditions are

$$Q_o = 0 \quad \text{and} \quad Q_n = P . \tag{40}$$

In the case of a *reinforcing strip* of symmetrical design with respect to its middle cross section, the boundary conditions are

$$Q_o = 0$$

at both ends, and

$$\partial_{n+1} = 0 \quad \text{or} \quad f_{n+1} = P_{n+1} = 0 \tag{41}$$

at the middle plane of symmetry.

If, instead of one row of fasteners, there are m parallel rows, the load transferred by each fastener becomes

$$P_i = (Q_i - Q_{i-1})/m \tag{42}$$

and f_i must be replaced by f_i/m in Equation (42).

5.3.2 Example of Elasticity Computations of Load Transfer and Stress Concentrations in a Reinforcing Strip

As for other examples treated later, this example corresponds to actual fatigue damage occurring during a full-scale fatigue test carried out in the open air with the aircraft fuselage immersed in a tank of water. Following the analysis of this damage, practical improvements in inspection and maintenance procedures have eliminated any risk of damage occurring in actual service. In some cases the original data have been modified so as to make possible a simplified explanation of the technical aspects of the problem, but the stress levels and values of the stress concentration factors have been preserved in order to retain the full value of the conclusions.

The reinforcing strip is represented in Figure 56. This strip was attached to the inside surface of an aircraft wing lower skin between two adjacent stringers.

The problem data are as follows:

- Skin of 2024-T3 aluminium alloy sheet. Thickness a = 4.8 mm, E_a = 70,000 N/mm² . 2024-T3 extrusion stringers. Cross-sectional area of the skin and of the associated stringer, A_a = 1000 mm² .
- Reinforcing strip made from 2024-T3 aluminium alloy sheet. Thickness varying from 1.5 mm at the ends to 3 mm at the middle cross section; width = 65 mm, $E_{strip} = E_a$.
- 4 mm-diameter steel rivets in two rows 45 mm apart. The part of the strip associated with one row of rivets is 32.5 mm wide. $E_{rivet} = E_f$ = 210,000 N/mm² .
- Ratios:

  The effective width of the skin and its associated stringer may be taken as $A_a/2a$ = 104 mm ; d/w = 4/104 = 0.04 and k = (1 − d/w)E/0.8 = 1.2E .

  The corresponding ratio E_f/k is 210,000/(70,000 x 1.2) = 2.5.

  In the reinforcing strip, d/w = 4/32.5 = 0.123 and k = 0.877E/0.8 = 1.1E and E_f/k = 2.73 . The cross-sectional areas of the strip are given in Figure 56. a/d = 4.8/4 = 1.2 .

  In the computation of ∂ , the average value E_f/k = 2.6 is used. b/a varies from 1.59/4.8 = 0.33 to 3/4.8 = 0.625 .

Computations not reproduced here show that the part of the load transferred by the first, most critical rivet depends only little on the exact values of $Ef_i = E\partial/P = (E/P)[K_{q_a} + (a/b)K_{q_b}]$. Therefore, the interpolation used to derive values of K_{q_a} and K_{q_b} from Figures 50 to 53 may be quite crude.

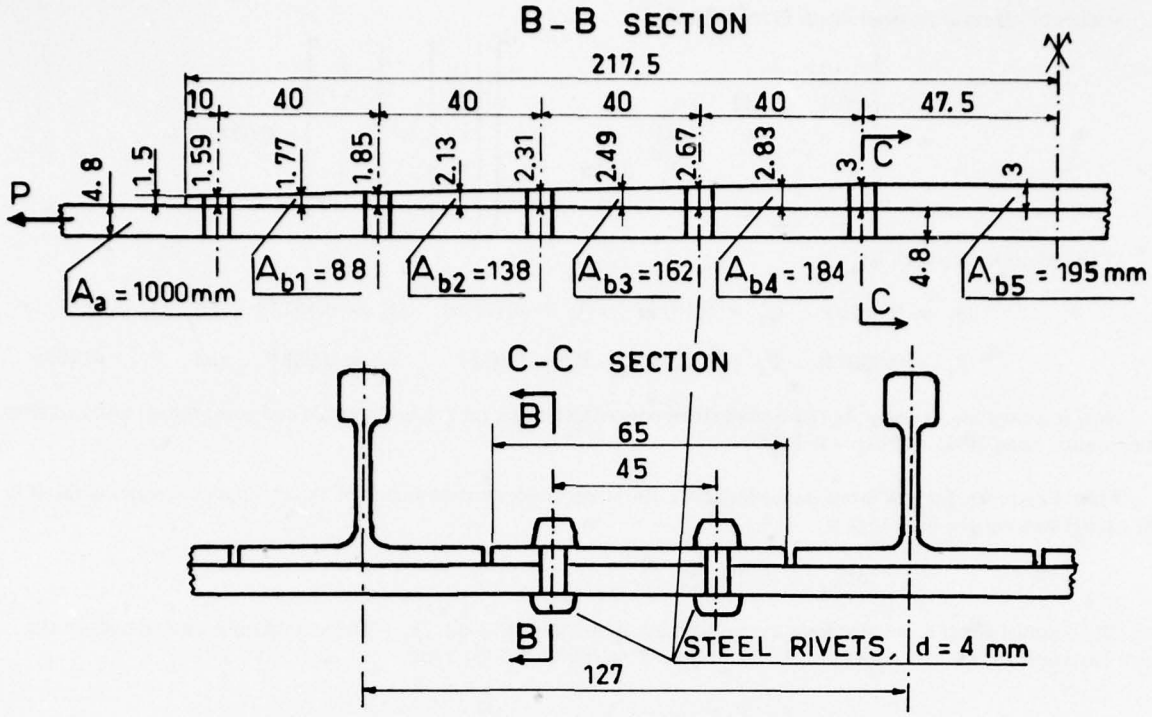

Figure 56

On the average, for *pins with free ends*, $\partial = 10\,P/ka$ and $Ef_i = E\partial/P = (\partial ka/P)(E_f/k)(E/E_f)/a = 10 \times 2.6(70{,}000/210{,}000)/4.8 = 1.806$; for the other limiting *case of clamped rivet heads*, $\partial = 5.7\,P/ka$ and $Ef_i = 0.98$. For two rows of rivets and with the correction factor $0.8 + 0.3(E/E_f) = 0.9$,

$$Ef_i/2 = \begin{cases} 0.81 & \text{for pins with free ends, and} \\ 0.44 & \text{for the clamped head case.} \end{cases}$$

Dividing f_i by 2 and multiplying all the terms of the Equation (39) by $E_a = E_b = E$, we have

$$-Q_{i-1}\frac{Ef_i}{2} + Q_i\left[\frac{Ef_i}{2} + \frac{Ef_{i+1}}{2} + \frac{\alpha_i l_i}{A_{ai}} + \frac{\beta_i l_i}{A_{bi}}\right] + Q_{i+1}\frac{Ef_{i+1}}{2} = \frac{\alpha_i l_i}{A_{ai}}P\,. \tag{43}$$

The terms $\alpha_i l_i/A_{ai}$ have the values 0.041 for $i = 1, 2, 3$ and 4 and 0.049 for $i = 5$. The values of the terms $\beta_i l_i/A_{bi}$ are 0.475, 0.29, 0.26, 0.23 and 0.255 for $i = 1, 2, 3, 4$ and 5, respectively. From this, the following matrix equations are obtained after their elements have been multiplied by a common factor so that all subdiagonal elements become equal to -1.

– *Case of pins with free ends* (loose rivets):

$$\begin{bmatrix} 2.637 & -1 & & & \\ -1 & 2.409 & -1 & & \\ & -1 & 2.372 & -1 & \\ & & -1 & 2.335 & -1 \\ & & & -1 & 1.365 \end{bmatrix}\begin{bmatrix} Q_1 \\ Q_2 \\ Q_3 \\ Q_4 \\ Q_5 \end{bmatrix} = \begin{bmatrix} 1 \\ 1 \\ 1 \\ 1 \\ 1.195 \end{bmatrix} \times 0.0506P\,,$$

the solution of which is:

$$Q_1 = 0.0537P\,,\quad Q_2 = 0.091P\,,\quad Q_3 = 0.115P\,,\quad Q_4 = 0.131P \text{ and } Q_5 = 0.140P\,,$$

$$P_1 = 0.027P\,,\quad P_2 = 0.019P\,,\quad P_3 = 0.012P\,,\quad P_4 = 0.008P \text{ and } P_5 = 0.005P\,.$$

– *Case of clamped fastener heads* (very tight rivets):

$$\begin{bmatrix} 3.173 & -1 & & & & \\ -1 & 2.752 & -1 & & & \\ & -1 & 2.684 & -1 & & \\ & & -1 & 2.616 & -1 & \\ & & & -1 & 1.672 \end{bmatrix} \begin{bmatrix} Q_1 \\ Q_2 \\ Q_3 \\ Q_4 \\ Q_5 \end{bmatrix} = \begin{bmatrix} 1 \\ 1 \\ 1 \\ 1 \\ 1.195 \end{bmatrix} \times 0.0932P ,$$

the solution of which is:

$$Q_1 = 0.0614P , \quad Q_2 = 0.1017P , \quad Q_3 = 0.1252P , \quad Q_4 = 0.1413P \text{ and } Q_5 = 0.1511P ,$$

$$P_1 = 0.0307P , \quad P_2 = 0.020P , \quad P_3 = 0.012P , \quad P_4 = 0.008P , \text{ and } P_5 = 0.005P .$$

Now it is possible to compute the overall stress concentration factor for both tensile and compressive nominal stress. The nominal stress is $S_n = P/A_a = P/1000$.

From Figure 45, for low interference fasteners, the stress concentration factor of axially applied stresses is about 2. The partial stress at the hole edge is

$$\Delta S_{max\,1} = 2S_n ,$$

since the nominal stress is not significantly reduced by the transferred load $2P_i$. The second term corresponds to the mean bearing load. On the average of the two cases, $P_1 = 0.03P = 30S_n$, and

$$\Delta S_{max\,2} = \frac{P_1}{td}(1 + \lambda^2)/(1 - \lambda) = \frac{1.04 \times 30}{4 \times 4.8} S_n = 1.63S_n .$$

The third term corresponds to the secondary bearing load resulting from the inclination and bending of the fastener shank. It should be multiplied by a correction coefficient, $c \leqslant 1$, the value of which is not yet known and is taken as 1:

$$\Delta S_{max\,3} = \Delta S_{max\,2}(K_{q_a} - 1) ,$$

where $K_{q_a} = 5.3$ for pins with free ends (Figure 28 of Reference 57, a/d = 1.2, b/a = 0.33 and $E_f/k = 2.6$) and $K_{q_a} = 2.3$ for clamped fastener heads (Figures 52 and 53, a/d = 1.2, b/a = 0.33 and $E_f/k = 2.6$). Then,

$$\Delta S_{max\,3} = \begin{cases} 7S_n & \text{for pins with free ends, and} \\ 2.12S_n & \text{for clamped heads.} \end{cases}$$

In *tension* the overall maximum stress is

$$S_{max} = \begin{cases} 10.6S_n & \text{or} \\ 5.8S_n . \end{cases}$$

In *compression*, $S_n \leqslant 0$, for high negative S_n-values, the load transferred by a fastener tends to create tensile stresses at the hole edge. As long as the bearing load is transferred by the whole of the hole surface, owing to the pressure being reduced over one half of the hole surface and increased over the other half, the stress concentration due to the transferred load is divided by 2 as long as contact is maintained, i.e., longer in the presence of nominal compression than in the case of tension with an interference-fit fastener. Moreover, the stress concentration factor associated with the direct compressive load bypassing the hole will be 1. Therefore, an upper limit of the ratio S_{max}/S_n will be obtained by replacing $\Delta S_{max\,1}/S_n$ of the tensile case by -1, the other partial values being considered as upper limits for $\Delta S_{max\,2}/S_n$ and $\Delta S_{max\,3}/S_n$. In the present case, the values are:

$$\Delta S_{max\,1}/S_n = -1$$

$$\Delta S_{max\,2}/S_n \leqslant 1.63$$

$$\Delta S_{max\,3}/S_n \leqslant \begin{cases} 7 & \text{for pins with free ends, and} \\ 2.12 & \text{for clamped heads.} \end{cases}$$

Superimposing these values we obtain the upper limits of the tensile stress concentration factors for a compressive nominal stress:

$$S_{max}/S_n \leqslant \begin{cases} 7.63 & \text{for pins with free ends, and} \\ 2.78 & \text{for clamped heads.} \end{cases}$$

This means that fatigue cracks due to compressive nominal stresses would occur in compressed regions only at badly designed fasteners.

5.4 Computation of Damage Adjustment Factors

As defined in Section 5.1, the *damage adjustment factor*, k_{DA}, is mainly a multiplying factor for all load levels used in connection with laboratory S–N curves of notched specimens, to make the value 1 of the Miner damage correspond to the physical damage occurring during a full-scale fatigue test. The value of k_{DA} so computed may be used (a) in *comparative computation* of fatigue life with other loading spectra, and (b) in fatigue life evaluation *for the same environment* and a slightly modified local design.

5.4.1 Superposition of Stress Concentrations

To clarify our ideas, we consider the case of a wing box lower skin in a region containing a number of fuel tank access doors, some numbers in the example being modified for publication. In the course of a full-scale fatigue test in the open air, and after 8000 cycles of a severe loading programme that was applied on a flight-by-flight basis, fatigue cracks appeared at fastener holes of access doors in the machined skin. The seven cracked door frames and the neighbouring structural elements had the same technical design but differed in skin thickness, and the local stress levels varied slightly. The first visible crack appeared at a fastener hole in the less severely stressed door frame, which was attributed to a possible increase of scatter due to corrosion and control movements during operation. More careful investigation by means of an eddy current sensor then revealed other cracks, some tenths of a millimetre long, hidden under fasteners located at six access doors. Figure 57 shows (a) the sketch of the wing box structure considered, (b) the door assembly, (c) a schematic diagram of a typical problem, (d) the stress distribution on the door, the fastener holes being neglected, and (e) the superimposed stress distribution on the fastener.

In an infinitely extended plate, the stress distribution S_y under a stress of $S_x = S$, applied some distance from a circular hole of radius a, is

$$S_y/S = 1 + (a/x)^2[0.5 + 1.5(a/x)^2]\ ; \tag{44}$$

from the general expression for an elliptical hole (see Reference 21, p.140):

$$S_y/S = 1 + (1+k)u\left[\frac{1-k}{2} + (1-k)^2u(1.5+ku)\right],$$

where $$u = 1/(\xi^2 - k), \quad \xi = \frac{(1+k)}{2}\left[\frac{x}{a} + \sqrt{\left\{\left(\frac{x}{a}\right)^2 - \frac{4k}{(1+k)^2}\right\}}\right], \quad k = \frac{1-b/a}{1+b/a},$$

and then k is equated to zero.

For the plate of finite width, w, containing a circular hole of radius a, the distribution of S_y/S_{max} has been computed from numerical data (Howland[62]) as follows:

d/w	S_{max}/S	x/a →	1	1.025	1.05	1.075	1.1	1.15	1.20
0.5	4.32		1		0.875		0.770	0.700	0.637
0.4	3.74		1		0.886		0.795	0.723	0.665
0.2	3.14		1	0.944	0.894	0.850	0.810	0.742	0.686
0(w = ∞) 3			1	0.945	0.895	0.852	0.812	0.745	0.690

The last row is computed from the expression (44) with $S_{max}/S = 3$ and corresponds to an infinite plate. For $0 \leqslant d/w \leqslant 0.4$, this expression is sufficiently precise to be used in conjunction with an approximation to the stress concentration factor:

$$S_y/S = \frac{1}{3}\left[1 + \left(\frac{a}{x}\right)^2\left\{0.5 + 1.5\left(\frac{a}{x}\right)^2\right\}\right](S_{max}/S). \tag{45}$$

In the present case, $d/w = 300/1500 = 0.2$ and the stress concentration factor is $S_{max}/S = 3.14$. In the radial direction, the stress distribution is

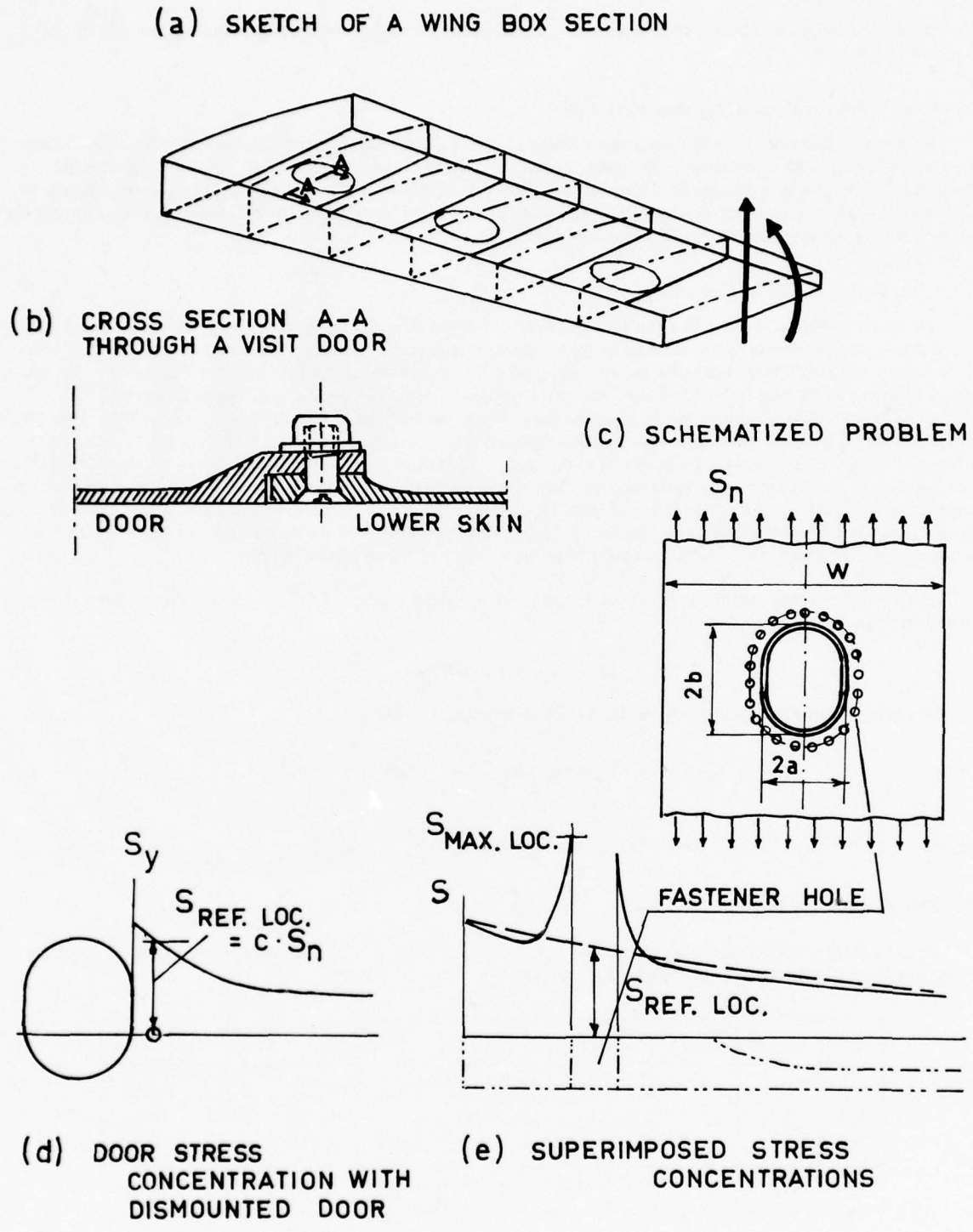
(a) SKETCH OF A WING BOX SECTION
A
A
(b) CROSS SECTION A-A
THROUGH A VISIT DOOR
DOOR
LOWER SKIN
(c) SCHEMATIZED PROBLEM
S_n
W
2b
2a
S_y
$S_{REF. LOC.}$
$= c \cdot S_n$
$S_{MAX. LOC.}$
S
FASTENER HOLE
$S_{REF. LOC.}$
(d) DOOR STRESS
CONCENTRATION WITH
DISMOUNTED DOOR
(e) SUPERIMPOSED STRESS
CONCENTRATIONS

Figure 57

(x − a) mm =	0	7.5	10	12.5	15	30
x/a =	1	1.05	1.067	1.083	1.1	1.2
S_y/S =	3.14	2.81	2.72	2.63	2.55	2.17

It may be seen that, near the edge of a large circular hole and around the position of a small hole not yet machined, $S_y/S = 2.72$ and the relative stress gradient in the radial direction is $(1/S)(\partial S/\partial n) = -0.013$. Using x/r as relative coordinate, where r is the curvature radius of an elliptic hole at the point of maximum stress and a is semi-major axis, it has been shown (Reference 21, p.142, Figure 4.12) that the distributions of S_y/S_{max} are similar for ellipses with r/a ranging from 0 (thin slot) to 0.1, and for the circle with $r/a = 1$. Extending this property to any plane stress concentration, it will be assumed from experience that the stress distribution is known, multiplying $S_{max}/S = K_T$ by

$$\frac{1}{3}\left[1 + \left(\frac{a}{x}\right)^2 \left\{0.5 + 1.5\left(\frac{a}{x}\right)^2\right\}\right].$$

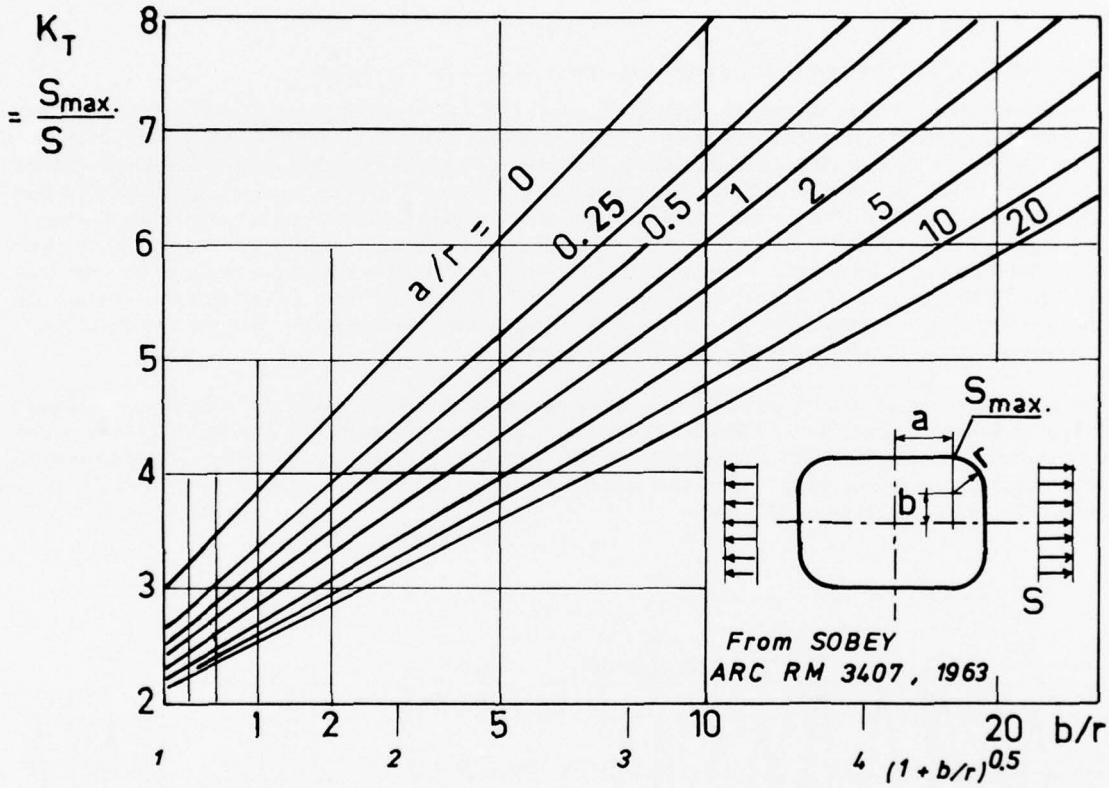

Figure 58

Returning to the actual rectangular door, for an infinite plate, Sobey[71] gave computed values of the stress concentration factor as shown in Figure 58. With $b/r = 0$ and $a/r = 50/150 = 0.33$, $K_T = 2.6$, instead of 3 for a circular hole. Multiplying the previous distribution by the correction factor 2.6/3 yields $S_y/S = 2.72 \times 0.87 = 2.37$ at the centre of the fastener hole.

For the fastener hole, considered alone, the model used would be that of Figure 59, the hole centre being distant 10 mm from the edge of an infinite plate[72]. With $d = 2a = 5$ mm and $c = 10$ mm, $a/c = 0.25$, hence $S_A/S = 3.19$, $S_B/S = 3.08$ and $S_C/S = 0.9$. At the edge of the fastener hole, the critical point is A where $S_{yA}/S = 3.19$ for $S = 2.37 S_n$.

Therefore, the stress concentration factor evaluated at point A in the door aperture would be $2.37 \times 3.19 = 7.56$. This value should be increased further by a possible contribution of the load transferred by the fastener. Although fasteners are installed with clearance, a stress level of 100 N/mm² might produce an elongation of $100 \times 100/70{,}000 = 0.14$ mm, which might destroy the clearance effect and give place to bearing stresses over the fastener hole surface.

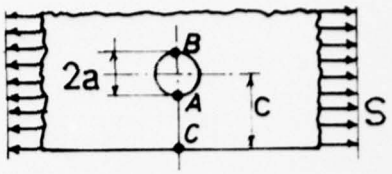

a/c	0	0.1	0.2	0.3	0.4	0.5	0.7
S_A/S	3	3.04	3.12	3.25	3.40	3.70	4.85
S_B/S	3	3.02	3.05	3.10	3.15	3.18	3.30
S_C/S	1	0.95	0.90	0.85.	0.80	0.70	0.50
$S_{AC\ mean}/S$	1	1.12	1.25	1.39	1.55	1.72	2.36

From MINDLIN SESA - V-No. 2, 1948.

Figure 59

5.4.2 Breakdown of Test or Flight Loading into Components for Damage Calculation

Independently of the formula used to compute numerical values of fatigue damage, the breaking down of time-dependent loading into components is very important in the practical interpretation of fatigue tests. In the early days, full-scale fatigue tests used for fatigue life determination of aircraft were performed by constantly applying to aircraft wings the equilibrium loads of level flight and by superimposing the repeated application of vertical gust loads corresponding to a gust velocity of 10 ft per second and occurring ten to twenty times during an average flight. Damage computations using the Miner-Palmgren rule were made by splitting the flight loads into a so-called ground-air-ground variation, between level flight and ground mean loads, and a series of alternating loads around each of the mean load values. This "ground-air-ground" component gave almost negligible computed damage, although some tests on small notched specimens or assemblies and the service behaviour of aircraft structures suggested that the actual effect of returning to the ground condition was important if not predominant.

In order to take account of the ground-air-ground transition, it has been proposed[73] to break down the diagram of loads applied during one flight into one fundamental component, defined by the highest and the lowest levels of the load programme, and complementary alternating loads. This *peak-to-peak* definition attributes to the ground-air-ground transition an importance comparable to the actual importance. Figure 60 illustrates the decomposition in the case used to explain the damage computation procedure.

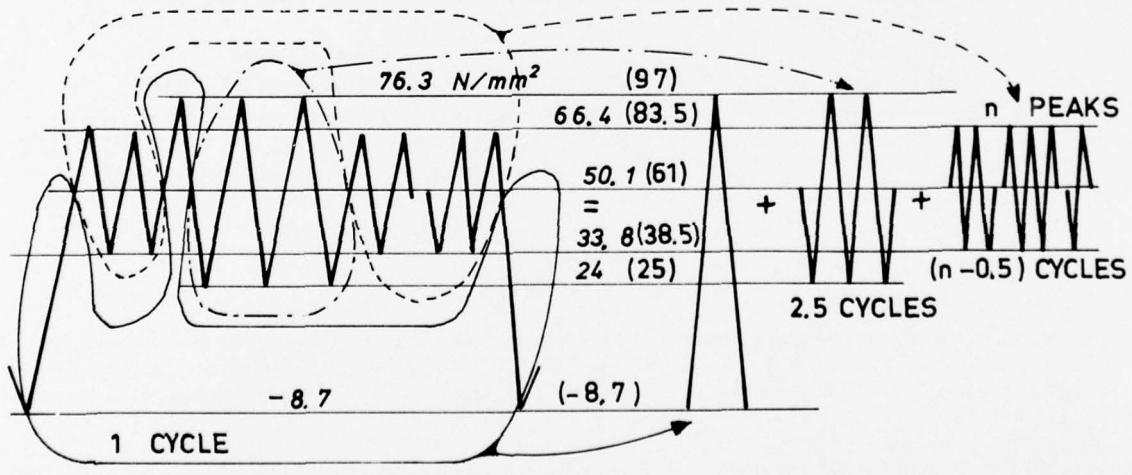

Fig.60 Breakdown of one-flight simulating test loading into constant amplitude components

For example, the nominal bending stresses applied to the structure considered previously are split into constant amplitude components as follows:

	S_{max}	S_{min}	S_{alt}	S_{mean}	n per programme
	N/mm²				
– for 1500 severe one-flight programmes:					
peak-to-peak	97	−8.7	52.85	44.15	1
alternating components:			36	61	2.5
			22.5	61	32.5 ;
– for 3500 moderate one-flight programmes:					
peak-to-peak	76.3	−8.7	42.35	33.8	1
alternating components:			26.1	50.1	2.5
			16.3	50.1	32.5

These nominal stresses would be too low to produce any damage in the absence of stress concentration. They must be multiplied by an appropriate factor so that the Miner damage may be computed, using a suitable region of the S–N curves. Figure 61 shows a set of $(K_T S_a - N) - K_T S_m$ curves for Alclad 2024-T3 aluminium alloy sheet and notched specimens having a notch radius $r = 1.5$ mm. These curves are considered representative for 3 mm- to 5 mm-diameter holes.

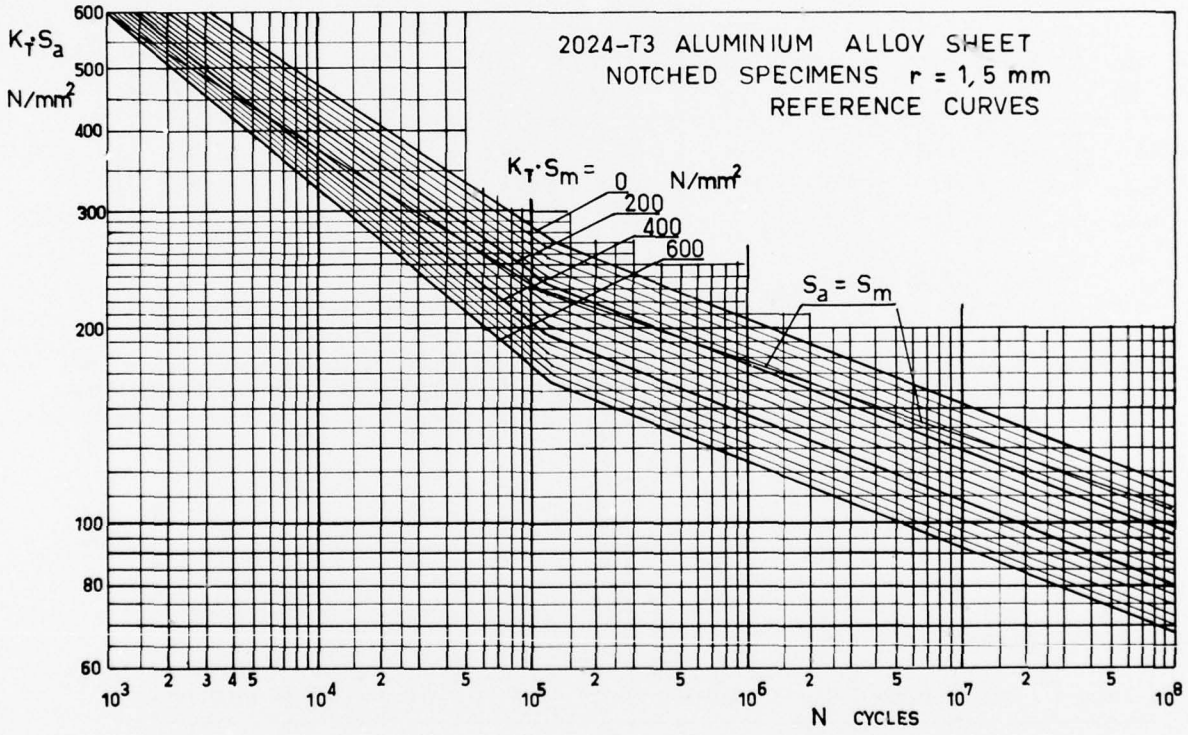

Figure 61

The multiplying factor may be applied to loads such as forces, bending moments, etc. and to stresses. Applied to nominal stresses, it becomes the damage-equivalent stress concentration factor, $K_{DE} = K_T k_{DA}$. In order to obtain comparable values of the damage adjustment factor, k_{DA}, the same set of S–N curves are used for structures made of Alclad 2024-T3 aluminium alloy sheet. This should allow us to clarify the relationship of k_{DA} to certain parameters of the assembly.

By a short trial-and-error procedure, the value $K_{DE} = 7.86$ has been determined such that the stresses $K_{DE}S$ correspond to unit value of the Miner damage:

S_{alt}	S_{mean}	n total	$N_{allowable}$	*Partial damage*
N/mm^2				
416	347	1,500	8,000	0.1875
283	479	3,750	23,000	0.1630
177	479	48,750	140,000	0.3482
333	266	3,500	21,000	0.1667
205	394	8,750	100,000	0.0875
128	394	113,750	2,700,000	0.0421

Overall Miner damage = *0.995*.

Now we assume a particular aircraft operation for which the cumulative frequency of flight load levels, $H = f(c)$, c being the flight load factor, has been evaluated. Taking account of the necessary breakdown of each one-flight load programme into one "fundamental", peak-to-peak, ground-air-ground load variation and alternating components around the 1g-level, the range of c will be divided into classes on each side of the value c_1 that would be reached or exceeded once per flight on the average. With $c \geqslant c_1$, each load is considered as occurring during one particular flight and the ground-air-ground variation must be used in damage computation. On the contrary, with $c < c_1$, the loads occur several times per flight and will be considered as alternating around the flight level load. In the present case and with one mean typical flight, the classes of the load programme would be as follows:

$c_1 = 0.488$; $\Sigma\Delta H = 1$

Δc	0.15	0.25	0.35	0.444	0.544	0.65	0.75	0.85	0.95	
ΔH	83.5	23.5	6.2	1.8	0.68	0.22	0.07	0.022	0.00	
ΔS	6.83	11.4	15.9	20	25	30	34	39	43	
S_{mean}	49	49	49	49	28.5	31	33	35.5	37.5	
S_{min}					−17	−17	−17	−17	−17	N/mm^2
S_{max}					74	79	83	88	92	
S_{alt}	6.83	11.4	15.9	20	45.5	48	50	52.5	54.5	

These nominal stress values must be multiplied by the damage-equivalent stress concentration factor, $K_{DE} = 7.86$, deduced from the fatigue test and corresponding to unit value of the Miner damage computed with the fatigue test duration corresponding to the actual damage considered. Then, the alternating and mean steady values of the stresses become

S_{alt}	53	90	125	157	358	377	393	413	428	N/mm^2
S_{mean}	385	385	385	385	224	244	259	279	295	
ΔH	83.5	23.5	6.2	1.8	0.68	0.22	0.07	0.022	0.008	
$N/10^4$	25,000	4000	400	70	2	1.4	1.1	0.9	0.67	
10^4 d	0.003	0.006	0.0155	0.0257	0.340	0.1571	0.064	0.0244	0.0119	

The damage per typical flight is $\Sigma\Delta H/N = 0.65 \times 10^{-4}$ and the fatigue life would be evaluated as 10,000/0.65 = 15,400 flights.

Using a reserve factor of 3 and considering an actual aircraft, it would be recommended to apply before 15,400/3 = 5100 flights the *maintenance procedure of hole reaming, eddy current control of the absence of microcracks, cold-work burnishing of the hole surface and the installation of fasteners of increased diameter.* This procedure eliminates possible microcracks, refreshes the metal and improves the surface condition by creating surface compressive residual stresses, thus extending the fatigue life considerably.

The damage computations are essentially comparative and the results are independent of any elasticity calculation. In the present problem, elasticity calculations related only to the limiting case where the fastener clearance was large enough for the access door to remained unstressed. The other limiting case of tight fasteners transferring some part of the load to the door is too complex and was not considered.

5.4.3 Interpretation of Fatigue Test Results on Joints in which Loads are Transferred Through Fasteners

In some cases, assemblies damaged during fatigue tests have simple local features facilitating the determination of the stress concentration factor. Numerous slight fatigue cracks, discovered after the completion of full-scale fatigue tests when dismantling assemblies in areas where damage occurred, have led to several numerical interpretations from which a relation might eventually be established between k_{DA} and certain assembly parameters.

We consider again the example of a reinforcing strip riveted onto the inside lower skin of an aircraft wing between two stringers and for which the elasticity calculation of Section 5.3.2 yielded the following values of the stress concentration factors:

$$K_T = \begin{cases} 10.6 & \text{for pins with free ends, and} \\ 5.8 & \text{in the clamped head case.} \end{cases}$$

Test stresses were computed from the test loading. Then compressive values of the nominal stresses were neglected and assumed to be zero since, as explained in Section 5.2.4, the predominant part of stresses is due to bearing pressures that are created by the loads transferred through the fasteners. For 7100 one-flight programmed loadings of two different degrees of severity, the nominal tensile stress variations were:

S_{alt}	75	48	30	69	44	27	} N/mm²
S_{mean}	75	100	100	69	95	95	
n	1500	3000	49,500	5600	11,200	185,000	

A short trial-and-error process supplied the value of the damage-equivalent stress concentration factor as $K_{DE} = 4.9$. The stresses become $K_{DE}S$ and, by using the reference curves of Figure 61, the computed partial Miner damages are:

S_{alt}	368	235	147	338	216	132	} N/mm²
S_{mean}	368	490	490	338	465	465	
n	1,500	3,000	49,500	5,600	11,200	185,000	
N	10,000	43,000	500,000	15,500	68,000	1.6×10^6	
d	0.150	0.116	0.099	0.361	0.165	0.115	

The overall damage, when the test damage occurs, is $D = 1$.

From the conclusions of investigations by damage computation of other test results, it seems that rivets or bolts installed with the usual axial tightening have a noticeable clamping effect and that it is suitable to use as reference the stress concentration factor computed in the limiting case of a theoretically perfect clamping of the fastener shank on the outside assembly surfaces through the head stiffness. This defines the k_{DA} damage adjustment factor as $k_{DA} = K_{DE}/K_T = 4.9/5.8 = 0.84$.

It is possible to arrive at a lower limit of the fatigue life increment due to the replacement of fasteners during maintenance. The beneficial effect might be provided (a) by a slight change in the distribution of loads transferred by the fasteners, (b) by a reduction of the bearing stresses and of the corresponding stress concentration factor due to increased fastener diameter, and (c) by improving the hole surface condition by finer machining and, in case of cold-work burnishing, owing to the surface compressive residual stresses delaying fatigue crack initiation before being reduced by fatigue accommodation. Only the items (a) and (b) may be refined by elasticity calculations.

In the present case of a reinforcing strip, it is assumed that the two end 4 mm-diameter rivets and the two nearest rivets are replaced by 5 mm-diameter rivets. The procedure described in Section 5.3.2 yields: average $E_f/k = 2.46$, average $Ef_i/2 = 0.42$, $\alpha_i l_i/A_{ai} = 0.047$ for $i = 1$ and 2, $\beta_i l_i/A_{bi} = 0.485$ for $i = 1$ and 0.309 for $i = 2$, $K_{q_a} = 1.82$ for $i = 1$. Other numerical data are not modified. The distribution of the transferred loads, which was: $P_1 = 0.0307P$, $P_2 = 0.020P$, $P_3 = 0.012P$, $P_4 = 0.008P$, $P_5 = 0.005P$ becomes: $P_1 = 0.0297P$, $P_2 = 0.0199P$, etc. It is seen that the load distribution is practically unaffected. The components of the maximum stress at the first fastener hole are

– direct tensile loading: $S_{max\,1} = 2S_n$ (not modified),

– mean bearing load: $S_{max\,2} = \dfrac{1.04 \times 30}{5 \times 4.8} S_n = 1.3S_n$

instead of $1.63S_n$ (increased rivet diameter),

– secondary bearing load: $S_{max\,3} = (K_{q_a} - 1)S_{max\,3} = 1.3 \times 0.82 = 1.07$.

The maximum stress at the critical end rivet hole becomes

$$S_{max} = 4.4S_n \quad \text{instead of} \quad 5.8S_n .$$

Assuming an actual aircraft, with the following statistical loading programme per mean typical flight:

S_{alt}	12.4	20.6	28.8	36.7	68.4	73	77	81	85	} N/mm²
S_m	92	92	92	92	68.4	73	77	81	85	
ΔH	83.5	23.5	6.2	1.8	0.68	0.22	0.07	0.022	0.008	

and using the preceding damage-equivalent stress concentration factors:

$$K_{DE} = \begin{cases} 4.9 & \text{before maintenance inspection and repair, and} \\ 3.7 & \text{after maintenance.} \end{cases}$$

$K_{DE}S$ stresses and the corresponding partial Miner damage are as follows:

– Without or before maintenance repair:

$K_{DE}S_{alt}$	61	101	141	180	335	358	377	397	417	} N/mm²
$K_{DE}S_{mean}$	451	451	451	451	335	358	377	397	417	
ΔH	83.5	23.5	6.2	1.8	0.68	0.22	0.07	0.022	0.008	
N	3×10^8	1.2×10^7	10^6	1.6×10^5	16,000	13,000	11,000	7500	6000	
$10^4\, d_i$	0.003	0.02	0.062	0.113	0.425	0.169	0.063	0.029	0.013	

The overall damage is 0.9×10^{-4} per flight. With a reserve factor of 3 the safe life before maintenance inspection and repair would be:

$$10{,}000/(0.9 \times 3) = 3700 \text{ flights} .$$

– After maintenance repair:

$K_{DE}S_{alt}$	46	76	107	146	253	270	285	300	315	} N/mm²
$K_{DE}S_{mean}$	340	340	340	340	253	270	285	300	315	
ΔH	83.5	23.5	6.2	1.8	0.68	0.22	0.07	0.022	0.008	
N	5×10^9	2×10^8	1.8×10^7	3×10^6	70,000	50,000	42,000	29,000	24,000	
$10^4\, d_i$	0.0002	0.0012	0.0034	0.0060	0.097	0.044	0.017	0.008	0.003	

The overall damage is $d = 0.180 \times 10^{-4}$ per flight. With a reserve factor of 3, the safe life before the next maintenance inspection would be:

$$10{,}000/(0.18 \times 3) = 18{,}500 \text{ flights after the previous maintenance and repair.}$$

This conservative evaluation takes no account of the improvement obtained by reaming to produce a finer surface condition.

6. CONCLUSIONS

A survey of available data on the fatigue behaviour of notched specimens made from commercial aluminium alloys yields the following conclusions:

(a) In the representation of fatigue test results on notched specimens, the stress concentration factor K_T is not a sufficient parameter. Here the effect of the stress gradient is accounted for by using the surface stress K_TS and the notch radius r .

(b) Even with 3 to 6 specimens at each load level, the experimental set of results, $(K_TS_a - N) - K_TS_m$, for several notch radii, does not give a coherent set of curves. In no case was the number of specimens sufficient to eliminate the effect of the scatter in determining mean S–N curves.

(c) The surface conditions of thin sheets, such as are produced by cold-working, electrolytic polishing, aluminium cladding, etc., produce a larger fatigue life variation than that corresponding to various aluminium alloys for a similar surface condition.

(d) The effect of the loading time-frequency is known only from laboratory tests on small specimens or very simple assemblies.

(e) The corrosion effect of outdoor day-night temperature variations, and hence water condensation, and of similar ground-altitude-ground variations were investigated only by flexure bending of small notched specimens made of 2024-T3 and 7075-T6 aluminium alloy sheet materials at the NACA Langley Field Laboratory, and during the fatigue crack propagation by axial loading of centre-notched specimens made of the same material. It is not yet possible to evaluate whether the fatigue life of actual structures under the service environment differs broadly or little from those obtained in laboratory tests where the room temperature is almost constant.

The interpretation of full-scale fatigue tests on aircraft structures or components undertaken by several manufacturers or laboratories would yield data of general use only if all the details were published or if a general consensus were reached on the interpretation methods and particularly on the reference S–N curves to be used in the interpretation. In the absence of S–N curves representative of the service environment or outdoor full-scale fatigue tests, an arbitrary modified set of $(K_T S_a - N) - K_T S_m$ curves (see Figure 61) for Alclad 2024-T3 aluminium alloy sheet has been used in France in the interpretation of a number of fatigue tests.

Two examples of interpretation are given. Despite some changes in the data, stress levels and stress concentration factors have retained the orders of magnitude of the original data.

Using Miner's formula for cumulative damage, interpretation consists in obtaining values of the "damage-equivalent" stress concentration factor, K_{DE}, and then comparing them with the theoretical stress concentration factors, K_T, that result from elasticity calculations. When the reference specimens, the fatigue tests of which are represented by the S–N curves used in computing K_{DE}, are made of the same material as the structure considered, have a comparable notch radius and are machined using the same manufacturing process, the ratio $K_{DE}/K_T = k_{DA}$ is close to 1. This result indicates a correct assessment of K_T and supports the use of the same computation procedure and the same value of k_{DA} in any evaluation of the fatigue life of the structure, either after a slight design change or for modified load spectra corresponding to a different service use.

In actual structures, the loads are transferred in joints through the shear of fastener shanks. The most critical stress concentrations exist at fasteners stressed in single shear. Approximate evaluations of stress concentration factors in single shear from numerically computed curves result from a general theory with two simplifying hypotheses for the confirmation of which no information yet exists. Assessment of the change in fatigue life due to load variation or to a slight local change in design is made by a reverse procedure which is theoretically exact when no change exists and which minimizes the errors when the change is small, as in the case of fastener replacement after hole reaming, eddy current control and installation of a fastener of increased diameter.

It may be expected that any improvement in the elasticity computation of stress concentrations will further reduce assessment errors. A constant calculation procedure including the reference S–N curves, the theory of elasticity calculations with its hypotheses, the method of decomposing varying loads, etc., may supply values of K_T, K_{DE} and k_{DA}, namely the stress concentration factor, the damage-equivalent stress concentration factor and the damage adjustment factor, such that relationships might be found between k_{DA} and geometric or elastic parameters of the assemblies investigated.

REFERENCES

1. Gassmann, H. — *Schädigung und Schadensakkumulation bei hochfestes Stall.* Thesis, Technischen Hochschule, Stuttgart, 1966.

2. Crichlow, W.J.; McCulloch, A.J.; Young, I.; Melcon, M.A. — *An Engineering Evaluation of Methods for the Prediction of Fatigue Life in Airframe Structures.* Technical Report ASD-TR-61-434, Wright-Patterson Air Force Base, Ohio, March 1962.

3. Dixon, J.R. — Journal of the Royal Aeronautical Society, March 1960.

4. Grover, H.J.; Bishop, S.M.; Jackson, L.R. — *Fatigue Strength of Aircraft Materials.* TN 2324, NACA, 1951. Results from Figure 9 of the paper.

5. Grover, H.J. Bishop, S.M. Jackson, L.R. — *Fatigue Strength of Aircraft Materials.* TN 2389, NACA, 1951. Concerns notched specimens with $K_T = 2$ and 4.

6. Grover, H.J. Bishop, S.M. Jackson, L.R. — *Fatigue Strength of Aircraft Materials.* TN 2390, NACA, 1951. Notched specimens, $K_T = 5$.

7. Grover, H.J. Hyler, W.S. Jackson, L.R. — *Fatigue Strength of Aircraft Materials.* TN 2639, NACA, February 1952. Notched specimens, $K_T = 1.5$.

8. Esquerre — *Essais de fatigue sur alliages légers.* Etude 229M, Rapport No.4, EAT, Toulouse, 1956.

9. – — Test results from CEAT, Toulouse, lost reference.

10. Beckett, R.C. Vann, A. — Note ARL – SM 307, Melbourne, April 1960.

11. – — Laboratorium für Betriebsfestigkeit, Report 1079, not published, Darmstadt, 1968.

12. – — From CEAT fatigue tests, not published.

13. Auvinet, Notton — CEAT Report M6-6153, Toulouse, February 1968.

14. Auvinet, Marquier, Notton — CEAT Report M7-6161, Toulouse, February 1968.

15. Auvinet, Notton — CEAT Report M3-7873, Toulouse, May 1965.

16. Auvinet, et al. — CEAT Report M6-7487, Toulouse.

17. Auvinet, Oulie — CEAT Report M6-7325, Toulouse, December 1966.

18. Marin, H.I. — *Fatigue Strength of Aircraft Structural Elements.* In Russian, pp.74-75, Moskow, 1968.

19. Leleu, Notton — *Frequency Influence on Rotating Bending Fatigue of A-U2GN Aluminium Alloy Specimens.* CEAT Report NO-5525-1, Toulouse, March 1974, in French. English summary in: Barrois, W.: Some Investigations on Aeronautical Fatigue in France, Period 1973-1975, ICAF Conference, Lausanne, 1975.

20. Maurin, E. Barrois, W. — *Influence de la frèquence et de la température d'essai sur la durée en fatigue d'éprouvettes et d'assemblages en tôle A-U2GN-T6. Intéraction fatigue-fluage.* In l'Aéronautique et l'Astronautique, No.9, Paris, 1969. English version in ICAF Proceedings, Stockholm, 1969.

21. Barrois, W. — *Manual on Fatigue of Structures.* Vol.I: Fundamental and Physical Aspects, AGARD-MAN-8-70, Paris, pp.65, 66 and 271, March 1970.

22. Finney, J.M. Mann, J.Y. — *Abnormally High Fatigue Strengths in Aluminium Alloy Extruded Bar.* Nature, Vol.182, pp.1366-1367, November 1958.

23. Shabalin, V.I. — *On the Discontinuity in Fatigue Curves of Duralumin.* Soviet Physics – Doklady, Vol.3, No.5, pp.1022-1024, September–October 1958.

24. Finney, J.M. — *A Review of the Discontinuity or Hump Phenomenon in Fatigue S–N Curves: Theories and Further Results.* ARL Report SM 314, Melbourne, March 1967.

25. Luther, R.G. Williams, T.R.G. — *Discontinuities in S–N Curves, from Fatigue Tests on EnIA Steel.* Metals and Materials, pp.357-362, August 1973.

26. Korbacher, G.K. et al. — *Failure Mechanisms and Statistical Aspect of Metal Fatigue.* Technical Progress Report on period November 1964 to October 1966, University of Toronto, Institute for Aerospace Studies.

27. Mori, L. — *Characteristics of Fatigue of Light Alloys: Influence of the Test Speed.* Alluminio, Vol.30, pp.175-180, 1961.

28. Austin, C.W. — *Rotating Beam Fatigue and Corrosion Fatigue Properties of Aluminium and Magnesium Alloys.* Army Ballistic Missile Agency, Engineering Materials Section, Report DS-TN-169, Abstract number: AD 606552, February 1958.

29. Auvinet, Leleu — CEAT Report No.5861, Toulouse, April 1972.

30. Vialatte, M. Pinochet, S. — *Centre d'Essai des Propulseurs.* Report 2758-LM-76, Saclay, February 1976.

31. Dixon, J.R. — Journal of the Royal Aeronautical Society, London, March 1960.

32. Donaldson, D.R. Anderson, W.A. — *Crack Propagation Behaviour of Some Airframe Materials.* Crack Propagation Symposium, Cranfield, September 1961.

33. Hartman, A. Jacobs, F.A. Nederveen, A. De Rijk, P. — *Some Tests on the Effect of the Environment on the Propagation of Fatigue Cracks in Aluminium Alloys.* NLR Report NLR-TN M.2182, Amsterdam, May 1967.

34. Schijve, J. De Rijk, P. — *The Effect of Temperature and Frequency on the Fatigue Crack Propagation in 2024-T3 Alclad Sheet Material.* NLR Report NLR-TR M.2138, Amsterdam, January 1965.

35. Kemsley, D.S. Ryan, N.E. Jost, G.S. — *Environmental Effects on Fatigue Crack Initiation and Propagation in Ultra-High Strength Steels.* 1975 ICAF Symposium, Lausanne.

36. Speidel, M.O. — *Dynamic and Static Embrittlement of a High-Strength Steel in Water.* International Congress on Hydrogen in Metals, Paris, 1972. Science et Industrie ed., Paris.

37. Boyd, W.K. — *Survey Paper on Current Research and Development on Stress-Corrosion Cracking of Aircraft Metals in the United States.* AGARD Symposium on Stress Corrosion, Torino, April 1967.

38. Figge, I.E. Hudson, C.M. — *Crack Propagation, Delayed Failure and Residual Static Strength of Titanium, Aluminium and Stainless Steel Alloys in Aqueous Environments.* NASA TN D-3825, February 1967.

39. Ryder, J.T. Petitt, D.E. Krupp, W.E. Hoeppner, D.W. — *Evaluation of Mechanical Property Characteristics of IMI 685.* Final Report, Fracture Mechanics Laboratory, Lockheed California Co., Burbank, October 1973.

40. Speidel, M.O. — *Corrosion Fatigue Crack Growth in High-Strength Aluminium Alloys.* 1975 ICAF Symposium, Lausanne.

41. Hartman, A. — *On the Effect of Oxygen and Water Vapour on the Propagation of Fatigue Cracks in 2024-T3 Alclad Sheets.* International Journal of Fracture Mechanics, Vol.1, No.3, p.167, 1965.

42. Van Leeuwen, H.P. Boogers, J.A.M. Stentler, C.J. — *The Contribution of Corrosion to the Stress Corrosion Cracking of Al-Zn-Mg Alloys.* Corrosion, Vol.31, No.1, pp.23-29, January 1975.

43. Leybold, H.A. Hardrath, H.F. Moore, R.L. — *An Investigation of the Effects of Atmospheric Corrosion on the Fatigue Life of Aluminum Alloys.* NACA TN 4331, Langley Field, September 1958.

44. Leybold, R.A. — *The Effects of Combined Prior Stress and Atmospheric Corrosion on the Fatigue Life of Aluminum Alloys.* NASA TN D-2359, Langley Research Center, Va., August 1964.

45. Schijve, J.
De Rijk, P.
The Crack Propagation in Two Aluminium Alloys in an Indoor and an Outdoor Environment Under Random and Programmed Load Sequences. NLR-TR M.2156 Report, Amsterdam, November 1965.

46. Anderson, W.E.
Fatigue of Aircraft Structures. International Metallurgical Reviews, Vol.17, pp.240-263, 1972.

47. Harpur, N.F.
Troughton, A.J.
The Value of Full-Scale Fatigue Testing. ICAF 1965 Munich Symposium on Fatigue Design Procedures, edited by Gassner and Schutz, Pergamon Press, pp.343-373, 1969.

48. Anderson, W.E.
Corrosion Fatigue — Or — How to Replace the Full-Scale Fatigue Test? AGARD Lecture Series No.62, Paris, May 1973.

49. Hayes, J.E.
An Analytic Method for Predicting Aircraft Fatigue Life. Proceedings of the WADC Symposium 1959 on Fatigue of Aircraft Structures, WADC Report TR 59-107, Wright-Patterson, Ohio, August 1959.

50. Barrois, W.
Interrelated Aspects of Service Safety Arising from Consideration of Safe Life, Fail-Safe, Manufacturing Quality and Maintenance Procedure. London 1973 ICAF Symposium, edited by A.M.Stagg and published as Report TR.73183 by the Royal Aircraft Establishment, Farnborough, Vol.1, pp.1.2/1 to 1.2/37, December 1973.

51. Deneff, G.V.
Fatigue Prediction Study. Douglas Company, Technical Report WADD TR 61-153, Wright-Patterson Air Force Base, Ohio, January 1962.

52. Jarfall, L.
Fatigue Cycling of Riveted or Bolted Joints. FFA Report HF-1239, Stockholm, June 1969; also in the ICAF Proceedings of the Melbourne Symposium, Pergamon Press, 1972.

53. Vogt, F.
The Load Distribution in Bolted or Riveted Joints in Light-Alloy Structures. RAE Report No.SME 3300, Royal Aircraft Establishment, Farnborough, or NACA TM 1135, October 1944.

54. Volkersen, O.
Die Nietkraftverteilung in zugbeansprichten Nietverbindungen mit konstanten Laschenquerschnitten. Luftfahrtforschung, Vol.15, No.1/2, pp.41-47, 1938.

55. Rosenfeld, S.J.
Analytical and Experimental Investigation of Bolted Joints. NACA TN 1458, Washington D.C., October 1947.

56. Harris, G.H.
Ojalvo, J.U.
Hooson, R.E.
Stress and Deflection Analysis of Mechanically Fastened Joints. AFFDL-TR-70-49, Wright-Patterson Air Force Base, Ohio, May 1970.

57. Barrois, W.
Stresses and Displacements Due to Load Transfer by Fasteners in Structural Assemblies. First Part: Double symmetrical shearing. Second Part: Single shearing. September 1976, Paris, to be published in Engineering Fracture Mechanics.

58. Theocaris, P.S.
The Stress Distribution in a Strip Loaded in Tension by Means of a Central Pin. Journal of Applied Mechanics, pp.85-90, March 1940. Vol.23, No.1 NACHS 1956.

59. Frocht, M.M.
Hill, H.N.
Stress Concentration Factors at the Edge of a Circular Hole in a Plate Loaded by Means of a Pin. Journal of Applied Mechanics, March 1940. Vol.7, pp.A5-A9.

60. Jessop, H.T.
Snell, C.
Holister, G.S.
Photoelasticity Investigation on Plates With Single Interference-Fit Pin With Load Applied (a) To Pin and (b) To Pin and Plate Simultaneously. Aeronautical Quarterly 9, pp.147-163, 1958.

61. Bickley, W.G.
Distribution of Stress Round a Circular Hole in a Plate. Royal Society of London, Series A, Vol.2227, pp.383-415, 1928.

62. Howland, R.C.J.
On the Stresses in the Neighbourhood of a Circular Hole in a Strip Under Tension. Phil. Trans. Royal Society, London, Series A, Vol.229, pp.49-86, 1930.

63. Elsner
Diplomarbeit D 45, Institut für Luftfahrzeugbau (ILTUB), Berlin, 1966, quoted in Hertel, H., p.269.

64. Hertel, H.
Ermüdungsfestigkeit der Konstruktionen. Springer-Verlag, 1969.

65. Heywood, R.B. — *Designing By Photoelasticity*. Chapman and Hall, London, 1952.

66. Cowper, G.R. — *The Shear Coefficient in Timoshenko's Beam Theory*. Journal of Applied Mechanics, Vol.33, No.2, pp.335-340, 1966.

67. Tate, M.B. Rosenfeld, S.J. — *Preliminary Investigations of the Loads Carried by Individual Bolts in Bolted Joints.* NACA TN 1051, May 1946.

68. Schijve, J. Jacobs, F.A. — *Fatigue Tests on Unnotched and Notched Specimens of 2024-T3 Alclad, 2024-T8 Alclad and 7178-T6 Extruded Materials.* Report NLR-TR 68017 U, Amsterdam, February 1968.

69. Schütz, D. Lowak, H. — *The Effect of Secondary Bending on the Fatigue Strength of Joints.* LBF Report FB-113, translated from German into English by the RAE (No.1858), Darmstadt, 1974 (German original).

70. — CEAT Fatigue Laboratory, private communication on an investigation in progress, Toulouse, November 1976.

71. Sobey, A.J. — *Stress Concentration Factors of Rectangular Holes With Rounded Corners in Infinite Sheets.* ARC R&M/3407, November 1963.

72. Mindlin — Society for Experimental Stress Analysis (SESA), Vol.V, No.2, 1948.

73. Barrois, W. — *Physical Interpretation of Metal Fatigue.* ICAF Conference, Bruxelles, October 1957. Also in French: "Sur la fatigue des cellules d'avions", Métaux-Corrosion-Industries, No.364, December 1955.

REPORT DOCUMENTATION PAGE			
1. Recipient's Reference	**2. Originator's Reference**	**3. Further Reference**	**4. Security Classification of Document**
	AGARD-AG-228	ISBN 92-835-1250-2	UNCLASSIFIED

5. Originator Advisory Group for Aerospace Research and Development
North Atlantic Treaty Organization
7 rue Ancelle, 92200 Neuilly sur Seine, France

6. Title USE OF GENERAL FATIGUE DATA IN THE INTERPRETATION OF FULL-SCALE FATIGUE TESTS

7. Presented at

8. Author(s)	**9. Date**
W. Barrois	October 1977
10. Author's Address	**11. Pages**
42, rue Larmeroux – 92170 Vanves, France	78

12. Distribution Statement This document is distributed in accordance with AGARD policies and regulations, which are outlined on the Outside Back Covers of all AGARD publications.

13. Keywords/Descriptors

Fatigue tests	Stress concentration	Elastic properties
Data processing	Shear tests	
Notch tests	Fasteners	

14. Abstract

The fatigue behaviour of notched specimens depends on two elasticity parameters, namely the stress concentration factor and the relative stress gradient or the radius of curvature at the notch root. Laboratory fatigue test results are not always representative of the environmental conditions within aircraft structural assemblies, particularly because of water condensation in gaps and recesses. The frequency effect is mainly ascribable to humidity, and therefore to corrosion, owing to hydrogen penetration.

In assemblies, stress concentrations due to load transfer through fasteners are investigated for the case of asymmetric single shear. The breakdown of the applied loadings must include the peak-to-peak, ground-air-ground variation. In load transfer by fastener bearing stresses, the low compressive loads may be neglected, the local highest stresses varying from zero to the maximum. Interpretation of full-scale fatigue test results, either for a different loading or for a slightly modified local design of the structure, is essentially comparative.

In order to locate the computation points within a suitable region, the stress concentration factor is multiplied by a damage adjustment factor, k_{DA}, such that the Miner damage is 1 for the local failure of the structure considered. A structure may provide as many k_{DA} values as the failures observed during the full-scale fatigue test. A number of further investigations would enable the variation of k_{DA} with structural assembly parameters to be investigated.

This AGARDograph was sponsored by the Structures and Materials Panel of AGARD.

AGARDograph No.228
Advisory Group for Aerospace Research and Development, NATO
USE OF GENERAL FATIGUE DATA IN THE INTERPRETATION OF FULL-SCALE FATIGUE TESTS
W.Barrois
Published October 1977
78 pages

The fatigue behaviour of notched specimens depends on two elasticity parameters, namely the stress concentration factor and the relative stress gradient or the radius of curvature at the notch root. Laboratory fatigue test results are not always representative of the environmental conditions within aircraft structural assemblies, particularly because of water condensation in gaps and

P.T.O.

AGARD-AG-228

Fatigue tests
Data processing
Notch tests
Stress concentration
Shear tests
Fasteners
Elastic properties

AGARDograph No.228
Advisory Group for Aerospace Research and Development, NATO
USE OF GENERAL FATIGUE DATA IN THE INTERPRETATION OF FULL-SCALE FATIGUE TESTS
W.Barrois
Published October 1977
78 pages

The fatigue behaviour of notched specimens depends on two elasticity parameters, namely the stress concentration factor and the relative stress gradient or the radius of curvature at the notch root. Laboratory fatigue test results are not always representative of the environmental conditions within aircraft structural assemblies, particularly because of water condensation in gaps and

P.T.O.

AGARD-AG-228

Fatigue tests
Data processing
Notch tests
Stress concentration
Shear tests
Fasteners
Elastic properties

AGARDograph No.228
Advisory Group for Aerospace Research and Development, NATO
USE OF GENERAL FATIGUE DATA IN THE INTERPRETATION OF FULL-SCALE FATIGUE TESTS
W.Barrois
Published October 1977
78 pages

The fatigue behaviour of notched specimens depends on two elasticity parameters, namely the stress concentration factor and the relative stress gradient or the radius of curvature at the notch root. Laboratory fatigue test results are not always representative of the environmental conditions within aircraft structural assemblies, particularly because of water condensation in gaps and

P.T.O.

AGARD-AG-228

Fatigue tests
Data processing
Notch tests
Stress concentration
Shear tests
Fasteners
Elastic properties

AGARDograph No.228
Advisory Group for Aerospace Research and Development, NATO
USE OF GENERAL FATIGUE DATA IN THE INTERPRETATION OF FULL-SCALE FATIGUE TESTS
W.Barrois
Published October 1977
78 pages

The fatigue behaviour of notched specimens depends on two elasticity parameters, namely the stress concentration factor and the relative stress gradient or the radius of curvature at the notch root. Laboratory fatigue test results are not always representative of the environmental conditions within aircraft structural assemblies, particularly because of water condensation in gaps and

P.T.O.

AGARD-AG-228

Fatigue tests
Data processing
Notch tests
Stress concentration
Shear tests
Fasteners
Elastic properties

recesses. The frequency effect is mainly ascribable to humidity, and therefore to corrosion, owing to hydrogen penetration.

In assemblies, stress concentrations due to load transfer through fasteners are investigated for the case of asymmetric single shear. The breakdown of the applied loadings must include the peak-to-peak, ground-air-ground variation. In load transfer by fastener bearing stresses, the low compressive loads may be neglected, the local highest stresses varying from zero to the maximum. Interpretation of full-scale fatigue test results, either for a different loading or for a slightly modified local design of the structure, is essentially comparative.

In order to locate the computation points within a suitable region, the stress concentration factor is multiplied by a damage adjustment factor, k_{DA}, such that the Miner damage is 1 for the local failure of the structure considered. A structure may provide as many k_{DA} values as the failures observed during the full-scale fatigue test. A number of further investigations would enable the variation of k_{DA} with structural assembly parameters to be investigated.

This AGARDograph was sponsored by the Structures and Materials Panel of AGARD.

ISBN 92-835-1250-2

recesses. The frequency effect is mainly ascribable to humidity, and therefore to corrosion, owing to hydrogen penetration.

In assemblies, stress concentrations due to load transfer through fasteners are investigated for the case of asymmetric single shear. The breakdown of the applied loadings must include the peak-to-peak, ground-air-ground variation. In load transfer by fastener bearing stresses, the low compressive loads may be neglected, the local highest stresses varying from zero to the maximum. Interpretation of full-scale fatigue test results, either for a different loading or for a slightly modified local design of the structure, is essentially comparative.

In order to locate the computation points within a suitable region, the stress concentration factor is multiplied by a damage adjustment factor, k_{DA}, such that the Miner damage is 1 for the local failure of the structure considered. A structure may provide as many k_{DA} values as the failures observed during the full-scale fatigue test. A number of further investigations would enable the variation of k_{DA} with structural assembly parameters to be investigated.

This AGARDograph was sponsored by the Structures and Materials Panel of AGARD.

ISBN 92-835-1250-2

recesses. The frequency effect is mainly ascribable to humidity, and therefore to corrosion, owing to hydrogen penetration.

In assemblies, stress concentrations due to load transfer through fasteners are investigated for the case of asymmetric single shear. The breakdown of the applied loadings must include the peak-to-peak, ground-air-ground variation. In load transfer by fastener bearing stresses, the low compressive loads may be neglected, the local highest stresses varying from zero to the maximum. Interpretation of full-scale fatigue test results, either for a different loading or for a slightly modified local design of the structure, is essentially comparative.

In order to locate the computation points within a suitable region, the stress concentration factor is multiplied by a damage adjustment factor, k_{DA}, such that the Miner damage is 1 for the local failure of the structure considered. A structure may provide as many k_{DA} values as the failures observed during the full-scale fatigue test. A number of further investigations would enable the variation of k_{DA} with structural assembly parameters to be investigated;

This AGARDograph was sponsored by the Structures and Materials Panel of AGARD.

ISBN 92-835-1250-2

recesses. The frequency effect is mainly ascribable to humidity, and therefore to corrosion, owing to hydrogen penetration.

In assemblies, stress concentrations due to load transfer through fasteners are investigated for the case of asymmetric single shear. The breakdown of the applied loadings must include the peak-to-peak, ground-air-ground variation. In load transfer by fastener bearing stresses, the low compressive loads may be neglected, the local highest stresses varying from zero to the maximum. Interpretation of full-scale fatigue test results, either for a different loading or for a slightly modified local design of the structure, is essentially comparative.

In order to locate the computation points within a suitable region, the stress concentration factor is multiplied by a damage adjustment factor, k_{DA}, such that the Miner damage is 1 for the local failure of the structure considered. A structure may provide as many k_{DA} values as the failures observed during the full-scale fatigue test. A number of further investigations would enable the variation of k_{DA} with structural assembly parameters to be investigated.

This AGARDograph was sponsored by the Structures and Materials Panel of AGARD.

ISBN 92-835-1250-2

B319
4

AGARD
NATO OTAN
7 RUE ANCELLE · 92200 NEUILLY-SUR-SEINE
FRANCE
Telephone 745.08.10 · Telex 610176

DISTRIBUTION OF UNCLASSIFIED AGARD PUBLICATIONS

AGARD does NOT hold stocks of AGARD publications at the above address for general distribution. Initial distribution of AGARD publications is made to AGARD Member Nations through the following National Distribution Centres. Further copies are sometimes available from these Centres, but if not may be purchased in Microfiche or Photocopy form from the Purchase Agencies listed below.

NATIONAL DISTRIBUTION CENTRES

BELGIUM
Coordonnateur AGARD – VSL
Etat-Major de la Force Aérienne
Caserne Prince Baudouin
Place Dailly, 1030 Bruxelles

CANADA
Defence Scientific Information Service
Department of National Defence
Ottawa, Ontario K1A OZ2

DENMARK
Danish Defence Research Board
Østerbrogades Kaserne
Copenhagen Ø

FRANCE
O.N.E.R.A. (Direction)
29 Avenue de la Division Leclerc
92 Châtillon sous Bagneux

GERMANY
Zentralstelle für Luft- und Raumfahrt-
dokumentation und -information
Postfach 860880
D-8 München 86

GREECE
Hellenic Armed Forces Command
D Branch, Athens

ICELAND
Director of Aviation
c/o Flugrad
Reykjavik

ITALY
Aeronautica Militare
Ufficio del Delegato Nazionale all'AGARD
3, Piazzale Adenauer
Roma/EUR

LUXEMBOURG
See Belgium

NETHERLANDS
Netherlands Delegation to AGARD
National Aerospace Laboratory, NLR
P.O. Box 126
Delft

NORWAY
Norwegian Defence Research Establishment
Main Library
P.O. Box 25
N-2007 Kjeller

PORTUGAL
Direccao do Servico de Material
da Forca Aerea
Rua de Escola Politecnica 42
Lisboa
Attn: AGARD National Delegate

TURKEY
Department of Research and Development (ARGE)
Ministry of National Defence, Ankara

UNITED KINGDOM
Defence Research Information Centre
Station Square House
St. Mary Cray
Orpington, Kent BR5 3RE

UNITED STATES
National Aeronautics and Space Administration (NASA),
Langley Field, Virginia 23365
Attn: Report Distribution and Storage Unit

THE UNITED STATES NATIONAL DISTRIBUTION CENTRE (NASA) DOES NOT HOLD STOCKS OF AGARD PUBLICATIONS, AND APPLICATIONS FOR COPIES SHOULD BE MADE DIRECT TO THE NATIONAL TECHNICAL INFORMATION SERVICE (NTIS) AT THE ADDRESS BELOW.

PURCHASE AGENCIES

Microfiche or Photocopy
National Technical
Information Service (NTIS)
5285 Port Royal Road
Springfield
Virginia 22151, USA

Microfiche
Space Documentation Service
European Space Agency
10, rue Mario Nikis
75015 Paris, France

Microfiche
Technology Reports
Centre (DTI)
Station Square House
St. Mary Cray
Orpington, Kent BR5 3RF
England

Requests for microfiche or photocopies of AGARD documents should include the AGARD serial number, title, author or editor, and publication date. Requests to NTIS should include the NASA accession report number. Full bibliographical references and abstracts of AGARD publications are given in the following journals:

Scientific and Technical Aerospace Reports (STAR),
published by NASA Scientific and Technical
Information Facility
Post Office Box 8757
Baltimore/Washington International Airport
Maryland 21240, USA

Government Reports Announcements (GRA),
published by the National Technical
Information Services, Springfield
Virginia 22151, USA

Printed by Technical Editing and Reproduction Ltd
Harford House, 7–9 Charlotte St, London W1P 1HD

ISBN 92-835-1250-2